Institute of Energy Technology ■ Aalborg University ■ PED9 Autumn 2001

Pontoppidanstræde 101 ■ 9220 Aalborg East ■ Tlf.: 9635 8080

TITLE: Optimized Design of Power Supply for CubeSat at Aalborg University

THEME: Design Oriented Analysis of Electric Machines and Power Electronic Systems

PROJECT PERIOD: 1.09.2001 to 4.01.2002

PROJECT GROUP: PED9-17C

AUTHORS:

Radu Dan Lazar
Vasile Bucelea
Ales Loidl
Lukas Formanek
Thomas Chlubna

SUPERVISOR:

Søren Bækhøj Kjær

NUMBER OF COPIES: 7

NUMBER OF PAGES

Report: 139

Appendices: 24

COMPLETED: 4.01.2002

ABSTRACT

This project deals with the design and implementation of a power supply for the CubeSat student satellite. The satellite will be constructed and operated by students at Aalborg University.
Design of the power supply will be an optimized design which will take into account problems like redundancy, reliability and efficiency.
The main objective for this present project work is to realize a design oriented analysis over a real challenge. A student satellite is to be launched in space and the power supply subsystem must be realized. In order to accomplish the task, few topologies of the power supply will be analyzed. The best solution is chosen, efficiency of the system being one of the most important criteria.
For practical implementation, components are selected taking into account space reserved for the board inside the satellite and the operating temperature range.
Thermal analysis of the power subsystem is performed and basis for a more extended analysis for the whole satellite are stated.
Housekeeping data must be acquired for the solar cells, batteries and different users.
Partial measurements performed are showing that the system designed can work in concordance with the requirements and future improvements will be added, if they are necessary.

Preface

This present project "Optimised Design of Power Supply for CubeSat at Aalborg University" is written by Group PED9-17C at the 9th semester on the Master of Science Education in Electrical Engineering at Aalborg University. The project period is 1.09.2001 to 4.01.2002.
The main goal of the project is designing and practical realization of the power supply for the CubeSat sattelite.

The report consists of two parts: a main part and an appendix part.

The main part consists of seven parts (1-7), defining the demands for the application in which the power supply is seen as a subsystem. Based on critical comparison between simulations and measurements, conclusions will be drawn concerning the accuracy of the proposed models and the use of the chosen control solution concerning the application.

The appendix part contains five parts (A-E) where the used additional material is presented, and circuit diagrams are included. A list with symbols and common used abbreviations can be found in Appendix E.

The report uses SI-units. Literature references are stated by [*Author, Year, Page*], for example [*Mohan, 1995, p.164*]. A complete list of used literature may be found at the last page of the main part of the report. Figures and equations are numbered in succession within each chapter and appendix, for example, figure three in chapter 4 is named *figure 4.3*, and equation three in chapter 4 is named (4.3).

Aalborg, 4.01.2002

Radu Dan Lazar   Vasile Bucelea   Ales Loidl

Lukas Formanek   Thomas Chlubna

Table of Contents

Appendix

Chapter 1
Introduction

Abstract

This present project deals with practical design and implementation of a power supply for CubeSat satellite. The satellite is entirely developed by the students at the Aalborg University.

The first chapter, the introduction, presents a background of the project as well as some general guidelines about the work enclosed in the project.

1.1. Background of the project

The development of a student satellite is about to be initiated at Aalborg University. It should be finished by May 2002. The object of the project is to involve project groups in development of an AAU satellite across different departments of the Faculty of Engineering and Science.

The electronic functions on board and the choice of the materials are totally up to the CubeSat groups. The only restrictions deal with weight, space environment, launching requirements and international regulations. The satellite will be located in a Low Earth Orbit (LEO) at a height of approximately 600 kilometers from the surface of the Earth.

The satellite is designed, developed, implemented, tested and operated by students. A number of student groups are established within the participating fields and subsystems.

1.2. Aims of the project

The aim of the project is to design and realize the power subsystem for the CubeSat satellite. It is considered an optimized design, therefore some considerations about redundancy, operational thermal domain, reliability and efficiency of the power supply must be taken into account. It is a requirement that the efficiency is as high as possible, considering thermal problems caused by waste heat as no kind of convection is available. All power dissipation from the satellite is done by radiation. At the same time, high efficiency will result in savings of the solar cells.

1.3. System description

In figure 1.1 is presented a general description of the satellite architecture. The flow of power is illustrated, in order to offer an overview of the general power problem.

The mission of the satellite is to take snapshots of the Danish landscape. In order to achieve this task, a few separate subsystems must be implemented. The payload consists in a 5 V supplied CCD camera, 1.3 mil. pixels.

Orientation of the satellite is provided by the Attitude Control System (ACS) by means of interaction of 3-axis coils magnetic field with Earth's magnetism. Communication Module (COM) ensures the link with the ground control station, situated in Aalborg. It is also the task of the COM to downlink the pictures and information about each subsystem. Optional, the COM may incorporate a beacon module.

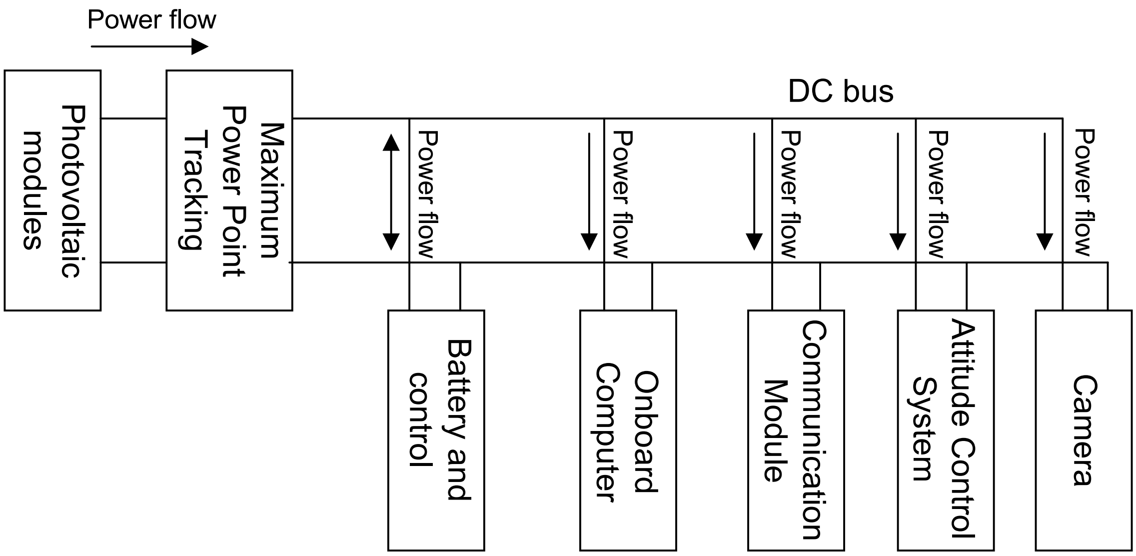

Figure 1.1 Overview of the simplified satellite system

Supervision of the well-behavior of all subsystems is done by the Onboard Computer (OBC), which will also decide in critical situations.

All subsystems will be supplied with proper voltages by the Power Supply Unit (PSU). The PSU contains Photovoltaic module (PV), Maximum Power Point Tracking (MPPT) and Battery Unit (BAT).

1.4. Strategy for achieving the aims

The strategy for achieving the aims is stated as follows:

- Analysis of entire structure of the satellite, revealing the most important aspects concerning the power subsystem.
- After the analysis is performed, the best solution for practical implementation of the different parts of the power supply is chosen, considering also the specifications for the system.
- Solution chosen is verified through simulation.
- The thermal regime is studied for a better positioning of the components of the power supply. This will provide a feedback for a more accurate analysis of the system.

- Finally, chosen topology is practical implemented.
- Measurements are performed on the real model of the power supply and efficiency is evaluated.
- Based on the results, final conclusion about the design is drawn.

1.5. Content of the project

The main goal of the present project is to realize an optimized design for a power supply used in CubeSat satellite.

The main part of the project consists of seven chapters, defining the demands for the application in which the power supply is to be used, and the power subsystem itself.

Based on the comparison between simulations and measurements, conclusions will be drawn, considering the chosen topology in respect with the application.

In the first chapter, the problem dealt in the project is stated and the goal of the project is defined, as well as the strategy for achieving the aims. A general scheme is shown and a description of the power subsystem is made.

The second chapter presents the specifications for the system.

In the third chapter, an analysis of the system is performed. Several ways to connect the solar cells and topologies for the power supply are presented and the best solution, in respect with the demands of the application, is chosen.

In the fourth chapter, the design is definitivated and the final analysis is performed using as a feedback the experience gained in the previous chapter. The protection circuits are designed and preliminary considerations about the temperature range inside the satellite are stated. The implementation of the power supply final design is also presented.

The fifth chapter deals mainly with problems related to EMC considerations and with the thermal analysis.

The sixth chapter is dedicated to experimental measurements. The experimental setup is presented and the methods used for measurements are presented. On the basis of the data obtained in this chapter, a conclusion is drawn in the final chapter, the seventh.

Chapter 2
Specifications of the system

Abstract

This chapter presents the characteristics of the satellite, seen as a whole system. The most important problems in respect with the project, reside from the characteristics of the power supply subsystem. Other important aspects, like orbit and space environment or mechanical structure are presented as general requirements for the system.

2.1. Introduction

For the purpose of understanding the role of the power supply in good-functioning of the satellite and to design it in a proper way, the specifications for the entire system must be known. The job of the electrical power subsystem is to provide uninterrupted power to on-board electronics both in sunlight and in eclipse.

There are five types of power sources in use today:

- Solar cells also denoted Photovoltaic (Silicon,Gallium-Arsenide)
- Secondary batteries (rechargeable) – used as energy storage medium to supply power during eclipse or adverse pointing of the solar arrays.
- Primary batteries (non-rechargeable) – used only on launchers and on small experimental missions with a lifetime of a few days.
- Fuel cells – producing electricity by electrochemically "burning" oxygen and hydrogen to water. Used presently only on the Space Shuttle.
- Radioisotope Thermal Generators (RTG) – using the heat produced by radioactive decay of Plutonium-238 to produce electricity via thermo-electrical cells. Used only on interplanetary missions to the outer planets.

For the CubeSat mission, two types of power sources are used: photovoltaic and rechargeable Li-Ion batteries.

2.2. General requirements

In this section, a few specifications for the system, named as "general" requirements, will be presented. Note that some values are absolute, others will provide only guidelines for final design.

- Efficiency for the power subsystem is not stated. An objective of the current project work is, therefore, to achieve as high efficiency, as possible. Also, reliability of the components, which will reflect into entire power subsystem reliability, must be taken into account.
- EMC characteristics must meet actual standards.
- Temperature inside the satellite must not exceed the limits for normal operation of the components.

- Dimensions and weight. For PSU is at disposal at most 290 grams mass which must be divided into batteries, solar cells, etc. For solar cells are also given maximum dimensions: solar cells on each hand side 80 x 95 mm and on the top side 80 x 80 mm. For each battery is given 83.3 x 39 x 4.9 mm [Conceptual-Structural-Design-271001-rev1-0-pdf.pdf].

2.3. Electrical specifications

2.3.1. Inputs and outputs specifications for power subsystem

Energy from the Sun is the main source of power for the satellite. However, there are lot of other sources of radiation in space (cosmic radiation, albedo from the Moon etc), but only a few of them are significant.

In table 2.1, three sources of energy, at disposal for Cubesat, are shown.

Type of heat	Solar radiation	Albedo of the Earth	Infrared radiation of the Earth
Energy (W/m^2)	1353	406	237

Table 2.1 Main energy sources

As can be seen in a table 2.1, the solar irradiation is the most powerful source of energy. This source can be taken into account only when the satellite is illuminated from the Sun. Due to the multi junction technology (used in solar cells) the infrared spectrum (from 700 nm to 1000 nm) can also be included [http://www.ipac.caltech.edu/Outreach/Edu/infrared.html].

Albedo is the fraction of light that is reflected by a surface. It is commonly used in astronomy to describe the reflective properties of planets, satellites, and asteroids. Bond albedo, defined as the fraction of the total incident solar radiation reflected by a planet back to space, is a measure of the planet's energy balance. The value of bond albedo is dependent on the spectrum of the incident radiation because such albedo is defined over the entire range of wavelengths. Earth-orbiting satellites have been used to measure the Earth's bond albedo. The most recent values obtained are approximately 33% [http://zebu.uoregon.edu/~js/glossary/albedo.html].

The power subsystem is designated to supply all the users in the satellite. The users, in the CubeSat satellite are: OBC (Onboard Computer), ACS (Attitude Control System), CAM (Camera), COM (Communication module).

In Table 2.2, the power budget for the loads is presented.

Consumer	Voltage [V]	Current [A]	Power [W]
OBC	5	0.092	0.46
COM module	5	1.8	9 (16min)
Camera	5	0.06	0.3
ACS	5	0.05	0.25
Total Power			**10.01**

Table 2.2 Power budget for the loads

In designing of the power supply subsystem, it has to be decided as the most convenient and high-efficient solution as possible.

2.3.2. Batteries and solar panels requirements

During the time eclipse, when the satellite is in shadow and also when bus needs more power than solar cells can provide, batteries must be used. They will be also back up in the case of failure on the solar cells and simultaneously as storage for redundancy energy. Due to the orbit conditions they must operate in big amount of temperatures. Weight and size must be kept as low as possible.

Due to these brief considerations, batteries chosen to equip CubeSat have the following specifications [http://www.danionics.dk]:

- Type: Li-Ion Polymer
- Dimensions: 69 x 39 x 4.9 [mm]
- Weight: 26 [g]
- Capacity: 920 [mAh]
- Nominal voltage: 3.7 [V]
- Voltage range: 3.0 – 4.2 [V]

Solar cells are semiconductor devices that convert sunlight directly into electricity. Conventional solar electric systems use solar cells, encapsulated in "flat-plate" weatherproof "modules". Solar cells cover the entire flat-plate module area and are uniformly illuminated with unconcentrated sunlight. The solar cells selected for the current application have the following specifications [http://www.emcore.com]:

- Size of one cell: 69 x 40 [mm]
- Thickness: 140 [μm]
- Weight: 2.25 [g]
- Advanced triple junction InGaP/GaAs, Ge substrate cell
- Efficiency (BOL) = min. 27.5 [%]
- Efficiency (EOL) = min. 25 [%]
- Open circuit voltage: 2.616 [V]
- Short circuit current: 462 [mA]

2.4. Interface and orbit specifications

There are two main parts of the interface – data and power. The power bus will provide energy for all systems in the satellite and the data bus will provide communication with OBC.
The loads on the satellite, as described in section 1.3, are: onboard computer, attitude control system, communication system (radio, associated circuits) and camera circuits.

The power bus must deliver energy from power source to these loads and must grant all values (ripple, voltage level etc.) with as high accuracy as possible. All systems are using 5V as an input voltage. For the radio transmitter, this comprises an internal converter, to transform 5V voltage to required voltage level (9V). This is done completely independent, so in respect with the tasks of the power supply, the transmitter module is seen as another user supplied at 5V. Another important task for PSU is to provide protections for the users, these protections must avoid any dangerous situations which can occur in user's circuits.

The data bus should provide communication to/from onboard computer. All housekeeping data will flow through this bus and all control signals will also use this bus.

The satellite will be placed on a circular Low Earth Orbit with the inclination of 96 degrees and height of approx. 600 km. Velocity of the satellite on orbit is estimated to be 27000 km/h.
Based on these parameters, revolution time has been computed:

- T_{orbit}: 100 min
- T_{sun}: 65 min
- $T_{eclipse}$: 35min

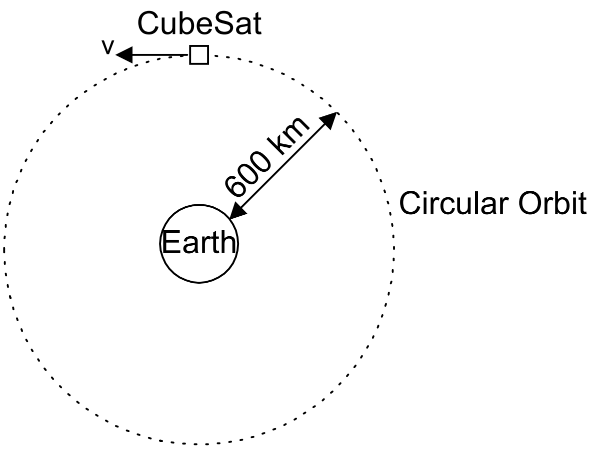

Figure 2.1 Sketch of the satellite orbit

2.5. Summary

In this chapter, general and special requirements for the system and for the Power Supply Unit, respectively, are presented. In section 2.2, requirements for the power subsystem regarding dimensions and weight are presented.

Some of them will be detailed in the next chapter, where a more detailed analysis of the system will be done.

Chapter 3
System analysis

Abstract

This chapter deals mainly with the analysis of the system. An important space is reserved to power sources in satellite: photovoltaic module and batteries. For both, the possible choices of connection are shown, with all advantages and disadvantages. In presentation of the photovoltaic module, a theoretical background is included. For the power supply the proposed layouts are analyzed in section 3.2.

3.1. Introduction

For the purpose of understanding function of the power supply, an analysis of the power subsystem has to be set. It is a requirement that the efficiency of the power supply to be as high as possible, considering thermal problems occurring in vacuum. In section 3.2, an overview of possible layouts of the power supply is done. In respect with efficiency, the best solution has been chosen for further implementation and deeper analysis, performed in the next chapter.

To obtain a robust system, the interface between the DC bus and the users must be examined. Protection of all users has to be implemented, also set up different priorities for users, according to their importance for the continuous functionality of the satellite.

3.2. Power supply topologies

Four different layouts have been proposed for the power supply.

In this section it will be explained the advantages and disadvantages for each of them and the best configuration is to be chosen.

In figure 3.1, the first possible configuration for the power subsystem is shown.

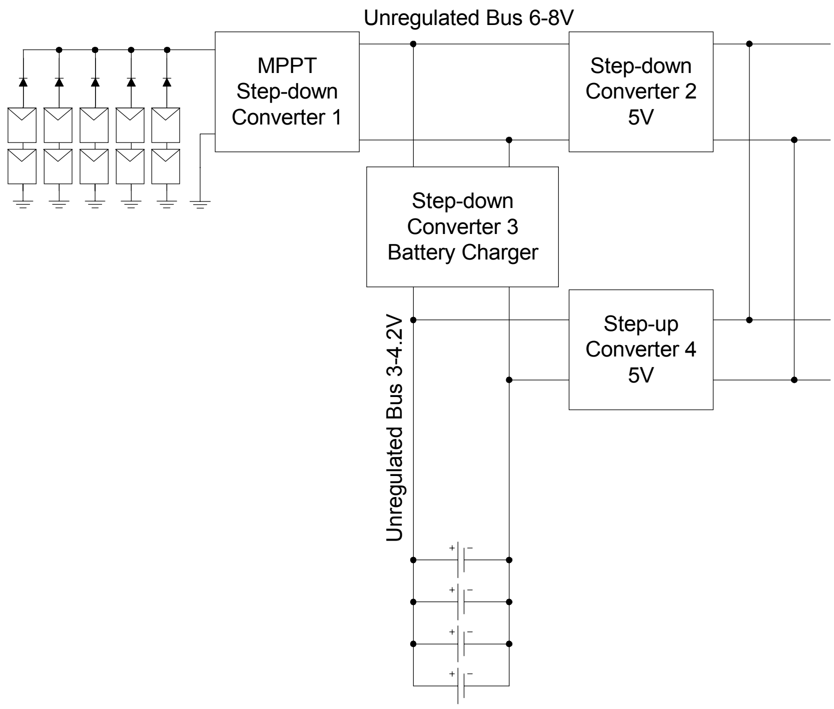

Figure 3.1 Proposal for power supply layout using 4 converters and 2 unregulated buses

In this configuration, four converters are to be used.

The MPPT converter is supplying the unregulated bus with voltage between 6V and 8V. This bus is feeding two step-down converters. One of them is charging the batteries and the other one realizes the 5V stabilized voltage used for OBC, ATC and camera. From the unregulated battery bus is supplied another converter for 5V. The 5V converter is working in parallel with the other one for a better redundancy.

Advantages:

- Good redundancy for 5V supply – there are two independent 5V sources

Disadvantages:

- Low efficiency – three converters are in series, final efficiency is product of each converter's efficiency
- Large amount of converters (4) – too big complexity
- Poor reliability – more components imply less reliability

In figure 3.2, the second possible topology is presented. Instead of the unregulated bus 6-8V, a 5V regulated bus is used. In this way is used one converter less.

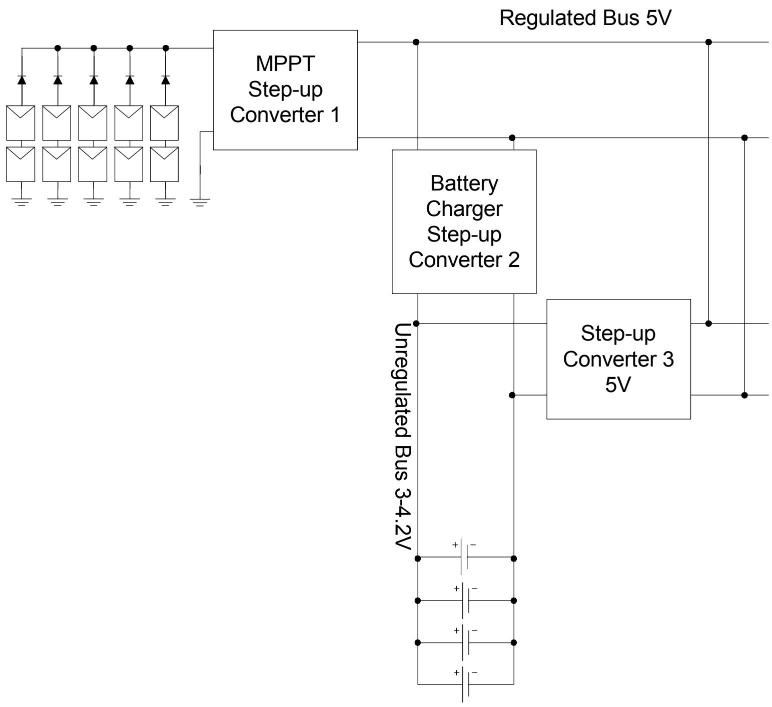

Figure 3.2 Proposal for power supply layout using 3 converters and an unregulated bus

Advantages:

- Good redundancy for 5V supply – there are two independent 5V sources (until batteries are charged)

Disadvantages:

- Low efficiency – again three converters in series

In the third case, presented below, the batteries are placed directly on the unregulated bus and the MPPT converter is also the battery charger. That results in one converter less, comparing with the other topologies.

The layout is depicted in figure 3.3.

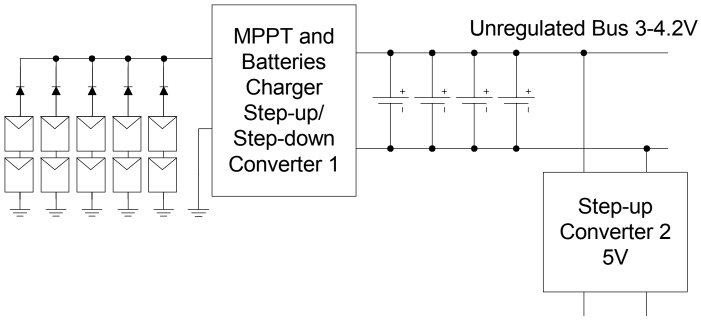

Figure 3.3 Proposal for power supply layout using 2 converters and an unregulated bus

Advantages:

- Good reliability – low number of components
- Good efficiency – only two converter in series

Disadvantages:

- There is not too wide variety of buck-boost converters, from which can be chosen proper one, in case of such a small input voltage.

The proposed layout for the power supply in the last case, is presented in figure 3.4. The configuration comprises two converters, one supplying the unregulated bus from the solar arrays. The second converter fed from the unregulated bus is stabilizing the voltage for the 5 V bus.

The first converter is controlled in order to achieve the maximum power point from the solar cells and to charge the batteries. Each battery string is using a protection circuit, which is disconnecting the battery string in case of overcharging, over discharging and over current.

The regulated 5V bus is supplied from a step-down converter fed by the unregulated bus. From the 5V bus each user is supplied using separate wires, but with common ground. Common ground is chosen because every user, which is connected to I^2C bus must use the same ground wire.

Protection circuits are provided for every load. The main function is to limit the output current to a safe level and to give a flag to the micro-controller unit (MCU), indicating an overcurrent. It can also be driven externally to connect or disconnect the user. The current is measured as housekeeping data for each user.

The protection for MCU is different than that for regular users. It is used a self-protected 5V voltage regulator with internal limiting and thermal shutdown features.

The MCU is used for gathering and computing the housekeeping data, taking decisions for connecting/disconnecting users in case of failure and communication with OBC.

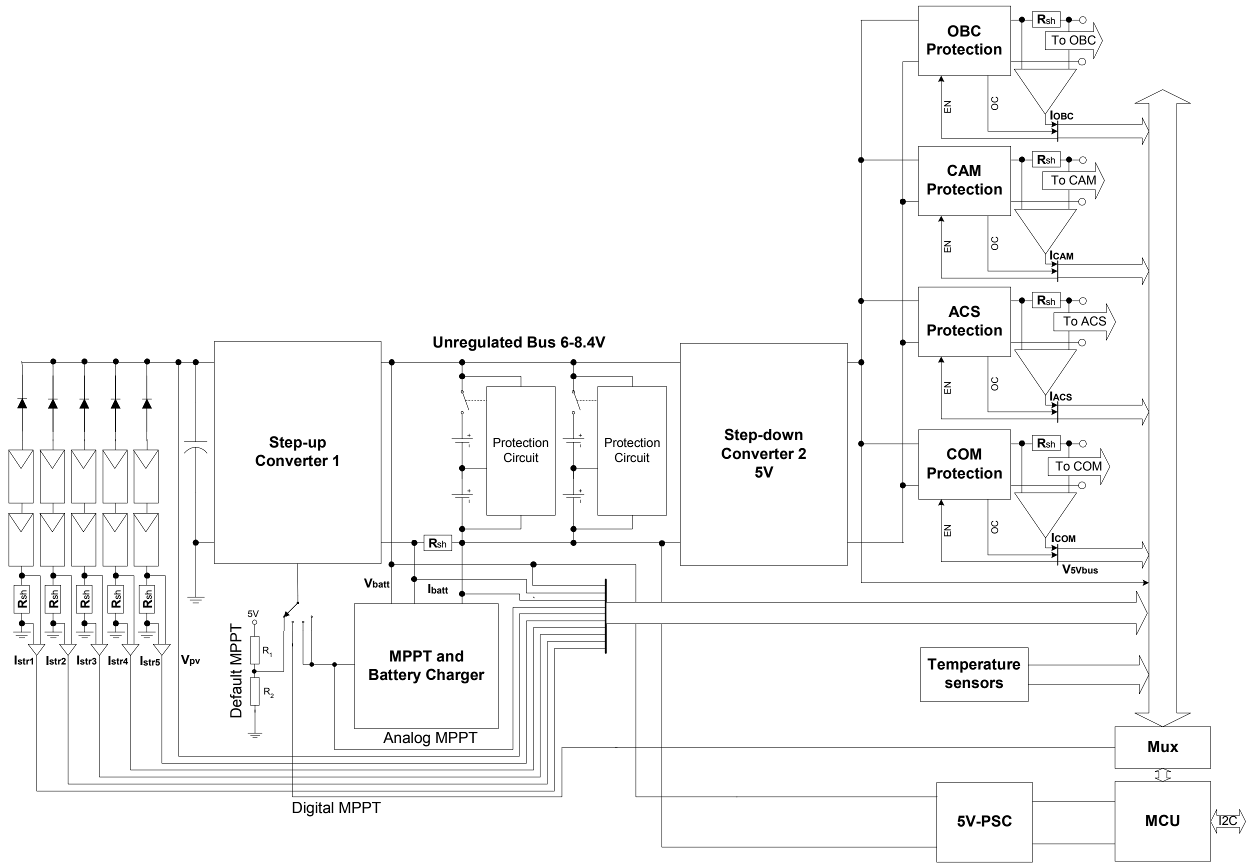

Figure 3.4 Proposed power supply layout using 2 converters and an unregulated bus

Taking into account all the advantages and disadvantages, for the presented configurations, it has been decided to use the last configuration, depicted in figure 3.4.

3.3. Power sources analysis

The Power Supply Unit (PSU) can be divided in three modules, as described in section 1.3: Photovoltaic module (PV), Battery unit (BAT) and Power Conditioning Unit (PCU). In this section, the first two modules will be analyzed, the third will follow in the next section. The reason of splitting the analysis in this way resides from the function fulfilled by each of the modules: PV and BAT are sources of energy while PCU main function is to provide loads with current from the common bus.

3.3.1. Photovoltaic considerations

Solar cells are composed of various semiconductor materials. Semiconductors are materials, which become electrically conductive when they are supplied with light or heat, but which operate as insulators at low temperatures. There are two effects that might provide the conversion of energy from sun into electric energy [*Fitzgerald, 2001*].

If a photon is incident upon a semiconductor then, if the photon energy is higher than the band-gap energy, the photon may be absorbed and an electron elevated from the valence band to the conduction band. This creates an electron-hole (e-h) pair; mobile charge carriers produced in this manner are called *photo-carrier*s. In a homogeneous semiconductor, the electron and hole will wander about (due to their thermal motion) and eventually recombine, either with each other or with other electrons and holes executing similar motion. When carriers recombine they annihilate each other and emit a photon corresponding to the band-gap energy. Under certain conditions the charge carriers may be collected before the combine to form a *photocurren*t. Depending on the material, band-gap energies range from several eV to a few tens of eV to. This process is called *photovoltaic effect.*

In the *photoelectric effect*, a photon strikes a metal and ejects an electron. No electrons will be ejected unless the photon energy, hf, exceeds the work function of the metal. (h is Planck's constant and f is the photon frequency). Unfortunately, work functions are typically 5-10 eV while most of the Sun's energy is concentrated in photons having energy 1-2 eV. Thus, the photoelectric effect would not be able to extract energy from most the Sun's radiation, and hence, would be very inefficient at converting sunlight to electric energy.

Ideal characterization and basic parameters of solar cells

The simplified equivalent circuit of a solar cell consists of a diode and a current source that are connected in parallel, as shown in figure 3.5.

The current source generates the photocurrent I_{ph}, which is directly proportional to the solar irradiance S and also temperature T. The p-n transition area of the solar cell is equivalent to a diode that is also integrated in the figure 3.5. In shadow, a solar cell is just a diode.

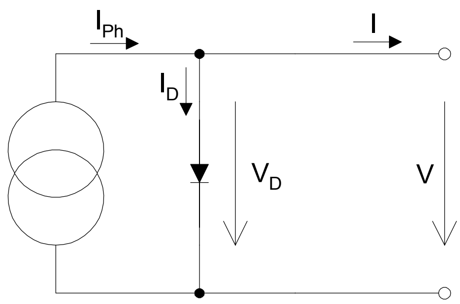

Figure 3.5 Simplified equivalent circuit of the solar cell.

The current-voltage characteristic of an ideal diode is given by the following formula:

$$I_D = I_{rs} \cdot (e^{\frac{q \cdot V_D}{A \cdot k \cdot T}} - 1) \tag{3.1}$$

where, I_{rs} is the reverse saturation current,

q = 1.6 x 10^{-19} [C] is the fundamental unit of charge,

k = 1.38 x 10^{-23} [J/K] is Boltzmann's constant,

A is diode quality factor (1÷5, 1 means ideal p-n junction),

V_D is voltage drop across the diode [V],

T is absolute temperature [K], 0°C = 273.15 K

The theoretical behavior under illumination is represented by

$$I = I_{Ph} - I_D \tag{3.2}$$

where I_{Ph} represents the photo current, I_D is diode current described above.

In figure 3.6a are illustrated I-V characteristics of ideal cell in two different positions [*Fitzgerald, 2001*]. The dark color curve shows an ideal solar cell that is shadowed. The light color curve in figure 3.6a shows the I-V characteristic of an ideal solar cell measured under 1000 W/m^2 illumination. For an ideal solar cell, the I-V characteristics are simply shifted down due to the light-generated current, I_{ph}. In case of shadowed cell can appear a situation of negative current through the solar cells. This is due to the behavior of the solar cell acting like a p-n junction in parallel with a current source. In order to avoid this inadvertent situation can be used a string diode which is connected in series with solar cell in negative polarization (figure 3.6b).

On the I-V curve are shown some points typical for solar cell. The *open circuit voltage* V_{OC}, the *short circuit current* I_{SC}, the *maximum power point voltage* V_{MPP}, the *maximum power point current* I_{MPP}. Then can be defined these parameters typical for solar cells.

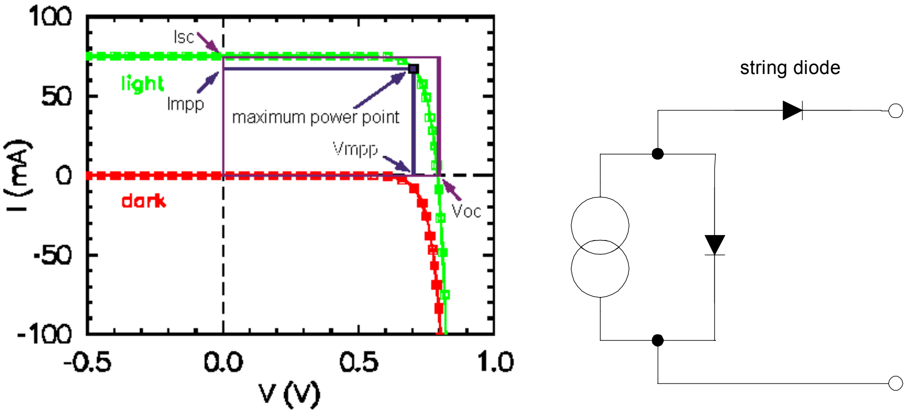

a b

Figure3.6 a) I-V curves for solar cell b) solar cell with string diode

The *fill factor* as a ratio of maximum power and product of short circuit current and open circuit voltage, is given by:

$$FF = \frac{V_{MPP} \cdot I_{MPP}}{V_{OC} \cdot I_{SC}} \tag{3.3}$$

The fill factor is always less than unity; the closer it is to unity the better the quality of the solar cell. One of the most important characteristic about a solar cell is its energy conversion efficiency, η:

$$\eta = \frac{Maximum\_electric\_power}{incident\_light\_power} \tag{3.4}$$

Real solar cell, influence of the temperature and incident light over I-V curve

In figure 3.7 is shown the equivalent circuit for real solar cell. In real solar cells a voltage loss on the way to the external contacts could be observed. This voltage loss could be expressed by a series resistor R_S. Furthermore leakage currents could be observed, which could be described by a parallel resistor R_P. For description of this circuit can be used relations mentioned above with proper modifying involving also influence of temperature.

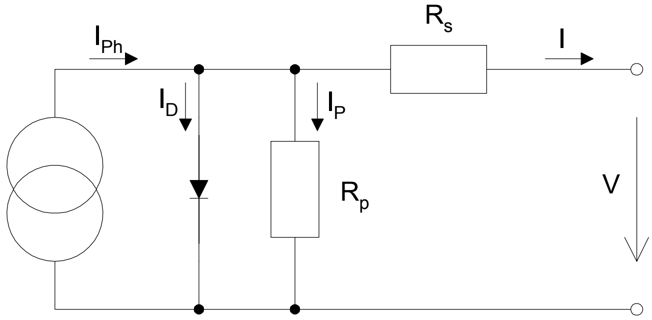

Figure 3.7 Circuit diagram for real solar cell

Equation (3.5) relates the I-V characteristics of a real diode to a number of device parameters [*Hussein et.al., 1995*]:

$$
\begin{aligned}
I &= I_{Ph} - I_D - I_P = (I_{SC} + k_i \cdot (T - T_{ref})) \cdot \frac{S}{100} - \\
&- I_{RR} \cdot \left(\frac{T}{T_{ref}}\right)^3 \cdot e^{\frac{q \cdot E_G}{A \cdot k} \cdot \left(\frac{1}{T_{ref}} - \frac{1}{T}\right)} \cdot \left(e^{\frac{q \cdot (V + I \cdot R_S)}{A \cdot k \cdot T}} - 1\right) - \\
&- \frac{V + I \cdot R_S}{R_P}
\end{aligned}
\tag{3.5}
$$

Where, I_{SC} is short circuit current [A],

k_i is short circuit current temperature coefficient,

T is cell temperature [K],

T_{ref} is cell reference temperature [K],

S is solar radiation [mW/cm^2],

I_{RR} is reverse saturation current at T_{ref} [A],

q is the charge of an electron, equal with 1.6 x 10^{-19} [eV],

E_G is the band-gap energy of the semiconductor used in the cell [eV],

k is Boltzmann's constant, equal with 1.38 x 10^{-23} [J/K],

A idealizing factor (1÷5, 1 means ideal p-n junction),

R_S is series resistance of the cell [Ω],

R_P is shunt resistance of the cell [Ω].

Most of the parameters of the solar cell show a temperature dependency. The general equation to calculate the temperature coefficient *TC* for a value *y* is:

$$TC(y) = \frac{1}{y} \cdot \frac{\partial y}{\partial T} \tag{3.6}$$

In case of linear connection between *y* and temperature, then the equation (3.6) can be rewritten:

$$TC(y) = \frac{1}{y(T_0)} \cdot \frac{y(T_1) - y(T_0)}{T_1 - T_0} \tag{3.7}$$

The short circuit current is increasing a little at rising temperatures, while the open circuit voltage is lower (-0.4 [%/K]) [http://www.emsolar.ee.tu-berlin.de/lehre/english/pv1]. Therefore the power output is decreasing for increasing temperatures. The power loss is around 0.3-0.5 % per degree Celsius, so for an increase of 30°C in temperature the power is decreasing by 9-15 % as depicted in figure 3.8 [*Masoum et. al.*].

After absorption of the incoming radiation in the solar cell a portion of it is converted into electricity and diverted. The remaining heat flow gets from the cell through the encapsulation to the surface of the module (steady state heat flow) or increases the temperature of the module (non-steady state heat flow).

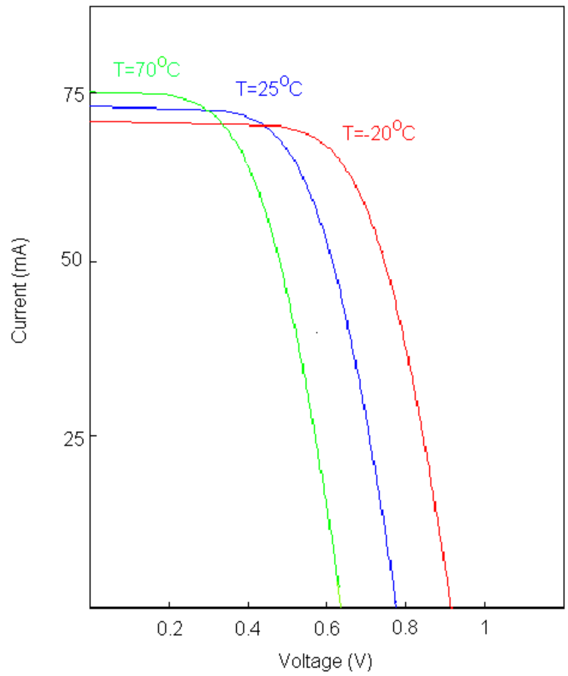

Figure 3.8 I-V curves dependent on temperature

The power that is obtained from solar cell is depended on the angle of incident light. In figure 3.9 is described a situation with changing angle φ [*Hishikawa et al., 2000, p.1465*].

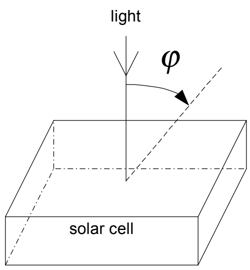

a

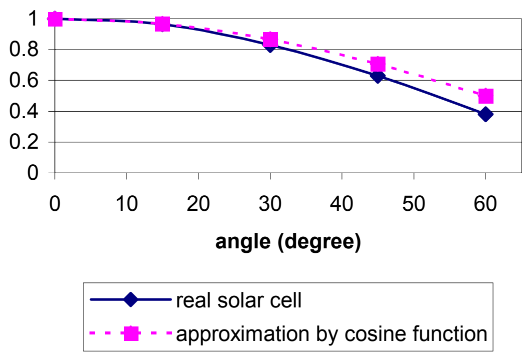

b

Figure 3.9 a) changing of the angle of incident light b) dependency of power from solar cell on angle of incident light

For description of this situation cannot be used any exact mathematic function. The best and also the most accuracy function used for this is cosine function. In figure 3.9b is shown per unit values of power from cell dependent on incident light for both real cell and cosine approximation. Approximation is accurate until approximately 15-degree angle.

Physical realization of solar cells

In these days can be found a lot of different structure of solar cells on markets. In order to choose proper cell for certain application must be compare behaviors together with prices. Nowadays there are three possible ways of internal structure: single, double and triple junction. More junctions indicate better efficiency due to cover wider spectrum of incident light. That, on the other hand, also implicates higher prices for those junctions.

The most efficient single junction space solar cell was fabricated from Galium-Arsenide (GaAs) substrate, which has a band-gap close to the theoretical ideal spectrum. It occurs also single junction fabricated from Germanium (Ge) substrate. Then on this substrate is applied a junction from GaAs. This junction can cover wavelength at intervals approximately 700-900 nm. It means that in this interval has the single junction the best quantum efficiency.

In order to cover also another wavelength is possible to add more junctions. The most often used material for this junction is Indium-Galium-Phosphorus (InGaP). In this case is possible to obtain energy from 300-650 nm interval of wavelength. If it is added directly on the substrate Ge junction, which forms third junction, the energy from 900-1600 nm could be also taken into account (figure 3.10).

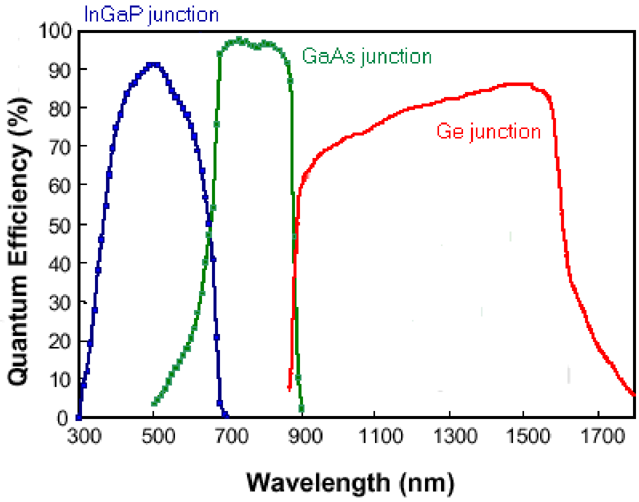

Figure 3.10 Different wavelength covered by typical triple junction solar cell
[www.emcore.com]

Connection of solar cells

There are two typical ways to connect solar cells to one module. Both of them have some advantages and also disadvantages.

In figure 3.11, series (a) and parallel (b) connection of the solar cells, into one module, are presented.

For the serial connection case, on the output from this connection can be obtain voltage which is sum of both cells and the current same for both cells. This is usually used in order to yield sufficient DC voltage for realizing higher conversion efficiency of converters.

For the parallel connection case, on the output from this connection can be obtain current which is sum of both cells and the voltage same for both cells.

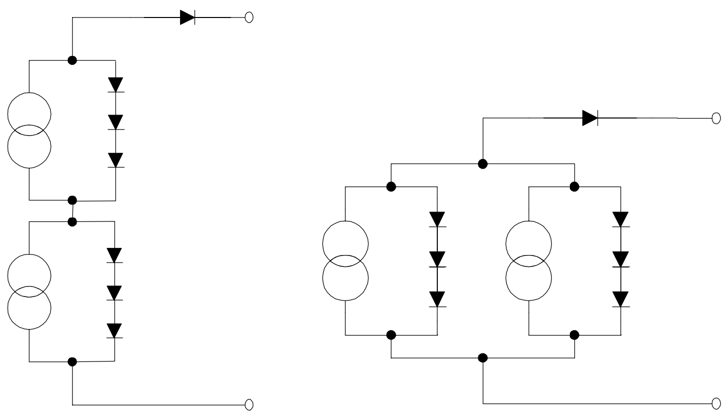

a b

Figure 3.11 Serial (a) and parallel (b) connection of two solar cells with string diode

The difference between the two connections resides in the shape of the output current and voltage.

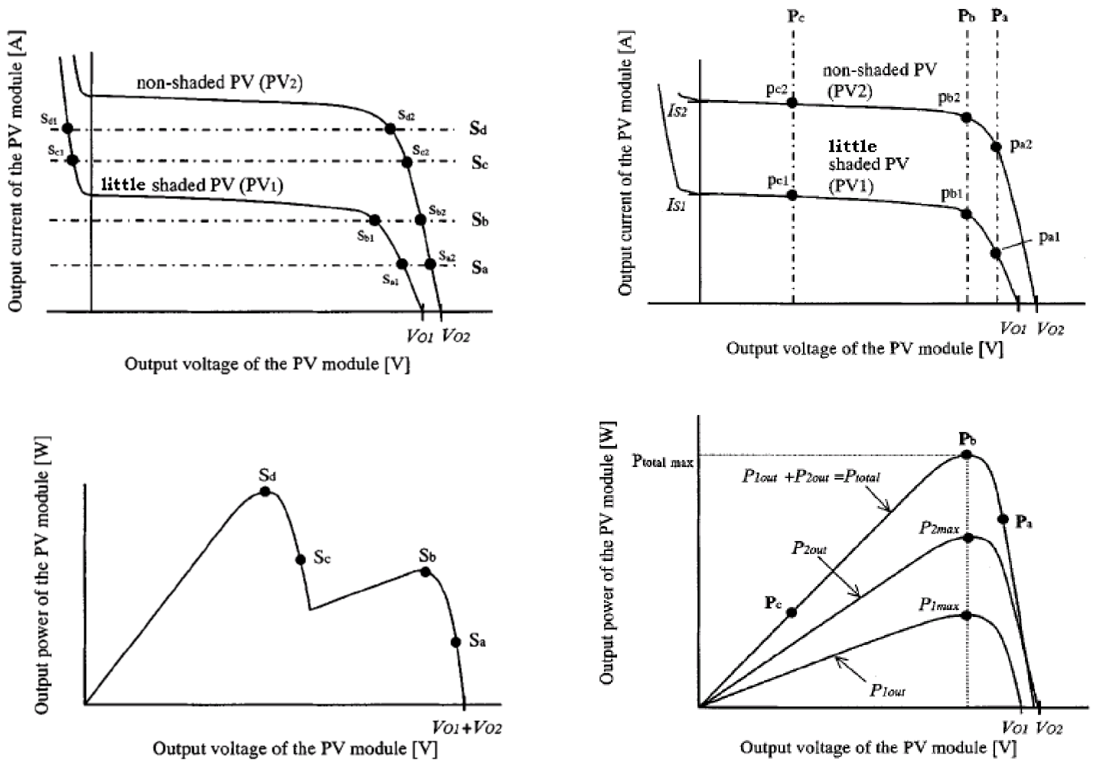

a b

Figure 3.12 Characteristics for two cells connected in series (a) and parallel (b)

For the serial connection, operation point for each cell is given by intersection of lines that are parallel to the x-axis (shown in figure 3.12a, up). When the output current is increased from zero to maximum current, the operation point is moving progressively from S_a>S_b>S_c>S_d. In the last two points, for instant, the little shaded solar cell has the negative voltage and it causes power loss. That is the reason for such a shape of power curve, shown on the figure 3.12a, bottom.

For parallel connection, the operation point for each cell is given by intersection of lines which are parallel to y-axis (shown in figure 3.12b, up). When the output current is increased from zero to maximum then the operation point is moving progressively from P_a>P_b>P_c. This points that not only the non shaded but also the little shaded cell can operate in area where can generate power. Then the final output power is sum of the power of each cell [*Shimizu, et. al, 2001*].

As it was mentioned before, for better behavior in supplying the satellite systems, is recommended to use cells in parallel connection. But for higher voltage is recommended to use serial connection. If the string diode is broken down then is conducting. In case of series connection is lost only one cell. In parallel connection appears a shortcut circuit and are lost all cells. For the current application it was decided to use on each side cells connected in series and then all sides connected in parallel as depicted in figure 3.13.

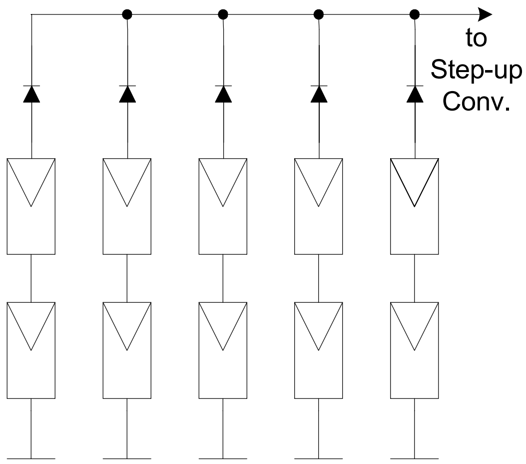

Figure 3.13 Final connection of solar cells

3.3.2. Input power calculation

Input power is influenced by a few factors. One of them is represented by type of energy source. As defined in chapter 2, section 2.3.1, there are three main sources of power in space. Due to the triple junction technology used in solar cells infrared radiation can be also taken into account. The input power, for one side of the satellite, considering only solar radiation, is:

$$P_{in1}^{*} = P_{sun} \cdot n \cdot A \cdot \eta \tag{3.8}$$

where, P_{sun} is the amount of energy radiated by Sun (Table 2.1), n represents the number of cells on one side, A is area of one cell and η represents the efficiency of solar cells. The efficiency, considered in calculations, is EOL (End Of Life) efficiency (25%).

The numerical value for the power is:

$$P_{in1}^{*} = 1353\left[\frac{\mathrm{W}}{\mathrm{m}^2}\right] \cdot 2 \cdot 0.00273\left[\mathrm{m}^2\right] \cdot 0.25 = 1.845\ [\mathrm{W}] \tag{3.9}$$

Losses caused by Schottky diode, at maximum power point, are:

$$P_{diode} = \langle I_{diode} \rangle \cdot \langle V_{diode} \rangle \quad , \quad P_{diode} = \frac{P_{in1}^{*}}{n_s \cdot V_{mpp}} \cdot V_{diode} \tag{3.10}$$

where V_{diode} is the voltage drop on a diode, V_{mpp} is the maximum power point voltage (which is a function of the incoming sunlight) and n_s is the number of serial solar cells in one string.

Replacing in equation (3.10) numerical values, the power dissipated in diode, for one side, is:

$$P_{diode1} = \frac{1.845\ [\mathrm{W}]}{2 \cdot 2.08\ [\mathrm{V}]} \cdot 0.3\ [\mathrm{V}] = 0.133\ [\mathrm{W}] \tag{3.11}$$

Then, the one side input power becomes:

$$P_{in1} = P_{in1}^{*} - P_{diode1} = 1.845 - 0.133 = 1.712\ [\mathrm{W}] \tag{3.12}$$

Furthermore, the power input is function of satellite position toward the sun, because illuminated area is changing after the way the satellite is spinning.

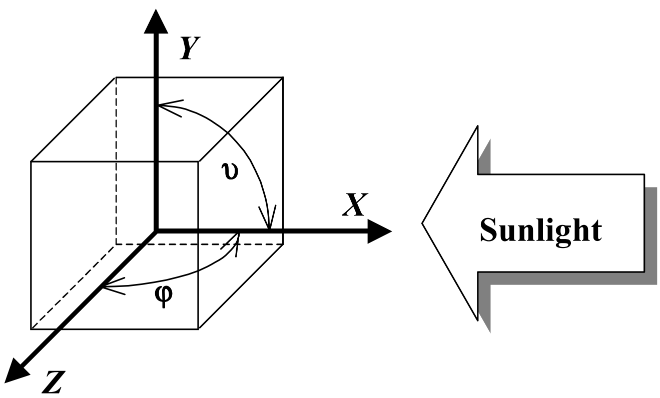

Figure 3.14 Definition of angles used for computation of input power

A function which will describe the illuminated area in dependency with angle have to be found. This function represents projection of side walls surface to plane normal to the Sun. For this simulation, Matlab software has been used and angles used in this program are shown in figure

3.14. Maximum three sides can be illuminated at a time. The area coefficients are defined for these three sides, as follows:

$$A_x = \cos(\varphi)\cdot\sin(\upsilon)\ ,\quad B_y = \sin(\varphi)\cdot\sin(\upsilon)\ ,\quad C_z = \cos(\upsilon) \tag{3.13}$$

This equations represent spherical coordinates.
[http://www.math.montana.edu/frankw/ccp/multiworld/multipleIVP/spherical/body.htm]
The total power available is the sum of powers for all sides:

$$P = (A_x + B_y + C_z)\cdot P_{in1} = (\cos(\varphi)\cdot\sin(\upsilon) + \sin(\varphi)\cdot\sin(\upsilon) + \cos(\upsilon))\cdot P_{in1} \tag{3.14}$$

The average power, calculated by a program in Matlab as an arithmetical average of all resulting values (Appendix A), is:

$$P_{av} = 2.48\ [\mathrm{W}] \tag{3.15}$$

But satellite has only five sides covered by solar cells, then the average power will be only 5/6, under the assumption that all sides are equally exposed to the Sun:

$$P_{av} = 2.48\cdot\frac{5}{6} = 2.07\ [\mathrm{W}] \tag{3.16}$$

Result of the input power as a function of the angles of incident light is plotted in figure 3.15.
Maximum value obtained from Matlab is:

$$P_{max} = \sqrt{3}\cdot P_{in1} = 2.965\ [\mathrm{W}] \tag{3.17}$$

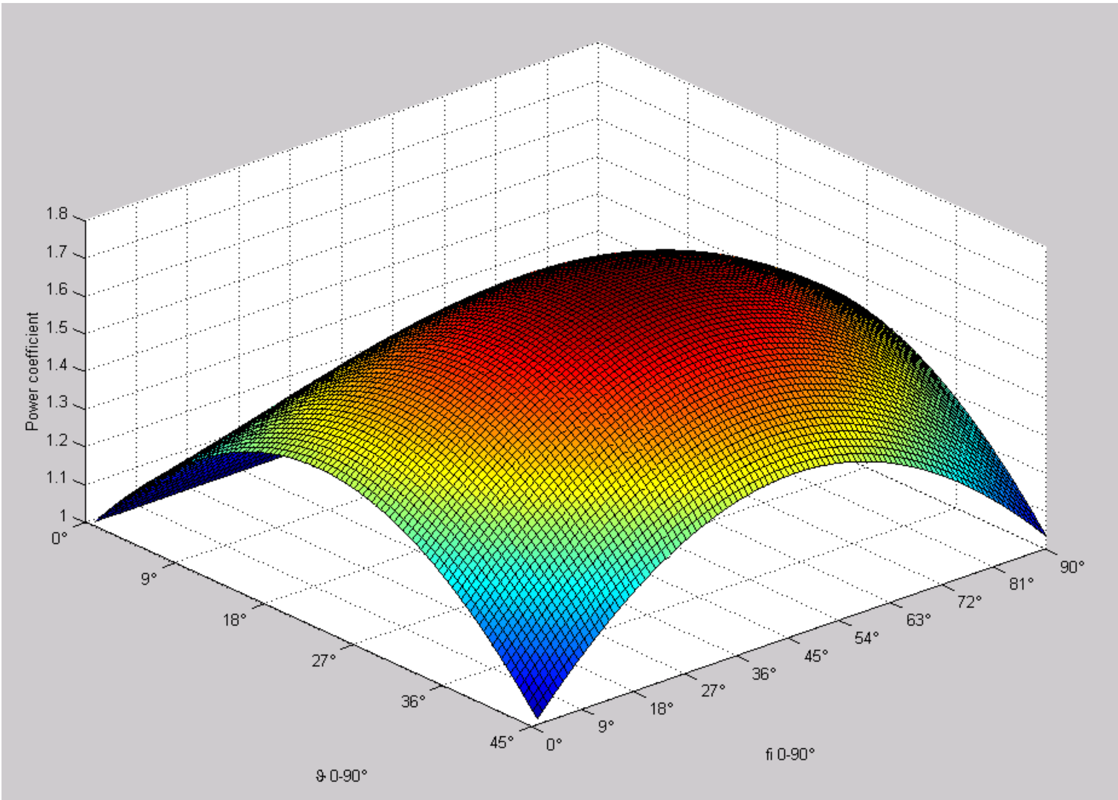

Figure 3.15 Input power as a function of incident light angles

And special case for two sides illuminated :

$$\mathrm{P}_{in2} = \sqrt{2} \cdot \mathrm{P}_{in1} = \sqrt{2} \cdot 1.712 = 2.42\ [\mathrm{W}] \tag{3.18}$$

In calculation of the input power, performed above, only the visible spectrum of the light, emitted by Sun has been considered. The Earth as a space object is source of energy and one of radiated components of this energy is in spectrum from 700 to 1000 nm. This energy is accepted by satellite during the whole orbit also in eclipse. That means that solar cells may convert this radiation into electrical power all the time. Some specific conditions must be fulfill for it. First, at least one of the sides with cells must point to the Earth and level of obtained current and voltage must be sufficient to drive switches (using of capacitor is necessary to accumulate power before MPPT). When the satellite is not in shadow there is no problem, energy from the Sun is summarized with infrared energy, so it adds a small amount of power in the system.

Input power from infrared radiation, for one side, is:

$$P_{IR}^{*} = P_{IR\_Earth} \cdot n \cdot A \cdot \eta \tag{3.19}$$

where, P_{IR_Earth} represents the amount of infrared energy radiated by the Earth (Table 2.1), n is the number of cells on one side, A is area of one cell and η represents the efficiency of solar cells. Like for equation (3.9), the efficiency is considered to be 25%.
Replacing numerical values in equation (3.19), yields:

$$P_{IR}^{*} = 237\left[\frac{\mathrm{W}}{\mathrm{m}^2}\right] \cdot 2 \cdot 0.00273\left[\mathrm{m}^2\right] \cdot 0.25 = 0.324\ [\mathrm{W}] \tag{3.20}$$

Analogical to the equation (3.17) maximum of this value, when three sides are illuminated, must be

$$P_{m\mathrm{IR}} = 0.324 \cdot \sqrt{3} = 0.560\ [\mathrm{W}] \tag{3.21}$$

If the albedo radiation is considered, the provided power is:

$$P_{ALB}^{*} = P_{ALB\_Earth} \cdot n \cdot A \cdot \eta \tag{3.22}$$

where, P_{ALB_Earth} represents the amount of albedo energy radiated by Earth (Table 2.1), n is the number of cells on one side, A is area of one cell and η represents the efficiency of solar cells (25%). Replacing in equation (3.22) corresponding numerical values, it yields:

$$P_{ALB}^{*} = 406\left[\frac{\mathrm{W}}{\mathrm{m}^2}\right] \cdot 2 \cdot 0.00273\left[\mathrm{m}^2\right] \cdot 0.25 = 0.554\ [\mathrm{W}] \tag{3.23}$$

and maximum value obtained from albedo is

$$P_{m\mathrm{ALB}} = \sqrt{3} \cdot 0.554 = 0.960\ [\mathrm{W}] \tag{3.24}$$

In calculation of infrared and albedo power, the specific levels of radiation can be found in chapter 2, table 2.1. If the values for infrared and albedo power are considered, this will give to the power subsystem a plus power of 0.878 [W] per one side.

3.3.3. Battery unit

According to the specifications batteries must be light and in minimum size. Two types of batteries are usually used in this kind of application: Lithium Ion (Li-Ion) and Nickel Cadmium (NiCd). Former satellites used NiCd batteries. The main advantage of these batteries is a longer lifetime, but in comparison to Li-Ion they are heavier and larger. Li-Ion offers a significant advantage of energy density and no memory effect. This was the main argument for choosing Li-Ion batteries. A comparison between usual types of batteries is shown in table 3.1.

Type	NiCd	NiMH	**Li-Ion**
Nominal voltage [V]	1.2 V	1.2 V	**3.7 V**
Density of energy [W·h/l]	140	180	**200**
Density of energy [W·h/kg]	39	57	**83**
Max. discharging current	20C	4C	**2C**
Self disc.[% per day]	1 %	1,5 %	**0,5 %**
Charging time (the fastest)	15 min	30 min	**1 h**
Thermal range for charging [°C]	0 to +50	0 to +45	**5 to+ 45**
Thermal range for discharging [°C]	-20 to +50	-20 to +50	**0 to +40**
Resistance against overcharging	Low	Low	**Middle**
Cathode material	NiOOH	NiOOH	**LiCoO2**
Anode material	Cd	alloy	**C**
Max number of cycles	1000	500	**400**

Table 3.1 Comparison of different types of batteries [http://www.mobil.cz/]

Theoretical background for Lithium Ion battery

A cell of a Li-Ion battery consists of a carbon-based negative electrode and a lithium transition metal oxide positive electrode. Upon charging, lithium ions are extracted from the positive electrode material and inserted into the negative electrode material. Upon discharging, the reverse process is taking place. Hence, the basic electrochemistry of the cell involves only the transfer of lithium ions between the two insertion electrodes. Due to the high cell voltage of up to 4V, the specific energy of this battery system is very favorable in comparison to the other known and commercialized secondary battery systems; however, an organic electrolyte solution must be used in the case of the lithium-ion battery.

Lithium-ion batteries are constructed by using a lithium oxide cathode and a carbon compound anode, with a high polymer separator and a non-aqueous electrolyte between the poles. Minute spaces are designed between the electrode materials to allow the lithium-ions to enter.

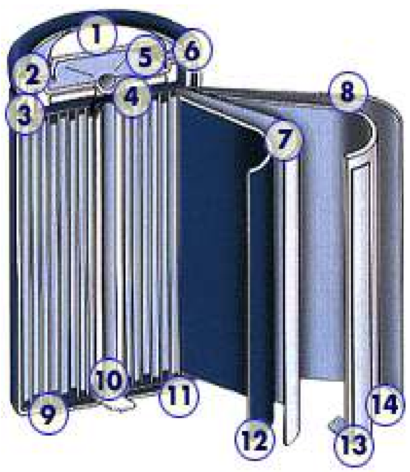

1.Cathode cover
2.Gasket
3.Insulator
4.Cathode lead
5.Safety vent
6.PTC
7.Separator
8.Separator
9. Insulator
10.Center pin
11.Anode container
12.Cathode
13.Anode lead
14.Anode

Figure 3.16 Section through a Li-Ion battery
[http://www.sony-media.com/en/technical/lithium-ion.html]

The way that a Li-Ion battery works is depicted in figure 3.17. Basically, as the battery is charged and discharged, the Lithium-ions shift back and forth between the cathode and anode.

DISCHARGING **CHARGING**

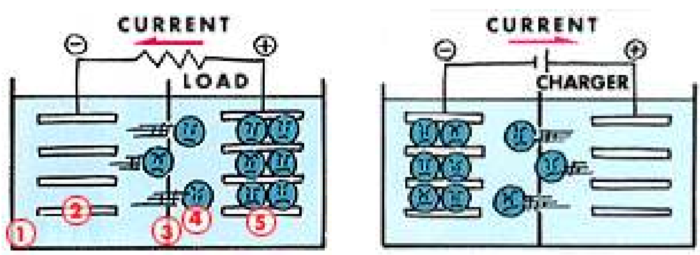

1.Electrolyte (organic solvent)
2.Cathode (lithium oxide)
3.Separator
4.Lithium ions
5.Anode (carbon compound)

Figure 3.17 Illustration of Li ions movement [http://ecl.web.psi.ch/lithium]

Power budget during one time period

The power budget will be computed taking in account the worst situation, when the satellite is in shadow for 35 minutes and transceiver is transmitting data for 15 minutes. Whole orbit lasts 100 minutes. In the table below are stated the consumers, the working time and the energy needed.

No.	Consumer	Power [W]	Time [s]	Energy [J]
1	OBC	0.46	6000	2760
2	Transmitter	9	900	8100
3	Camera	0.3 (while shooting)	10	3
4	Attitude Control	0.25	6000	1500
	Total	**-**	**-**	**12363**

Table 3.2 Power consumption for users, in the worst case

The energy is computed using the following formula:

$$E[\mathrm{J}] = P[\mathrm{W}] \cdot t[\mathrm{s}] \tag{3.25}$$

If it is considered a total efficiency for the converters η = 75%, the minimum available power will result:

$$E_{total} = \frac{E}{\eta} = \frac{12363\,[\mathrm{J}]}{0.75} = 16484\,[\mathrm{J}] \tag{3.26}$$

The Sun will provide energy for 65 minutes and the average input power will be around 2.07W (without albedo and infrared). So, the power obtained from solar cells is equal with:

$$E_{sun} = P_{av} \cdot t_{sun} = 2.07[\mathrm{W}] \cdot 65 \cdot 60[\mathrm{s}] = 8073\,[\mathrm{J}] \tag{3.27}$$

In this case the energy needed from the batteries is:

$$E^{n}_{batt} = E_{total} - E_{sun} = 16484[\mathrm{J}] - 8073[\mathrm{J}] = 8411\,[\mathrm{J}] \tag{3.28}$$

One battery fully charged can provide an energy of:

$$E_{batt} = \left(\frac{(U_{\max} + U_{\min})[\mathrm{V}] \cdot C[\mathrm{Ah}]}{2}\right) \cdot 3600[\mathrm{s}] = \left(\frac{(4.2+3)[\mathrm{V}] \cdot 0.92[\mathrm{Ah}]}{2}\right) \cdot 3600[\mathrm{s}] = 11923\,[\mathrm{J}] \tag{3.29}$$

where, U_{max} and U_{min} represents the limits of the voltage range for a Li-Ion battery and C is the capacity of the battery. Data for the batteries can be found in Chapter 2, section 2.3.2.
This yields to a needed number of batteries of:

$$n = ceil\left(\frac{E^{n}_{batt}}{E_{batt}}\right) = ceil\left(\frac{8411}{11923}\right) = ceil(0.705) = 1 \tag{3.30}$$

It can be seen from this results that one battery is giving enough power for one whole orbit if the solar panels are also used. But for avoiding to drain the batteries and also have a backup in case of failure will be used four of them.

If the batteries are particular discharged, to recharge them, the same amount of power must be obtained from the solar panels. If every load except OBC and ATC is off, the power consumption is:

$$E_{OBC} + E_{ATC} = 2760[\mathrm{J}] + 1500[\mathrm{J}] = 4260\,[\mathrm{J}] \tag{3.31}$$

This means that in each orbit the amount of energy:

$$E_{charge} = E_{sun} - E_{OBC} = 8073 - 4260 = 3813\,[\mathrm{J}] \tag{3.32}$$

is available to recharge batteries. Taking in account that there are four batteries, the energy requested for recharging from the solar panels is:

$$E^{r}_{charge} = \frac{n_{batt} \cdot E_{batt}}{\eta_t} = \frac{4 \cdot 9072[\mathrm{J}]}{0.8} = 45360\ [\mathrm{J}] \tag{3.33}$$

where η_t is the total efficiency of the MPPT converter series with the battery charger.

The time necessary for recharging the batteries, considering that every load is cut off after taking a picture and transmitting, will be:

$$t_{ch} = \frac{E^{r}_{batt}}{E_{charge}} \cdot 100 = \frac{8411[\mathrm{J}]}{3813[\mathrm{J}]} \cdot 100[\mathrm{min}] = 220.59\ [\mathrm{min}] \tag{3.34}$$

From this results can be seen, that if the OBC uses 0.46W it will take more than 2 orbits to recharge batteries back to initial state. The more OBC uses the idle mode with 5mW power consumption, the less time is needed to recharge them. Than the conclusion is that it is possible to take and send one picture daily, because we can transmit 4 times per a day. This is exactly what we need for sending one picture per a day.

Connection of batteries

There are three possibilities how to connect batteries: series, parallel or combination of both. If they are connected in parallel (figure 3.18), the voltage will be the same, but the current capability will be four times higher.

$$C_{parallel} = n \cdot C_{batt} = 4 \cdot 0.92\ [\mathrm{Ah}] = 3.68\ [\mathrm{Ah}] \tag{3.35}$$

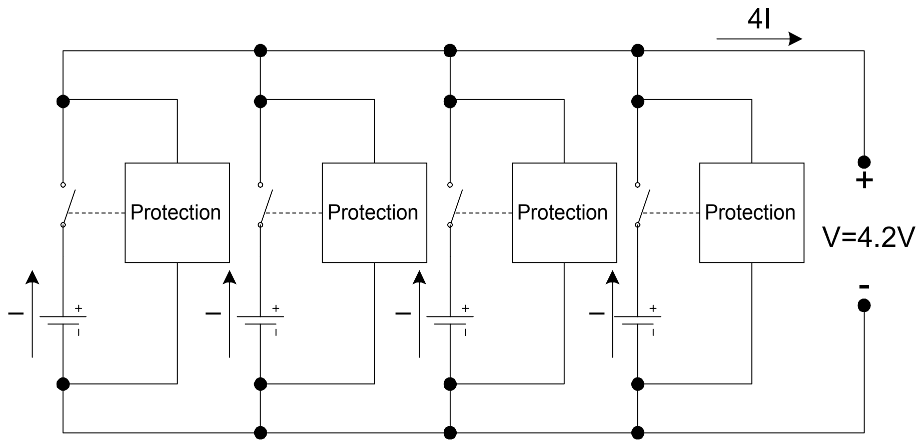

Figure 3.18 Parallel connection of the batteries

The reliability of parallel system is good, because when protection circuit will disconnect one battery, the other three can be still used. The only disadvantage of this configuration is the low voltage level.

If the batteries are connected in series (figure 3.19) the voltage level will be four times higher and the current will be the same.

$$V_{serial} = n \cdot V_{batt} = 4 \cdot 4.2[\mathrm{V}] = 16.8\,[\mathrm{V}] \tag{3.36}$$

Reliability of this system is lower because if the protection circuit is disconnecting one battery, the whole string might be lost.

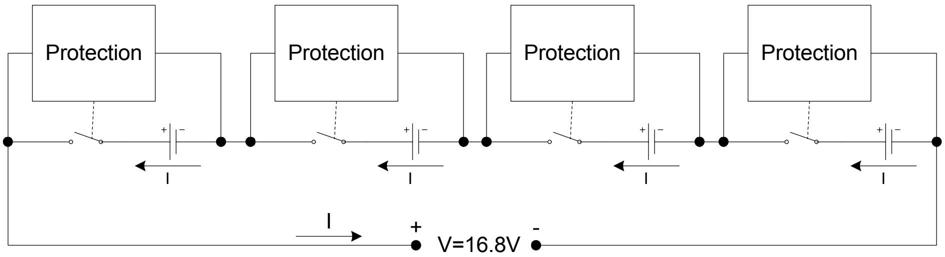

Figure 3.19 Serial connection of batteries

Last possibility is to use combination serial and parallel. Current and voltage levels will be:

$$\begin{gathered} C_{parallel} = n \cdot C_{batt} = 2 \cdot 0.92\,[\mathrm{Ah}] = 1.84\,[\mathrm{Ah}] \\ V_{serial} = n \cdot V_{batt} = 2 \cdot 4.2[\mathrm{V}] = 8.4\,[\mathrm{V}] \end{gathered} \tag{3.37}$$

Realization can be seen on a picture below:

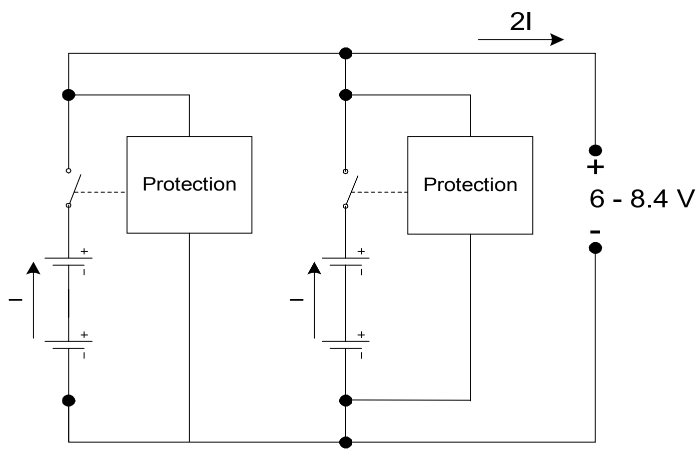

Figure 3.20 Serial and parallel connection of batteries

The last connection was chosen as the most suitable, despite the disadvantages of serial connection. Instead of this, the voltage level is higher and a step down with high efficiency converter may be used.

Position of batteries

Because of the temperature dependence, position of batteries is very important. All the batteries should have the same temperature for having the same operation parameters. Otherwise, can appear disequilibria between batteries and this situation is unwanted. It has been taken in consideration a thermal shield for them, in idea of a thermal stabilization and connection between batteries. Batteries are the largest component of the system and can be arranged in one pack of four or in two packs of two, function of available space in the cube and the thermal conditions.

For a better control of the satellite attitude, the center of mass must be placed as possible as in the middle of the satellite. Because of the large volume of the batteries and the thermal considerations, these should be placed as much inside the satellite as possible.

3.4. Power conditioning module analysis

3.4.1. Maximum power point tracker

Maximum power point tracker is an electronic device, which optimizes the point of operation of the solar cells in order to achieve maximum power delivered from the solar cells.

The output of a PV module is characterized by a performance curve of voltage versus current, (figure 3.21). The maximum power point of a PV module is the point along the I-V curve that corresponds to the maximum output power possible for the module. Maximum power point tracking enables PV arrays, to operate at its maximum power point.

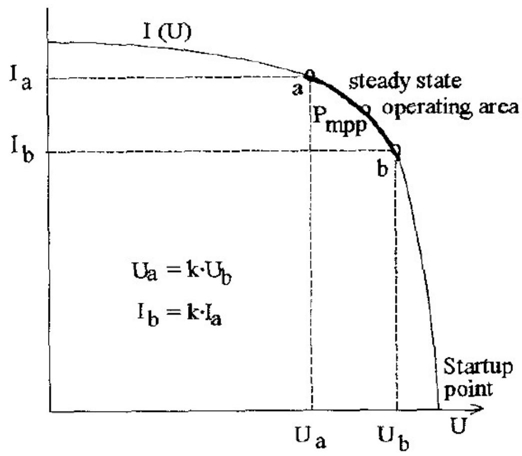

Figure 3.21 I-V isolation solar panel characteristic

There are several factors that will influence the amount of power gain one can expect; these factors are cell temperature, conversion losses, amount of available sunlight, cell structure and blocking diodes.

Some power is lost in the conversion from the voltage at the maximum power point to battery voltage. The efficiency of most maximum power point tracking units is usually around 93%. For crystalline modules, voltage will drop about 2.4mV/°C per cell. This yields a voltage drop of 1.73V, and shifts the I-V thus lowering the maximum power point closer to the battery voltage. As sunlight diminishes from the standard test condition of 1000W/m^2, the voltage corresponding to the maximum power point drops slightly, but the main component in the decrease of available power is the decrease in available current. In the case of amorphous silicon modules, the I-V curve will change current more dramatically as the voltage changes throughout the battery voltage and maximum power point ranges. This will translate into less gain seen by using the maximum power point tracker. Battery voltage will also play a major role in the amount of increased watt-hours one can expect from a module or array using a maximum power point tracker.

In practice are a lot of possibilities to implement a MPPT. An analog implementation of the MPPT (Maximum Power Point Tracker), which is to be used is stated in figure 3.22 [*Snyman, p.1243, 1993*].

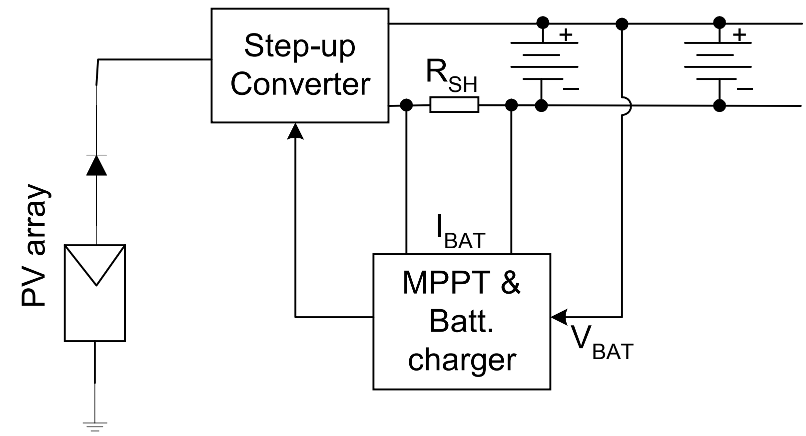

Figure 3.22 Analog implementation for MPPT

It is a feed-forward control, which combines a programmable current limit with a battery voltage limit to provide a constant current for charging the batteries. Only the output current is used as a feed-forward control parameter. The voltage regulation loop is converted into an overvoltage protection loop. This overvoltage protection loop becomes active only when the output voltage rises above a predetermined limit. Positive feedback of a signal proportional to the output current of the converter is therefore used as the input control signal to the current regulator (integrated in MPPT & Batt. charger, in figure), to perform maximum power point tracking. When the overvoltage loop is active, no maximum power point tracking can be performed.

The fundamentals of the maximum power point tracker are:

- When the time constant of changes in the output voltage of the converter is small compared to the switching period of the switching element, it is only necessary to maximize the output current of the converter in order to track the maximum power point of the PV array.
- Maximization of the output current by means of feeding the output current back in a positive way, is obtained since the I-V characteristics of the PV array are responsible for negative feedback when the output current tends to exceed the optimum current for the maximum power delivered by the PV array.
- Voltage feedback from the load is only necessary to protect the load against overvoltage

3.4.2. Converters used in power supply

For this given application is needed to be made only DC to DC conversion of energy. For this reason the types of converters to be used are: step-down (buck), step-up (boost) and step-down/step-up (buck-boost). For all the converters presented below is presumed that are working in continuous-conduction mode [*Mohan, p. 164, 1995*].

Step-down (buck) converter

As the name implies, a step down converter produces a lower average output voltage than the input voltage V_d. In the figure 3.23 can be seen a principle scheme for a buck converter.

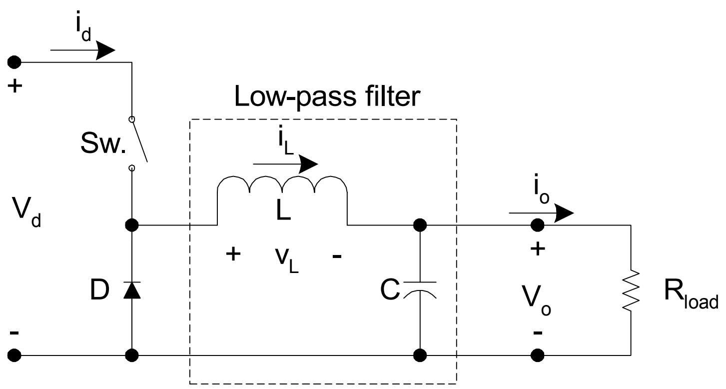

Figure 3.23 Step-down DC-DC converter

By varying the duty ratio t_{on}/T_s of the switch, V_0 the output voltage can be controlled (where t_{on} is conduction period for the switch and T_s is switching period). The voltage on the diode is fluctuating between 0 and V_d, but this is not acceptable in most of the applications. For this reason a low-pass filter is necessary.

During the interval when the switch is on (figure 3.24a), the diode becomes reverse polarized and the input energy is going to the load and in the same time is stored in the inductor. When the switch is turned off (figure 3.24b), the energy stored in the inductor will flow to the load through the diode.

The following equations imply that the areas A and B from the figure 3.24 must be equal. Therefore,

$$(V_d - V_o) \cdot t_{on} = V_o \cdot (T_s - t_{on}) \tag{3.38}$$

or,

$$\frac{V_o}{V_d} = \frac{t_{on}}{T_s} = D \tag{3.39}$$

This means that the output voltage varies linearly with the duty ratio for the switch for a given output voltage.

Neglecting the power loses caused by the circuit elements, the input power P_d equals with the output power P_o.

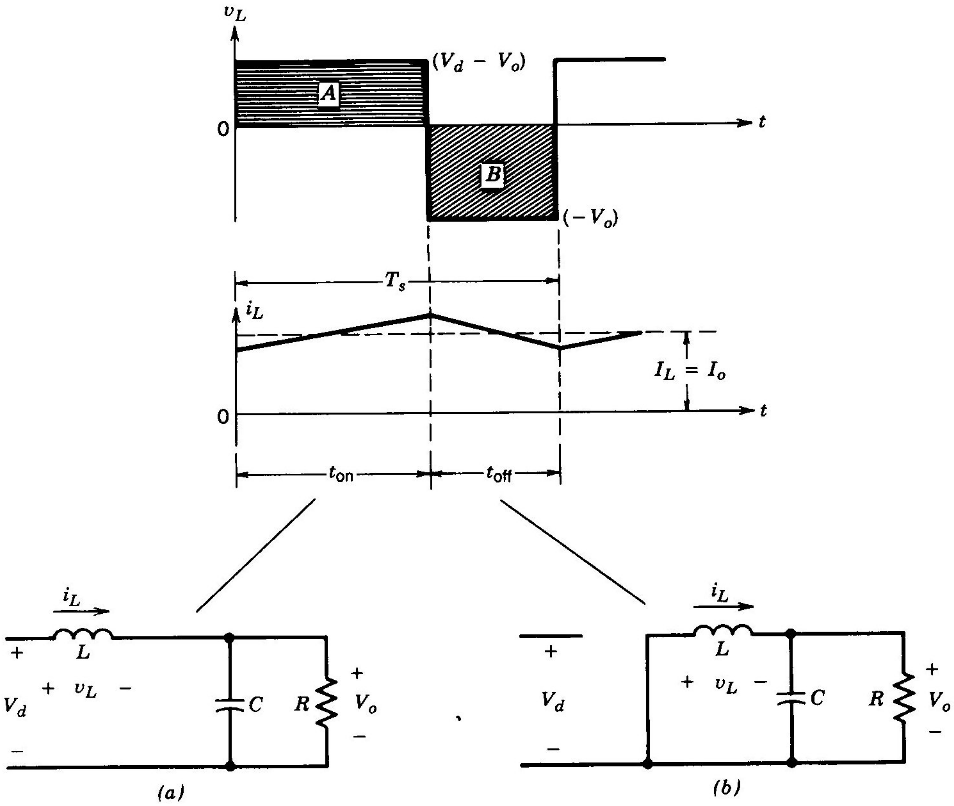

Figure 3.24 Step-down converter equivalent circuits when switch is turned on (a) or off (b).

It yields,

$$V_d \cdot I_d = V_o \cdot I_o \tag{3.40}$$

and

$$\frac{I_o}{I_d} = \frac{V_d}{V_o} = \frac{1}{D} \tag{3.41}$$

Therefore, in the continuous-conduction mode, the step-down converter is equivalent to a dc transformer where the turn's ratio of this equivalent transformer can be continuously controlled in a range from 0 to 1 controlling the duty ratio of the switch.

Step-up (boost) converter

As the name implies, the step-up converter produces a voltage higher than the input voltage V_d. In the figure 3.25 can be seen a principle scheme for a boost converter.

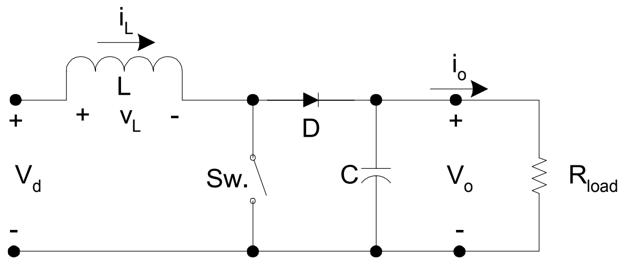

Figure 3.25 Step-down DC-DC converter

When the switch is on, the diode is reverse polarized isolating the output stage and the energy is stored in the inductor. When the switch is turned off, the load is receiving energy from the inductor as well as from the input.

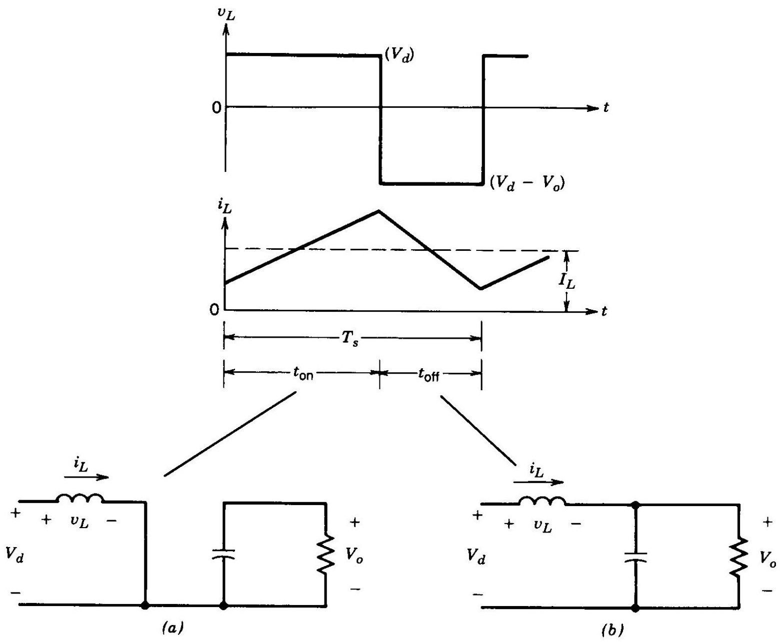

Figure 3.26 Step-up converter equivalent circuits when switch is turned on (a) or off (b).

Since in steady state the time integral of the inductor voltage over one time period must be zero,

$$V_d \cdot t_{on} + \left(V_d - V_o\right) \cdot t_{off} = 0 \tag{3.42}$$

Dividing both sides of equation (3.42) by T_s, and rearranging terms yields:

$$\frac{V_o}{V_d} = \frac{T_s}{t_{off}} = \frac{1}{1-D} \tag{3.43}$$

Assuming a lossless circuit, the input power P_d must be equal to the output power P_o:

$$V_d \cdot I_d = V_o \cdot I_o \tag{3.44}$$

Using formula (3.43), equation (3.44) yields:

$$\frac{I_o}{I_d} = \frac{V_d}{V_o} = 1 - D \tag{3.45}$$

3.4.3. Power supply interfaces

Power Bus

This bus should be used for transferring the electrical energy from the power subsystem to the users. Because PSU must also provide protection for each load, there are two possibilities in designing them:

- Protections can be mounted to each user's board and then there will be only two wires for supplying power to the users, but PSU must drive these protections with some logical/analog signals and it means high data traffic between the PSU and the users.
- All protections are put together to the PSU board. The advantage of this solution is that each user has its own power bus wire and it is more reliable to concentrate all the protections in one place, because connectivity problems between the protection circuits and MCU will disappear.

As a conclusion, it is more reliable to put all this protection circuits to one place where PSU system assure on/off on demand from OBC and/or also assure to turn off load in case of short circuit or overcurrent. It implies needs for independent wire for each user in the satellite. If short circuit occur there will be a higher voltage drop on the bus and that is why it is a better solution not to use common ground wire, but independent ground to each user. But because every user connected to I^2C bus must use the same ground wire, in that case, even though it is a worse solution it has to be used common ground.

Finally, the power bus will consists of four wires with 5V voltage and a common ground for all users.

Data Bus

I^2C bus used for data communication in the satellite is bi-directional 2-wire bus. Data flowing through this bus can be divided to two main categories.

From the first category, there is data to/from protection circuit, consisting in four flags describing safety status of each user (it means that user can be only turned on or off):

- status of the OBC
- status of the ACS
- status of the camera circuits
- status of the communication circuit

If the OBC send a flag to the PSU, PSU must react as fast as possible and turn on/off appropriate user. Other situation is if the protection circuit turns off the user, because of failure, a flag should be set and send to the OBC and it will decide what's going next. If the OBC is the user who has been turned off, this flag should be send to the OBC after a timer turn on power again only to tell the OBC that something went wrong.

Second category of data are housekeeping signals, this data might be used in other parts of the satellite like ACS, but their main task is to provide information to the OBC and help it to realize what is going on in the PSU. Also from the OBC this housekeeping data might be send to the ground station. From these conditions result high need for proper selected sensors, because after something wrong happen, the only way how to debug the system from the ground is from housekeeping data. The best solution is to measure all currents and voltages around the PSU, last but not least are thermal sensors, which must stick on the most dissipating parts of the satellite.

Each user can put at least one sensor to its system. All these signals will be presented as 12-bits numbers, except temperatures, which will be 8-bit in binary-complement format.

- currents from each solar panel (5 sensors)
- voltage on the solar panels (1 sensor)
- current flows from the MPPT (1 sensor)
- voltage on the batteries (1 sensor)
- voltage on 5V regulated bus (1 sensor)
- current flowing to each user (4 sensors)
- thermal sensors on most dissipative points in the satellite inc. PSU (7 sensors)

A summary of all the signals and sensors is depicted in figure 3.27.

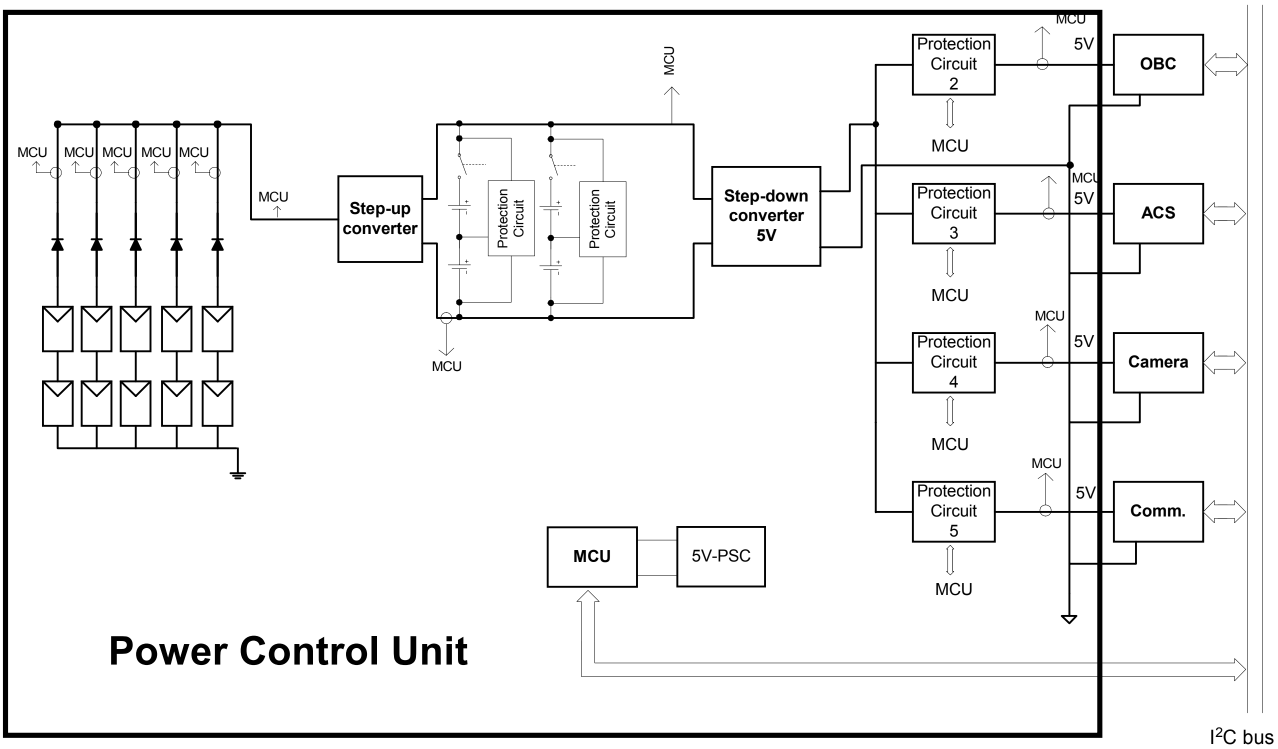

Figure 3.27 Power supply unit interfaces and sensors

3.5. Summary

This chapter presents the implementation solution of the power supply.

A few possible layouts are shown and the most reliable one is chosen. The final scheme of the power supply is presented in figure 3.4 and the way that different parts are interconnected and are working is explained. It is necessary a more accurate analysis for some of modules. This is to be used, further, in analysis of MPPT and power sources.

In section 3.3, the input power from the solar arrays is computed.

- Average input power, per one side: $P_{av} = 2.07$ [W]
- Albedo radiation power, for one side: $P^{*}_{ALB} = 0.554$ [W]
- Infrared radiation power, for one side: $P^{*}_{IR} = 0.324$ [W]

It is shown that the most favorable situation, in respect with the power, which can be delivered to users, is when three sides of the satellite are illuminated by Sun. Also, from characteristic of the solar cells, it is deducted that a certain amount of power can be delivered considering the infrared and albedo energy radiated by Earth. This quantity is calculated and it has been proposed as a mission statement to verify it through housekeeping data that will be send back to Earth. The power sources, photovoltaic module and rechargeable batteries, respectively, are inspected. A theoretical background about photovoltaic and batteries is presented, as well as an overview of different possibilities of implementation, existent on the market. Concerning the application and the specifications for the system, batteries are chosen to be Li-Ion type. Converters used in power supply are analyzed in section 3.4.2. It is not an exhaustive analysis, when appropriate components will be selected, a more accurate analysis will be perform.

The interfaces of the power supply (power interface and communication bus with OBC) are analyzed in section 3.4.3.

Chapter 4

Analysis and design of power subsystem

Abstract

In this chapter, a more detailed analysis of the system is made. All the circuitries are analyzed and computations are made. It is performed a analysis of the housekeeping data and the signals acquired for this. The hardware and the software used for Microcontroller Unit (MCU) are detailed.

4.1. Introduction

In this chapter, the design of the PSU is documented and detailed analysis is completed. In section 3.2, it was chosen the topology for PSU, as shown. In this respect, in the following, each part is detailed and physical implementation solution is presented.

The chapter is triturated after the most significant parts which consists the PSU. The circuits are presented as well as the devices. Then, for each part, if they require some specific computations, the formulas and results are presented. Finally, a conclusion is stated.

4.2. MPPT converter and battery charger

As described in Chapter 3, Section 3.4.1, the maximum power point tracker is an electronic device which optimizes the point of operation of the solar cells in order to achieve maximum power delivered by the solar cells.

The implementation solution implies a converter, to step-up the voltage from the solar cells, and which will provide the voltage to the unregulated bus. This converter is controlled by the positive feedback of the output current. Maximum power point tracking for such a PV system, with battery back-up is achieved by employing this simplified positive feedback control strategy to maximize the output current into the battery.

For all the devices, datasheet can be found on the attached CD of the project.

The step-up switching controller (MAX1771) provides 90% efficiency over a 30mA to 2A load. A unique current-limited pulse-frequency-modulation (PFM) control scheme gives this device the benefits of pulse-width-modulation (PWM) converters (high efficiency at heavy loads), while using less than 110µA of supply current (vs. 2÷10mA for PWM converters). This controller uses miniature external components. Its high switching frequency (up to 300kHz) allows surface-mount magnetics of 5 mm height and 9 mm diameter. It accepts input voltages from 2V to 16.5V. The output voltage is preset at 12V, or can be adjusted using two resistors. The MAX1771 optimizes efficiency at low input voltages and reduces noise by using a single 100mV current-limit threshold under all load conditions. The MAX1771 drives an external N-channel MOSFET switch, allowing it to power loads up to 24W. A functional diagram for the device can be seen in the figure below.

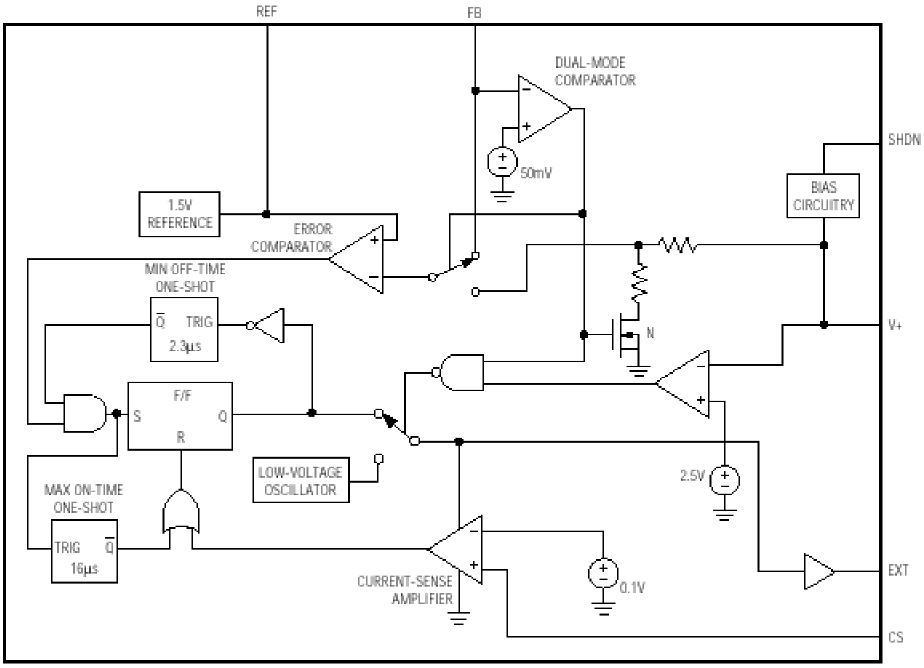

Fig. 4.1 Functional diagram for MAX1771 step-up converter

PIN	NAME	FUNCTION
1	EXT	Gate Drive for External N-Channel Power Transistor
2	V+	Power-Supply Input. Also acts as a voltage-sense point when in bootstrapped mode. Connected to ground for normal operation
3	FB	Feedback Input for Adjustable-Output Operation
4	SHDN	Active-High TTL/CMOS Logic-Level Shutdown Input. Connected to ground for normal operation
5	REF	1.5V Reference Output that can source 100mA for external loads. The reference is disabled in shutdown
6	AGND	Analog Ground
7	GND	High-Current Ground Return for the Output Driver
8	CS	Positive Input to the Current-Sense Amplifier

Table 4.1 Pin configuration for step-up converter

In bootstrapped mode, the IC is powered from the output (V_{OUT}, which is connected to $V+$) and the input voltage range is 2V to V_{OUT}. The voltage applied to the gate of the external power transistor is switched from V_{OUT} to ground, providing more switch gate drive and thus reducing the transistor's on-resistance. In non-bootstrapped mode, the IC is powered from the input voltage ($V+$) and operates with minimum supply current. In this mode, FB is the output voltage sense point. Since the voltage swing applied to the gate of the external power transistor is reduced (the gate swings from $V+$ to ground), the power transistor's on-resistance increases at low input voltages. However, the supply current is also reduced because $V+$ is at a lower voltage, and because less energy is consumed while charging and discharging the external MOSFET's gate capacitance. The minimum input voltage is 3V when using external feedback resistors. With supply voltages below 5V, bootstrapped mode is recommended. For the current application, the driver is supplied in bootstrapped mode.

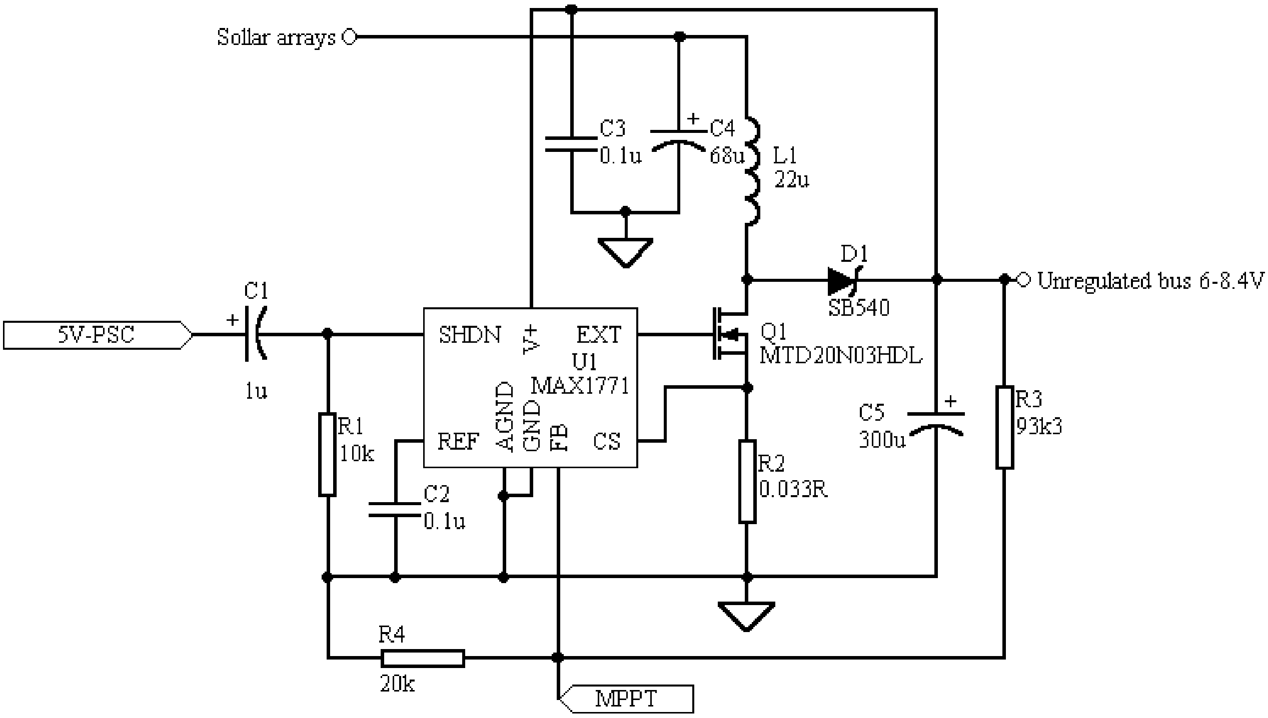

Figure 4.2 Scheme of application for the step-up converter MAX1771

Choose of external components

- **Setting the output voltage (Unregulated Bus 6-8.4V)**

To set the output voltage, first determine the mode of operation, either bootstrapped or non-bootstrapped. Bootstrapped mode provides more output current capability, while non-bootstrapped mode reduces the supply current.

The MAX1771's output voltage can be adjusted from very high voltages down to 3V, using external resistors R_3 and R_4 configured as voltage divider. For adjustable-output operation, the feedback resistor R_4 should be selected in the 10kΩ to 500kΩ range. R_3 is given by:

$$R_3 = R_4 \cdot \left(\frac{V_{OUT}}{V_{REF}} - 1 \right) \tag{4.1}$$

where V_{REF} equals 1.5V. If R_4 is chosen to have 20kΩ and U_{OUT} equals with 8.4V it occurs:

$$R_3 = 20 \cdot 10^3 \cdot \left(\frac{8.4}{1.5} - 1 \right) = 93.3k\Omega \tag{4.2}$$

Considering that the batteries are using their protection circuits is not needed a too precise voltage regulation.

The voltage on the FB pin will be regulated externally using three different types of inputs: a fixed one using a voltage divider, the output of battery charger and MPPT circuitry ADP3810AR-8.4 and the digital MPPT programmed in the MCU. These three inputs are selectable using a multiplexer.

- **Determining R_{SENSE} (R_2)**

To select R_{SENSE} theoretical output current curves shown in datasheet (figure 4.3) have been used. They were derived using the minimum (worst-case) current-limit comparator threshold value over the extended temperature range (-40°C to +85°C). No tolerance was included for R_{SENSE}. The voltage drop across the diode was assumed to be 0.5V, and the drop across the power switch $r_{DS(ON)}$ and coil resistance was assumed to be 0.3V.

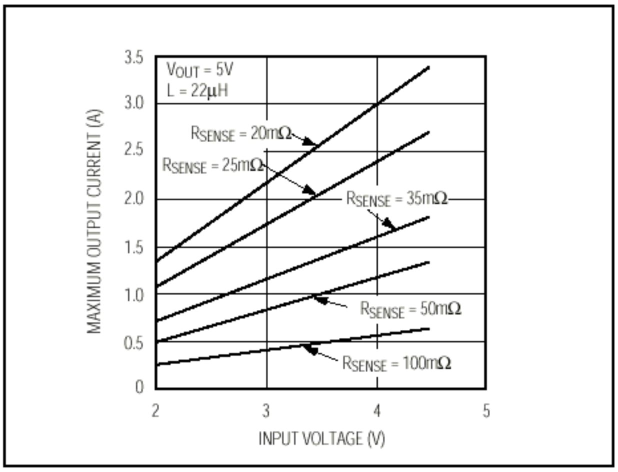

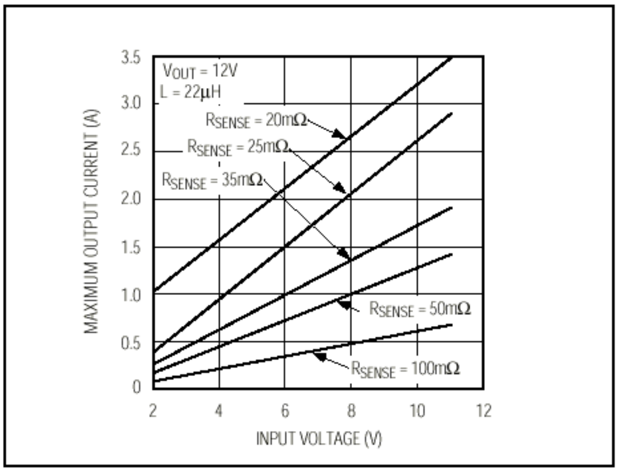

Figure 4.3 Maximum Output Current vs. Input voltage for V_{OUT} equal with 5V and 12V

Considering the curves from the figure 4.3 and the standardized values for shunt resistors, R_{SENSE} (R_2) was chosen to be 0.033Ω.

- **Determining the inductor (L)**

Practical inductor values range is from 10µH to 300µH. 22µH is a good choice for most applications. In applications with large input/output differentials, the IC's output current capability will be much less when the inductance value is too low, because the IC will always operate in discontinuous mode. If the inductor value is too low, the current will ramp up to a high level before the current-limit comparator can turn off the switch.

The minimum on-time for the switch ($t_{ON(\min)}$) is approximately 2µs; the inductor should be selected to allow the current to ramp up to I_{LIM}.

Standard operating circuits are using a 22µH inductor. If a different inductance value is desired, the inductor L will be selected such that:

$$L \geq \frac{V_{IN}(\max) \cdot 2\mu s}{I_{LIM}} \tag{4.3}$$

Considering that $V_{IN(\max)}$ is 5V and I_{LIM} equals with 1A results:

$$L \geq \frac{5(V) \cdot 2(\mu s)}{1(A)} \quad \Rightarrow \quad L \geq 10(\mu H) \tag{4.4}$$

The value for the inductor was chosen as being the same value indicated by the manufacturer of the device, in the datasheet, respectively 22μH.

Larger inductance values tend to increase the start-up time slightly, while smaller inductance values allow the coil current to ramp up to higher levels before the switch turns off, increasing the ripple at light loads. Inductors with a ferrite core or equivalent are recommended; powder iron cores are not recommended for use with high switching frequencies. It should be ensured that the inductor's saturation current rating (the current at which the core begins to saturate and the inductance starts to fall) exceeds the peak current rating set by R_{SENSE}. However, it is generally acceptable to bias the inductor into saturation by approximately 20% (the point where the inductance is 20% below the nominal value). For highest efficiency, is to be used a coil with low DC resistance, preferably under 20mΩ. To minimize radiated noise, will be used a toroid, a pot core, or a shielded coil.

- **Power Transistor Selection**

For selection of the N-FET, three important parameters are: the total gate charge (Q_g), on-resistance ($r_{DS(ON)}$), and reverse transfer capacitance (C_{RSS}).

Q_g takes into account all capacitances associated with charging the gate. The typical Q_g has to be used value for best results; the maximum value is usually grossly over-specified since it is a guaranteed limit and not the measured value. The typical total gate charge should be 50nC or less. With larger numbers, the EXT pins may not be able to adequately drive the gate. The EXT rise/fall time varies with different capacitive loads as shown in the datasheet, Typical Operating Characteristics section.

The two most significant losses contributing to the N-FET's power dissipation are I^2R losses and switching losses. The transistor should be selected with low $r_{DS(ON)}$ and low C_{RSS} to minimize these losses.

The maximum required gate-drive current is determined from the Q_g specification in the N-FET data sheet. The MAX1771's maximum allowed switching frequency during normal operation is 300kHz; but at start-up, the maximum frequency can be 500kHz, so the maximum current required to charge the N-FET's gate is $f_{(\max)} \cdot Q_{g(typ)}$.

For the MTD20N03HDL transistor, from the data sheet, the typical Q_g number is 13.4nC (for V_{GS}=5V). Therefore the current required to charge the gate is:

$$I_{GATE} = f_{(\max)} \cdot Q_g = 500[\text{kHz}] \cdot 13.4[\text{nC}] = 6.7[\text{mA}] \tag{4.5}$$

The bypass capacitor on $V+$ (C_3) must instantaneously furnish the gate charge without excessive droop (imposed less than 200mV):

$$\Delta V+ = \frac{Q_g}{C_3} = \frac{13.4[\text{nC}]}{0.1[\mu\text{F}]} = 134[\text{mV}] \tag{4.6}$$

The transistor recommended in the datasheet for MAX1771 is MTD20N03. The N-channel MOSFET chosen for the application has 20A continuous drain current and 30V drain-source voltage. Also, is required an on-resistance as small as possible. The $R_{\text{DS(on)}}$ of this device is 35mΩ.

- **Diode**

The MAX1771's high switching frequency demands a high-speed rectifier. Schottky diodes are recommended with average current rating exceeding the peak current limit set by R_{SENSE}, and that break-down voltage exceeding V_{OUT}. At heavy loads and high temperatures, the benefits of a Schottky diode's low forward voltage may outweigh the disadvantages of its high leakage current. Taking in consideration all of this, the diode chosen for this application is SB540 with $I_{F(AV)}$ = 5A, V_{RRM} = 40V and V_{RMS} = 28V.

- **Capacitor Selection**

Output Filter Capacitor (C_5)

The primary criterion for selecting the output filter capacitor (C_5) is low effective series resistance (ESR). The product of the peak inductor current and the output filter capacitor's ESR determines the amplitude of the ripple seen on the output voltage. Smaller-value and/or higher-ESR capacitors are acceptable for light loads or in applications that can tolerate higher output ripple. Since the output filter capacitor's ESR affects efficiency, low-ESR capacitors will be used for best performance. For reducing ESR is also possible to connect few capacitors in parallel.

The manufacturer is indicating for the applications like the presented one an output capacitor of 300μF. For reducing ESR of the output capacitor, will be used three capacitors of 100μF connected in parallel.

Input Bypass Capacitors (C_4)

The input bypass capacitor (C_4) reduces peak currents drawn from the voltage source and also reduces noise at the voltage source caused by the switching action of the MAX1771. The input voltage source impedance determines the size of the capacitor required at the $V+$ input. As with the output filter capacitor, a low-ESR capacitor is recommended. For output currents up to 1A, 68µF (C_4) is adequate, although smaller bypass capacitors may also be acceptable.

The IC is bypassed with a 0.1µF ceramic capacitor (C_3) placed as close to the V+ and GND pins as possible.

Reference Capacitor

REF pin is bypassed with a 0.1µF capacitor (C_2). REF can source up to 100µA of current for external loads. This reference is not used in present application.

Feed-Forward Capacitor

In adjustable output voltage and non-bootstrapped modes, parallel a 47pF to 220pF capacitor across R_2. The capacitor should have the lowest value that insures stability; high capacitance values may degrade line regulation. For this reason this capacitor has a value of 100pF.

- **Choosing the components for timed start-up**

After the kill switch is released (launch procedure) the step-up converter should start after a short period. For this reason a timer is used on the SHDN pin. Basically is an *RC* network formed from R_1 and C_1 (see figure 4.2) circuit which is keeping this input high for a period equal with the time constant of *RC* network.

For the chosen components R_1=10kΩ and C_1=1µF the time constant will be:

4.2.1. Battery charger circuitry and MPPT

The ADP3810 battery charger combines a programmable current limit with a battery voltage limit to provide a constant current, constant voltage battery charger controller. The circuitry includes two gain stages (GM), a precision 2.0V reference, a control input buffer, an Undervoltage Lock Out (UVLO) comparator, an output buffer and an over-voltage comparator.

The ADP3810 has internal thin-film resistors that are trimmed to provide a precise final voltage for LiIon batteries. Four voltage options are available, corresponding to 1-4 LiIon cells as follows: 4.2V, 8.4V, 12.6V and 16.8V.

Here are a few features of the ADP3810 circuit:

- Programmable charge current
- High precision battery voltage limit
- Precision 2.000V reference
- Low voltage drop current sense: 300mV full scale
- Full operation in shorted and open battery conditions

- Wide operating supply range: 2.7V to 16V
- Undervoltage lockout

A functional block diagram of the circuit is presented in figure 4.2.

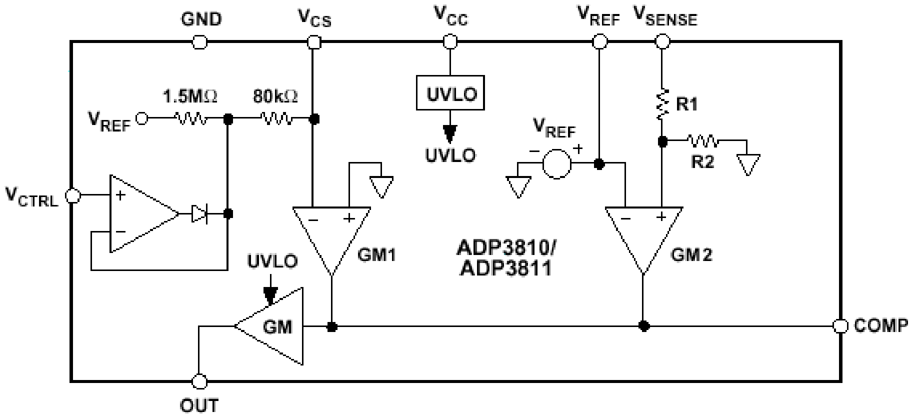

Figure 4.4 Simplified functional block diagram for battery charger

Pin Description

Pin	Name	Description
1	V_{SENSE}	Battery Voltage Sense Input.
2	V_{CS}	Current Sense Input.
3	COMP	External Compensation Pin.
4	OUT	Optocoupler Current Output Drive.
5	V_{CTRL}	DC Control Input to Set Current Limit, 0 V to 1.2 V.
6	GND	Ground Pin.
7	V_{REF}	Reference Output. Nominally 2.0 V.
8	V_{CC}	Positive Supply.

The ADP3810 contain the following blocks (shown in Figure 4.4):

- Two "GM" type error amplifiers control the current loop (GM1) and the voltage loop (GM2).
- A common COMP node is shared by both GM amplifiers such that an RC network at this node helps compensate both control loops.
- A precision 2.0V reference is used internally and is available externally for use by other circuitry. The 0.1µF bypass capacitor shown is required for stability.
- A current limited buffer stage (GM3) provides a current output, I_{OUT}, to control an external dc-dc converter. The dc-dc converter must have a control scheme such that higher I_{OUT} results in lower duty cycle. If this is not the case, a simple, single transistor inverter can be used for control phase inversion.
- An amplifier buffers the charge current programming voltage, V_{CTRL} , to provide a high impedance input.

- An UVLO circuit shuts down the GM amplifiers and the output when the supply voltage (V_{CC}) falls below 2.7V. This protects the charging system from indeterminate operation.
- A transient overshoot comparator quickly increases I_{OUT} when the voltage on the "+" input of GM2 rises over 120mV above V_{REF}. This clamp shuts down the dc-dc converter to quickly recover from overvoltage transients and protect external circuitry.

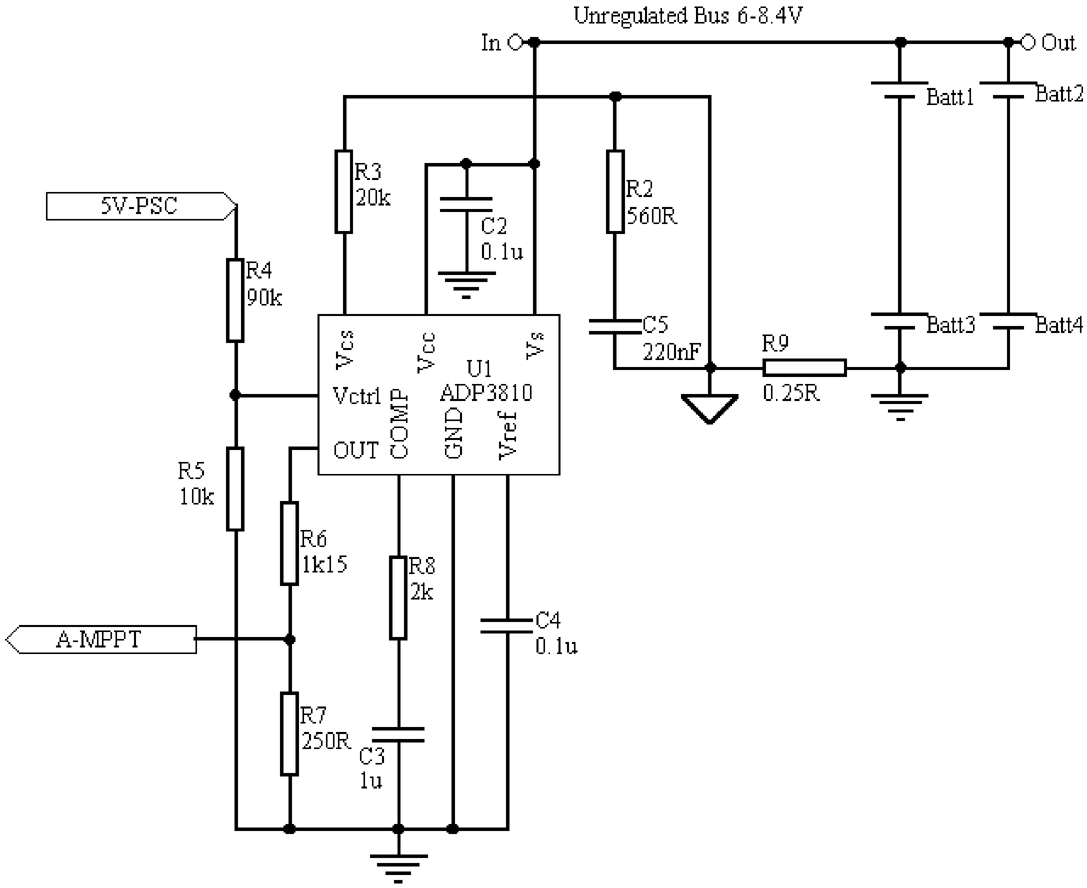

Figure 4.5 Application scheme for Battery Charger ADP3810

Functional description

The current limit amplifier senses the voltage drop across an external sense resistor to control the average current for charging a battery. The voltage drop can be adjusted from 25mV to 300mV, giving a charging current limit from 100mA to 1.2A with a 0.25Ω sense resistor. An external dc voltage on the V_{CTRL} input sets the voltage drop. As the battery voltage approaches its voltage limit, the voltage sense amplifier takes over to maintain a constant battery voltage. The two amplifiers essentially operate in an "OR" fashion. Either the current is limited, or the voltage is limited.

Description of Battery Charging Operation

The IC based system shown in figure 4.5 charges a battery with a dc current supplied by a dc-dc converter, which is most likely a switching type supply but could also be a linear supply where feasible. The value of the charge current is controlled by the feedback loop comprised of R_3, R_2, GM1, the external dc-dc converter and a dc voltage at the V_{CTRL} input. The actual charge current is set by the voltage, V_{CTRL}, and is dependent upon the choice for the values of R_3 and R_2 according to the formula below:

$$I_{CHARGE} = \frac{1}{R_3} \cdot \frac{R_2}{80k\Omega} \cdot V_{CTRL} \tag{4.8}$$

Typical values are $R_3 = 0.25\Omega$ and $R_2 = 20\text{k}\Omega$, which result in a charge current of 0.5A for a control voltage of 0.5V. The 80kΩ resistor is internal to the IC, and it is trimmed to its absolute value. The positive input of GM1 is referenced to ground, forcing the V_{CS} pin to a virtual ground. The resistor R_3 converts the charge current into the voltage at V_{RCS} , and it is this voltage that GM1 is regulating. The voltage at V_{RCS} is equal to $-(R_3/80\text{k}\Omega)\ V_{CTRL}$. When V_{CTRL} equals 1.0V, V_{RCS} equals –250mV. If V_{RCS} falls below its programmed level (i.e., the charge current increases), the negative input of GM1 goes slightly below ground. This causes the output of GM1 to source more current and drive the COMP node high, which forces the current, I_{OUT}, to increase. A higher I_{OUT} decreases the drive to the dc-dc converter, reducing the charging current and balancing the feedback loop. As the battery approaches its final charge voltage, the voltage loop takes over. The system becomes a voltage source, floating the battery at constant voltage thereby preventing overcharging. The constant voltage feature also protects the circuitry that is actually powered by the battery from overvoltage if the battery is removed. The voltage loop is comprised of R_1, R_2, GM2 (see figure 4.5) and the dc-dc converter. The final battery voltage is simply set by the ratio of R_1 and R_2 according to the following equation ($V_{REF} = 2V$):

$$V_{BATT} = 2[\text{V}] \cdot \left(\frac{R_1}{R_2} + 1 \right) \tag{4.9}$$

If the battery voltage rises above its programmed voltage, V_{SENSE} is pulled above V_{REF}. This causes GM2 to source more current, raising the COMP node voltage and I_{OUT}. As with the current loop, the higher I_{OUT} reduces the duty cycle of the dc-dc converter and causes the battery voltage to fall, balancing the feedback loop.

Charge Termination

If the system is charging a LiIon battery, the main criteria to determine charge termination is the absolute battery voltage. The ADP3810, with its accurate reference and internal resistors, accomplishes this task. The ADP3810's guaranteed accuracy specification of ±1% of the final battery voltage ensures that a LiIon battery will not be overcharged. This is especially important with LiIon batteries because overcharging can lead to catastrophic failure. It is also important to insure that the battery be charged to a voltage equal to its optimal final voltage (typically 4.2V per cell). Stopping at less than 1% of full-scale results in a battery that has not been charged to its full mAh capacity, reducing the battery's run time and the end equipment's operating time.

V_{CTRL} Input and Charge Current Programming Range

The voltage on the V_{CTRL} input determines the charge current level. This input is buffered by an internal single supply amplifier (labeled BUFFER) to allow easy programmability of V_{CTRL}. The guaranteed input voltage range of the buffer is from 0.0V to 1.2 V. Considering the input power from solar arrays, V_{CTRL} voltage is fixed at 0.5V using a voltage divider and a external 5V power supply, the same power supply used for all the power supply circuits, as in figure below.

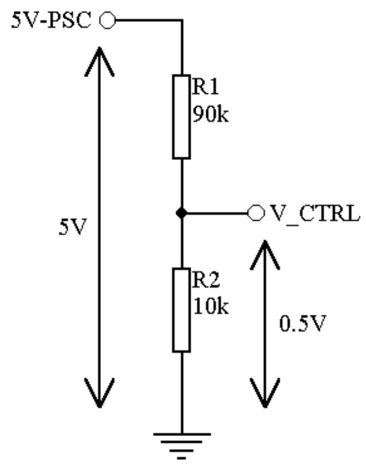

Figure 4.6 Set of V_{CTRL} value

$$U_{OUT} = \frac{R_2}{R_1 + R_2} \cdot U_{IN} \tag{4.10}$$

When V_{CTRL} is in the range of 0.0V to 0.5V, the output of the internal amplifier is fixed at 0.5V. This corresponds to a charge current of 500mA for $R_3 = 0.25\Omega$, $R_2 = 20\ \text{k}\Omega$.

V_{REF} Output

The internal band gap reference is not only used internally for the voltage and current loops, but it is also available externally if an accurate voltage is needed. The reference employs a pnp output transistor for low dropout operation. The reference is guaranteed to source 5mA with a dropout voltage of 400mV or less. The 0.1µF capacitor on the reference pin is integral in the compensation of the reference and is therefore required for stable operation. If desired, a larger value of capacitance can also be used for the application, but a smaller value should not be used. This capacitor should be located close to the V_{REF} pin.

Output Stage

The output stage performs two important functions. It is a buffer for the compensation node, and as such, it has a high impedance input. It is also a GM stage. The gain from the COMP node to the OUT pin is approximately 5mA/V. With a load resistor of 1 kΩ, the voltage gain is equal to five as specified in the data sheet. A different load resistor results in a gain equal to R_L·(5mA/V). The guaranteed output current is 5mA, which is much more than the typical 1mA to 2mA required in most applications.

Current Loop Accuracy Considerations

The accuracy of the current loop is dependent on several factors such as the offset of GM1, the offset of the V_{CTRL} buffer, the ratio of the internal 80kΩ compared to the external 20kΩ resistor, and the accuracy of R_3 . The specification for current loop accuracy states that the full-scale current sense voltage, V_{RCS}, of –300 mV is guaranteed to be within 15mV of this value. This assumes an exact 20kΩ resistor for R_2. Any errors in this resistor will result in further errors in the charge current value. For example, a 5% error in resistor value will add a 5% error to the charge current. The same is true for R_3, the current sense resistor. Thus, 1% or better resistors are recommended.

Voltage Loop Accuracy Considerations

The accuracy of the voltage loop is dependent on the offset of GM2, the accuracy of the reference voltage, the bias current of GM2 through R_1 and R_2, and the ratio of R_1/R_2. For the demanding application of charging LiIon batteries, the accuracy of the ADP3810 is specified with respect to the final battery voltage. This is tested in a full feedback loop so that the single accuracy specification given in the specification table accounts for all of the errors mentioned above.

STABILIZATION OF FEEDBACK LOOPS

The ADP3810 uses two transconductance error amplifiers with “merged” output stages to create a shared compensation point (COMP) for both the current and voltage loops as explained previously. Since the voltage and current loops have significantly different natural crossover frequencies in a battery charger application, the two loops need different inverted zero feedback loop compensations that can be accomplished by two series *RC* networks. One provides the needed low frequency (typical f_C<100Hz) compensation to the voltage loop, and the other provides a separate high frequency (f_C~1kHz–10kHz) compensation to the current loop. In addition, the current loop input requires a ripple reduction filter on the V_{CS} pin to filter out switching noise. Instead of placing both *RC* networks on the COMP pin, the current loop network is placed between V_{CS} and ground as shown in figure 4.5 (C_5 and R_2). Thus, it performs two functions, ripple reduction and loop compensation.

Loop Stability Criteria

1. The voltage loop has to be stable when the battery is floating.
2. The current loop has to be stable when the battery is being charged within its specified charge current range.
3. Both loops have to be stable within the specified input source voltage range.

4.3. Battery protection circuit

The batteries are provided a protection circuit for overcharging and overdischarging. In order to perform this function, the UCC3911 IC from Texas Instruments has been chosen. This device is able to ensure protection for a string of two series connected Li-Ion cells.

The UCC3911 is a two-cell lithium-ion (Li-Ion) and lithium-polymer (Li-Poly) battery pack protector device that incorporates an on-chip series FET switch thus reducing manufacturing costs and increasing reliability. The device's primary function is to protect both Li-Ion and Li-Poly cells in a two-cell battery pack from being either overcharged (overvoltage) or overdischarged (undervoltage). It employs a precision bandgap voltage reference that is used to detect when either cell is approaching an overvoltage or undervoltage state. When on-board logic detects either condition, the series FET switch opens to protect the cells. Principal characteristics of this IC are:

- provides protection against battery pack output shortcircuit
- extremely low power drain on batteries of about 20 μA
- used for two-cell battery packs
- low internal FET switch voltage drop
- user controllable delay for tripping short
- 3 A current capacity

A functional diagram for the device can be seen in figure 4.7. and a detailed pin description for the device is given in Table 4.2.

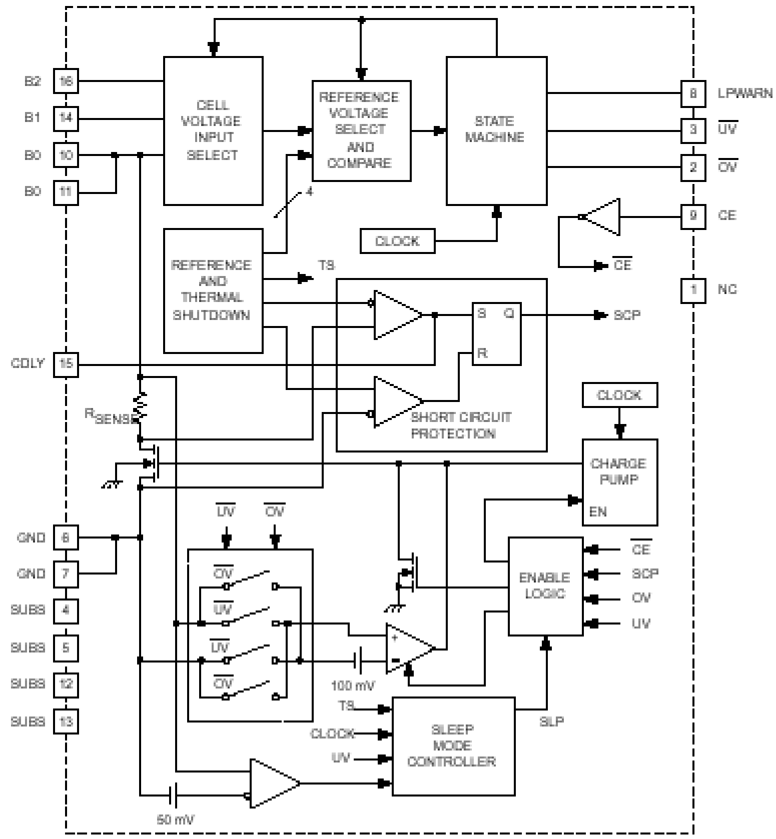

Figure 4.7 Functional diagram for battery protection circuit UCC3911

TERMINAL		I/O	DESCRIPTION
NAME	PACKAGE DP		
B0	10, 11	I	Connects to the negative terminal of the lower cell in the battery pack
B1	14	I	Connects to the junction of the positive terminal of the lower cell and the negative terminal of the upper cell in the battery pack
B2	16	I	Connects to the positive terminal of the upper cell in the battery pack. This pin also connects to the positive of the two terminals that are presented to the user of the battery pack
CDLY	15	I	Delay control pin for the short circuit protection feature
CE	9	O	Chip enable. The internal FET is disabled when CE is connected to B0
GND	6,7	–	In an overcharged state, current is allowed to flow only into this terminal. Similarly, in an over-discharged state, current is allowed to flow only out of this terminal
LPWARN	8	O	This active–high signal is the low Power Warning. The voltage on this pin goes high (to B2 potential) as soon as either of the battery's cells voltage falls below 3.0 V. Once the UV state is entered, this output goes back to low

$\overline{\text{OV}}$	2	O	This active–low signal indicates the state of the state machine's $\overline{\text{OV}}$ bit. When low, it indicates that one or both cells are overvoltage. Further charging is inhibited by the opening of the FET switch
SUBS	4,5,12,13	I	The substrate connections connect these points to a heat sink which is electrically isolated from all other device pins
$\overline{\text{UV}}$	3	O	This active–low signal indicates the state of the state machine's undervoltage bit. When low, it indicates that one or both cells are under voltage. Further discharging is inhibited by the opening of the FET switch

Table 4.2 Pin description for UCC3911

A negative feedback loop controls the FET switch when the battery pack is in either the overvoltage or undervoltage state. In the overvoltage state the action of the feedback loop is to allow only discharge current to pass through the FET switch. In the undervoltage state, only charging current is allowed to flow. The operational amplifier that drives the loop is powered only when in one of these two states. In the undervoltage state the chip enters sleep mode until it senses that the pack is being charged. The FET switch is driven by a charge pump when the battery pack is in a normally charged state to achieve the lowest possible $R_{DS(\mathrm{on})}$. In this state the negative feedback loop's operational amplifier is powered down to conserve battery power. Short circuit protection for the battery pack is provided and has a nominal delay of 100 µs before tripping.

An external capacitor may be connected between CDLY and B0 to increase this delay time to allow longer overcurrent transients. A chip enable (CE) pin is provided that when held low, inhibits normal operation of the device to facilitate assembly of the battery pack.

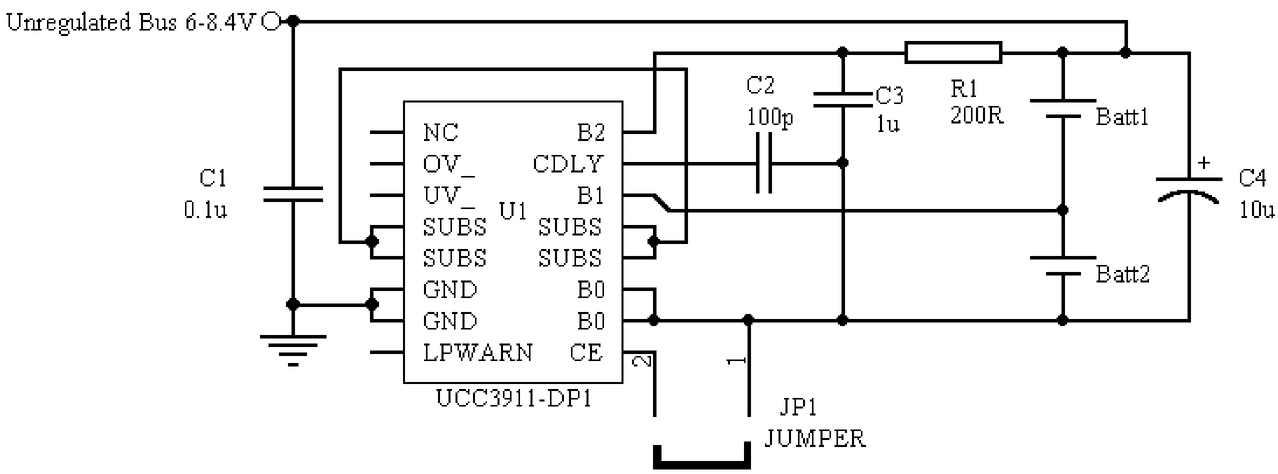

Figure 4.8 Scheme of application for battery protection circuit

Short-circuit protection

The demands of true short-circuit protection require that careful attention be paid to the selection of a few external components. In the application circuit shown in figure 4.8, C_1 protects the battery pack output terminals from inductive kick when the pack current is shut off due to an overcurrent or overvoltage/undervoltage condition. (It also increases the ESD protection level.)

The overcurrent delay capacitor (C_2), sets the time delay, after the overcurrent threshold is exceeded, before turning off the UCC3911's internal FET. If no capacitor is used, the nominal delay is 100μs. To charge large capacitive loads without tripping the overcurrent circuit, a small capacitor (typically less than 1000pF) is used to extend the delay time. The approximate delay time is given below and shown graphically in figure 4.9.

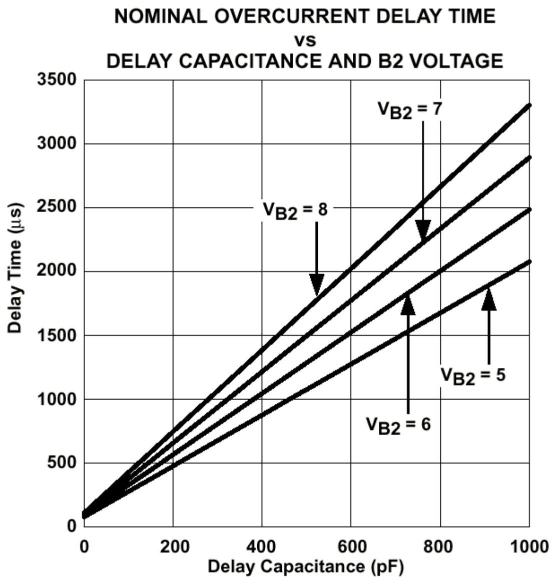

Figure 4.9 Nominal current delay time

$t_{DLY}[\mu s] = 25 + (25 + C_2[pF]) \cdot 0.4 \cdot V_{B2}$, therefore, for a capacitor C_2=100pF the minimum delay is:

$t_{DLY}(MIN) = 25 + (25 + 100) \cdot 0.4 \cdot 6 = 325[\mu s]$ when the battery voltage is minimum (6V) and the maximum delay:

$t_{DLY}(MAX) = 25 + (25 + 100) \cdot 0.4 \cdot 8.4 = 445[\mu s]$.

The amount of time required will be a function of the load capacitance, battery voltage, and the total circuit impedance, including the internal resistance of the cells, the UCC3911's on resistance, and the load capacitor ESR. The required delay time can be calculated from:

$$t = -R \cdot C \cdot \ln\left(\frac{I \cdot R}{V}\right) \tag{4.11}$$

In this equation, R is the total circuit resistance, C is the capacitor being charged, I is the overcurrent trip current (5.25A nominal), and V is the battery voltage. Using the minimum trip current of 3.5A and the maximum battery voltage of 8.4V, the worst case maximum delay time required is defined as:

$$t_{MAX}\,[\mu\text{s}] = -R \cdot C[\mu\text{F}] \cdot \ln\left(\frac{R}{2.4}\right) \tag{4.12}$$

Considering that C_{load} = 300µF, R = 0.2Ω (ESR from the capacitor added with resistance of the battery wires) it result:

$$t_{MAX} = -0.2 \cdot 300 \cdot \ln\left(\frac{0.2}{2.4}\right) = 149.094[\mu\text{s}] \tag{4.13}$$

To prevent a momentary cell voltage drop, caused by large capacitive loads, from causing an erroneous undervoltage shutdown, an *RC* filter is required in series with the two battery sense inputs, B1 and B2. If large capacitive loads (or other loads with surge currents above the overcurrent trip threshold) are not being applied to the pack terminals, the overcurrent delay time can be short and for B1 input the filter is not needed. In addition, the time constant of R_1 and C_3 (filter for B2 input) can be made much shorter. R_1 and C_3 are still necessary, however, to assure proper operation under short circuit conditions. It is important to maintain a minimum R_1/C_3 time constant of 100 µs.

If it is selected a time constant of 200µs, $\tau_{R1C3} = R_1 \cdot C_3 = 220[\mu\text{s}]$, it yields to R_1 = 200Ω and C_3 = 1µF.

Capacitor C_4 is recommended, in case the wires connecting to the top and bottom of the cell stack are more than an inch long (not likely in a small battery pack). In this case, a 10µF, low ESR capacitor is recommended to prevent excessive overshoot at turn-off due to wiring inductance.

4.4. Converter for the 5 V bus

For the 5V bus a step-down converter is to be used. The MAX174X family of ICs are step-down DC-DC controllers capable of handling up to 36V inputs. The MAX1744 device has been chosen because the output voltage is presetable for 5V. The main characteristics of this converter are:

- High-Voltage Operation (up to 36V IN)
- Efficiency >90%
- Output Power Capability Exceeds 50W
- 10-Pin µMax Package
- Low-Dropout Voltage

- 100% (max) Duty Cycle
- 90µA Quiescent Current
- 4µA Shutdown Current
- Up to 330kHz Switching Frequency
- Output Voltage
- 5V or 3.3V (MAX1744)
- Adjustable 1.25V to 18V (MAX1745)
- Current-Limited Control Scheme

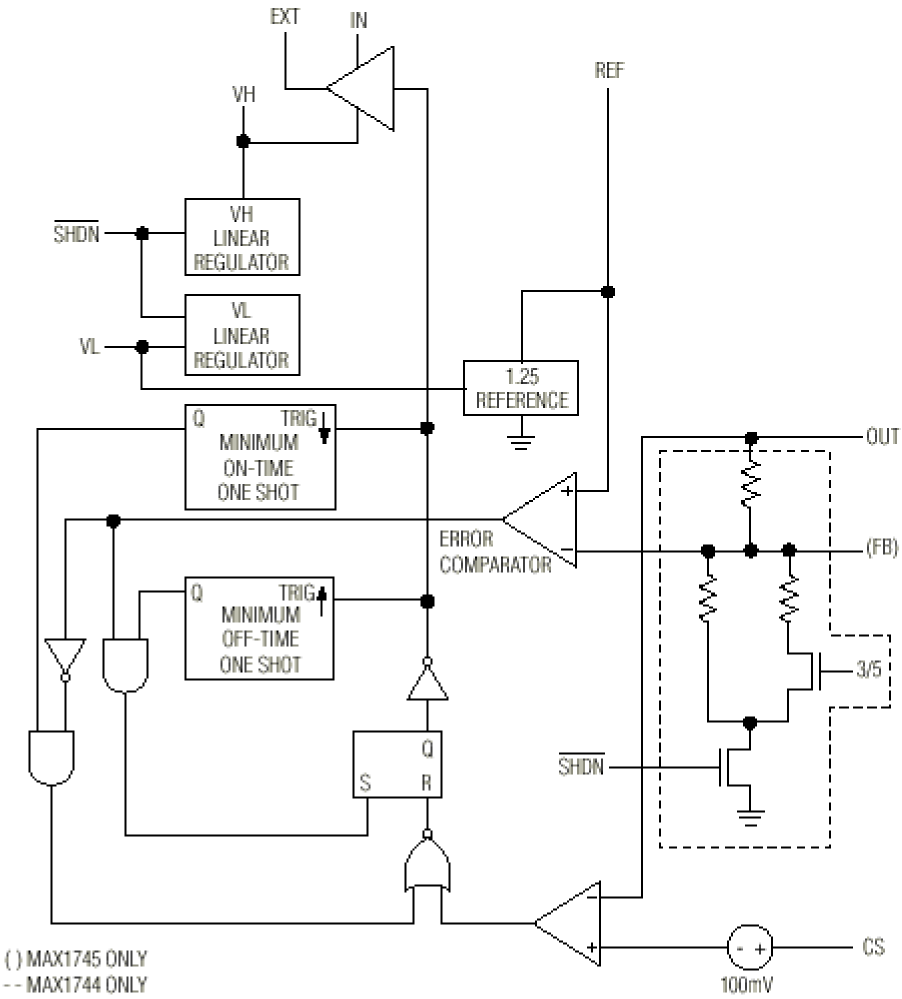

Figure 4.10 Functional diagram for step-up converter MAX1744

This part is using a proprietary current-limited control scheme for excellent light and full-load efficiency, while their 330kHz (max) switching frequency permits small external components for space-critical applications. Operation to 100% duty cycle permits the lowest possible dropout voltage. The MAX1744 contains an internal feedback network that provides a pin-selectable output voltage of either 3.3V or 5V.

Pin Description

PIN	PIN NAME	FUNCTION
1	GND	Ground
2	VL	Linear Regulator Output. VL provides power to the internal circuitry and can supply up to 1mA to an external load. Bypass VL to GND with 4.7uF or greater capacitor.
3	REF	1.25V Reference Output. REF can supply up to 100A to an external load. Bypass REF to GND with a 0.1uF or greater ceramic capacitor.
4	3/5	3.3V or 5V Selection. Connect 3/5 to GND to set the output voltage to 3.3V. Connect 3/5 to VL to set the output voltage to 5V.
5	OUT	Sense Input for Fixed 5V or 3.3V Output Operation (MAX1744) and Negative Current-Sense Input (MAX1744/5). OUT is connected to an internal voltage-divider (MAX1744). OUT does not supply current.
6	CS	Current-Sense Input. Connect the current-sense resistor between CS and OUT. External MOSFET is turned off when the voltage across the resistor is equal to or greater than the current limit trip level (100mV).
7	$\overline{\text{SHDN}}$	Active-Low Shutdown Input. Connect $\overline{\text{SHDN}}$ to IN for normal operation. Drive $\overline{\text{SHDN}}$ to low to shut the part off. In shutdown mode, the reference, output, external MOSFET, and internal regulators are turned off.
8	VH	High-Side Linear Regulator Output. VH provides a regulated output voltage that is 5V below IN. The external P-channel MOSFET gate is driven between IN and VH. Bypass VH to IN with a 4.7uF or greater capacitor (see Capacitor Selection).
9	EXT	Gate Drive for External P-Channel MOSFET. EXT swings between IN and VH.
10	IN	Positive Supply Input. Bypass IN to GND with a 0.47uF or greater ceramic capacitor.

The MAX1744 is high-voltage step-down DC-DC converter controller. These devices offer high efficiency over a wide range of input/output voltages and currents, making them optimal for use in applications such as telecom, automotive, and industrial control. Using an external P-channel MOSFET and current-sense resistor allows design flexibility and improved efficiency. The MAX1744 is automatically switching from PWM operation at medium and heavy loads to pulse-skipping operation at light loads to improve light-load efficiency. The low 90µA quiescent current further optimizes these parts for applications where low input current is critical. Operation to 100% duty cycle allows the lowest possible dropout voltage, which allows a wider input voltage variation. The small size, high switching frequency, and low parts count minimize the required circuit board area and component cost. figure 4.11 shows the MAX1744 typical application circuit.

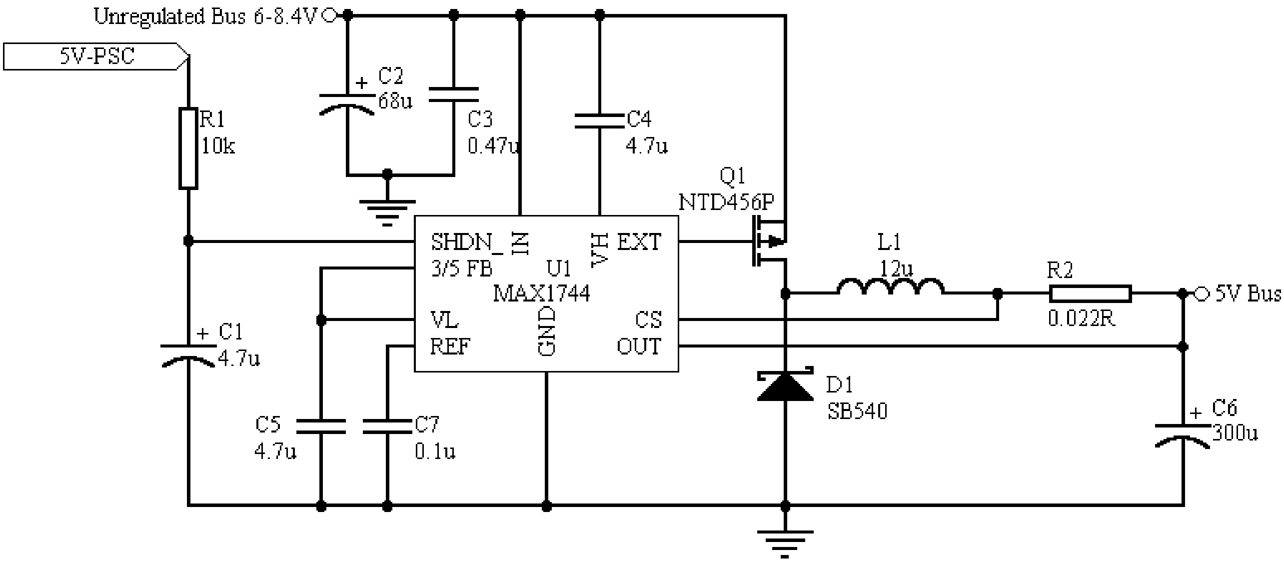

Figure 4.11 Application scheme for step-down converter MAX1744

Operating Modes

When delivering low output currents, the MAX1744 operate in discontinuous-conduction mode. Current through the inductor starts at zero, rises as high as the current limit, then ramps down to zero during each cycle. The switch waveform exhibits ringing, which occurs at the resonant frequency of the inductor and stray capacitance, due to residual energy trapped in the core when the commutation diode (D_1 in figure 4.11) turns off. When delivering medium-to-high output currents, the MAX1744 operate in PWM continuous-conduction mode. In this mode, current always flows through the inductor and never ramps to zero. The control circuit adjusts the switch duty cycle to maintain regulation without exceeding the peak switching current set by the current-sense resistor.

For the present application it can be considered that MAX1744 is operating in continuous-conduction mode.

Setting the Output Voltage

The MAX1744's output voltage can be selected to 3.3V or 5V under logic control by using the 3/5 pin. To ensure a 5V output the 3/5 pin is connected to VL.

VL Linear Regulator

The MAX1744 contains a 5V low-side linear regulator (VL) that powers the internal circuit and can supply up to 1mA to an external load. This allows the MAX1744 to operate up to 36V input, while maintaining low quiescent current and high switching frequency. When the input voltage goes below 5.5V, this regulator goes into dropout and the IN pin quiescent current will rise. VL should be bypassed with a 4.7µF or greater capacitor (C_5).

VH Linear Regulator

The MAX1744 is containing a high-side linear regulator (VH) that regulates its output to 5V below IN (the positive supply input voltage). This regulator limits the external P-channel MOSFET gate swing (EXT), allowing high input voltage operation without exceeding the MOSFET gate-source breakdown. VH is bypassed with a 4.7µF capacitor (C_4) between IN and VH.

Reference

The 1.25V reference is suitable for driving small external loads. It has a guaranteed 10mV maximum load regulation while sourcing load currents up to 100µA. The reference is turned off during shutdown. For normal operation the reference will be bypassed with 0.1µF (C_7). The bypass capacitor must be within 5mm of REF, with a direct trace to GND.

Current-Sense-Resistor Selection (R_2)

The current-sense comparator limits the peak switching current to V_{CS}/R_2, where R_2 is the value of the current-sense resistor and V_{CS} is the current-sense threshold. V_{CS} is typically 100mV. Minimizing the peak switching current will increase efficiency and reduce the size and cost of external components. However, since available output current is a function of the peak switching current, the peak current limit must not be set too low.

The peak current limit is set to 1.3 times the maximum load current by setting the current-sense resistor (R_2) to:

$$R_2 = \frac{V_{CS(MIN)}}{1.3 \cdot I_{OUT(MAX)}} \tag{4.14}$$

Considering the maximum output current as being 2A it yields to:

$$R_2 = \frac{0.085}{1.3 \cdot 2} = 0.0327\Omega \tag{4.15}$$

In concordance with standardized values for resistors R_2 was chosen to have 0.033Ω.

Inductor Selection

The essential parameters for inductor selection are inductance and current rating. The MAX1744 operate with a wide range of inductance values. In many applications, values between 4.7µH and 100µH take best advantage of the controller's high switching frequency.

The minimum inductance value is calculate as follows:

$$L_{(MIN)} = \frac{(V_{IN} - V_{OUT}) \cdot 1[\mu\text{s}]}{\frac{V_{CS(MIN)}}{R_2}} \tag{4.16}$$

where 1μs is the minimum on-time. Inductor values between 2 and 10 times $L_{(MIN)}$ are recommended. Therefore:

$$L_{(MIN)} = \frac{(8.4-5)\cdot 1}{\frac{0.085}{0.033}} = 1.32[\mu\text{H}] \tag{4.17}$$

and the final value for the inductance was chosen L = 12μH.

With high inductor values, the MAX1744 begin continuous-conduction operation at a lower fraction of the full load. The inductor's saturation and heating current ratings must be greater than the peak switching current to prevent overheating and core saturation. Saturation occurs when the inductor's magnetic flux density reaches the maximum level the core can support, and inductance starts to fall. The heating current rating is the maximum DC current the inductor can sustain without overheating. For optimum efficiency, the inductor winding's resistance should be less than the current-sense resistance.

External Switching Transistor

The MAX1744 drive a P-channel enhancement mode MOSFET. The EXT output swings from VH to IN. The MOSFET's on-resistance is should be specified for 5V gate drive or less.

Four important parameters for selecting a P-channel MOSFET are drain-to-source breakdown voltage, current rating, total gate charge (Q_g), and $R_{DS(\text{ON})}$. The drain-to-source breakdown voltage rating should be at least a few volts higher than V_{IN}. The MOSFET should be chosen with a maximum continuous drain current rating higher than the peak current limit:

$$I_{D(MAX} \geq I_{LIM(MAX)} \tag{4.18}$$

$$I_{LIM(MAX)} = \frac{V_{CS}}{R_2} = \frac{0.1}{0.033} = 3[\text{A}] \tag{4.19}$$

The Q_g specification should be 80nC or less to ensure fast drain voltage rise and fall times, and reduce power losses during transition through the linear region. Q_g specifies all of the capacitances associated with charging the MOSFET gate. $R_{DS(\text{ON})}$ should be as low as practical to reduce power losses while the MOSFET is on. It should be equal to or less than the current-sense resistor.

Considering the specifications listed above, the MOSFET transistor selected for the application is NDT456P with the following specifications: drain-to-source breakdown voltage $V_{DSS} = -30$V, on-state drain current $I_D = -7.5$A, total gate charge $Q_g = 47$nC, and static drain-source on-resistance $R_{DS(\text{ON})} = 0.041\Omega$ ($V_{GS} = -4.5$V, $V_{DS} = -5$V).

Diode Selection

The MAX1744's high switching frequency demands a high-speed rectifier. Schottky diodes, such as the 1N5817–1N5822 family or surface-mount equivalents, are recommended. Ultra-high-speed rectifiers with reverse recovery times around 50ns or faster should be used for high output voltages, where the increased forward drop causes less efficiency degradation. Diode's peak current rating should exceed the peak current limit set by R_2, and that its breakdown voltage exceeds V_{IN}. Schottky diodes are preferred for heavy loads due to their low forward voltage, especially in low-voltage applications.

The diode selected for the application is SB540 with the following characteristics: average forward current $I_{F(AV)} = 5$A, peak repetitive reverse voltage $V_{RRM} = 40$V and maximum RMS voltage $V_{RMS} = 28$V.

Capacitor Selection

The filter capacitors are chosen to service input and output peak currents with acceptable voltage ripple. ESR (Equivalent Series Resistance) in the output capacitor is a major contributor to output ripple, so low-ESR capacitors are recommended. Low-ESR tantalum, polymer, or ceramic capacitors are best. Low-ESR aluminum electrolytic capacitors are tolerable, but standard aluminum electrolytic capacitors are not recommended.

Voltage ripple is the sum of contributions from ESR and the capacitor value:

$$V_{RIPPLE} \approx V_{RIPPLE,ESR} + V_{RIPPLE,C} \tag{4.20}$$

For tantalum capacitors, the ripple is determined by the ESR, but for ceramic capacitors, the ripple is mostly due to the capacitance. Voltage ripple as a consequence of ESR is approximated by:

$$V_{RIPPLE,ESR} \approx (R_{ESR})\Delta I_{p-p} \tag{4.21}$$

The ripple due to the capacitance is approximately:

$$V_{RIPPLE,C} \approx \frac{L \cdot I_{PEAK}^2}{2 \cdot C \cdot V_O} \tag{4.22}$$

Estimation of the input (C_2) and output capacitor (C_6) values for given voltage ripple will be made as follows:

$$C_2 = \frac{\frac{1}{2} \cdot L_1 \cdot I_{\Delta L1}^2}{V_{RIPPLE,C3} \cdot V_{IN}} = \frac{\frac{1}{2} \cdot 12 \cdot 10^{-6} \cdot 2^2}{0.05 \cdot 8.4} = 57[\mu\text{F}] \tag{4.23}$$

$$C_6 = \frac{\frac{1}{2} \cdot L_1 \cdot I_{\Delta L1}^2}{V_{RIPPLE,C6} \cdot V_{OUT}} \cdot \left(\frac{V_{IN}}{V_{IN} - V_{OUT}} \right) = \frac{\frac{1}{2} \cdot 12 \cdot 10^{-6} \cdot 2^2}{0.05 \cdot 5} \cdot \left(\frac{8.4}{8.4 - 5} \right) = 237.176[\mu\text{F}] \qquad (4.24)$$

where $I_{\Delta L}$ is the change in inductor current and for continuous-conduction mode equals with output current and V_{RIPPLE} was chosen 50mV (1% from the output voltage). Considering the standardized values for capacitors, the chosen values for capacitors are $C_2 = 68\mu$F and $C_6 = 300\mu$F.

These equations are suitable for initial capacitor selection; final values should be set by testing a prototype. Pursuing output ripple lower than the error comparator's hysteresis (0.6% of the output voltage) is not practical, since the MAX1744 will switch at slower frequencies, increasing inductor ripple current threshold. The output capacitor will be chosen with a working voltage rating higher than the output voltage.

The input filter capacitor reduces peak currents drawn from the power source and reduces noise and voltage ripple at IN, caused by the circuit's switching action. It should be used a low-ESR capacitor. Two smaller-value low-ESR capacitors can be connected in parallel if necessary. The input capacitors should have the working voltage ratings higher than the maximum input voltage.

A surface-mount ceramic capacitor (C_3) will be placed very close to IN and GND. This capacitor bypasses the MAX1744, minimizing the effects of spikes and ringing on the power source (IN). The value for this capacitor is 0.47μF.

The REF pin is bypassed with 0.1μF (C_7). This capacitor should be placed within 5mm of the IC, next to REF, with a direct trace to GND.

Choosing the components for timed start-up

When the kill switch is released (launch procedure) the step-down converter should start in a short period after the step-up converter. For this reason a timer is used on the $\overline{SHDN}$ pin. Basically is an RC circuit, formed by R_1 and C_1 (see figure 4.11), circuit which is keeping this input low for a period equal with the time constant of the RC network.

For the chosen components $R_1 = 20\text{k}\Omega$ and $C_1 = 4.7\mu$F the time constant will be:

$$\tau_{R1-C1} = R_1 \cdot C_1 = 20 \cdot 10^3 \cdot 4.7 \cdot 10^{-6} = 94[\text{ms}] \qquad (4.25)$$

This time constant was chosen considering that this converter should start after the first converter is getting out from its transient domain.

4.5. Load protection circuits

Each user is using a protection circuit like in figure 4.12. The only difference between protections for different users is the current limit for power distribution switches TPS203x.

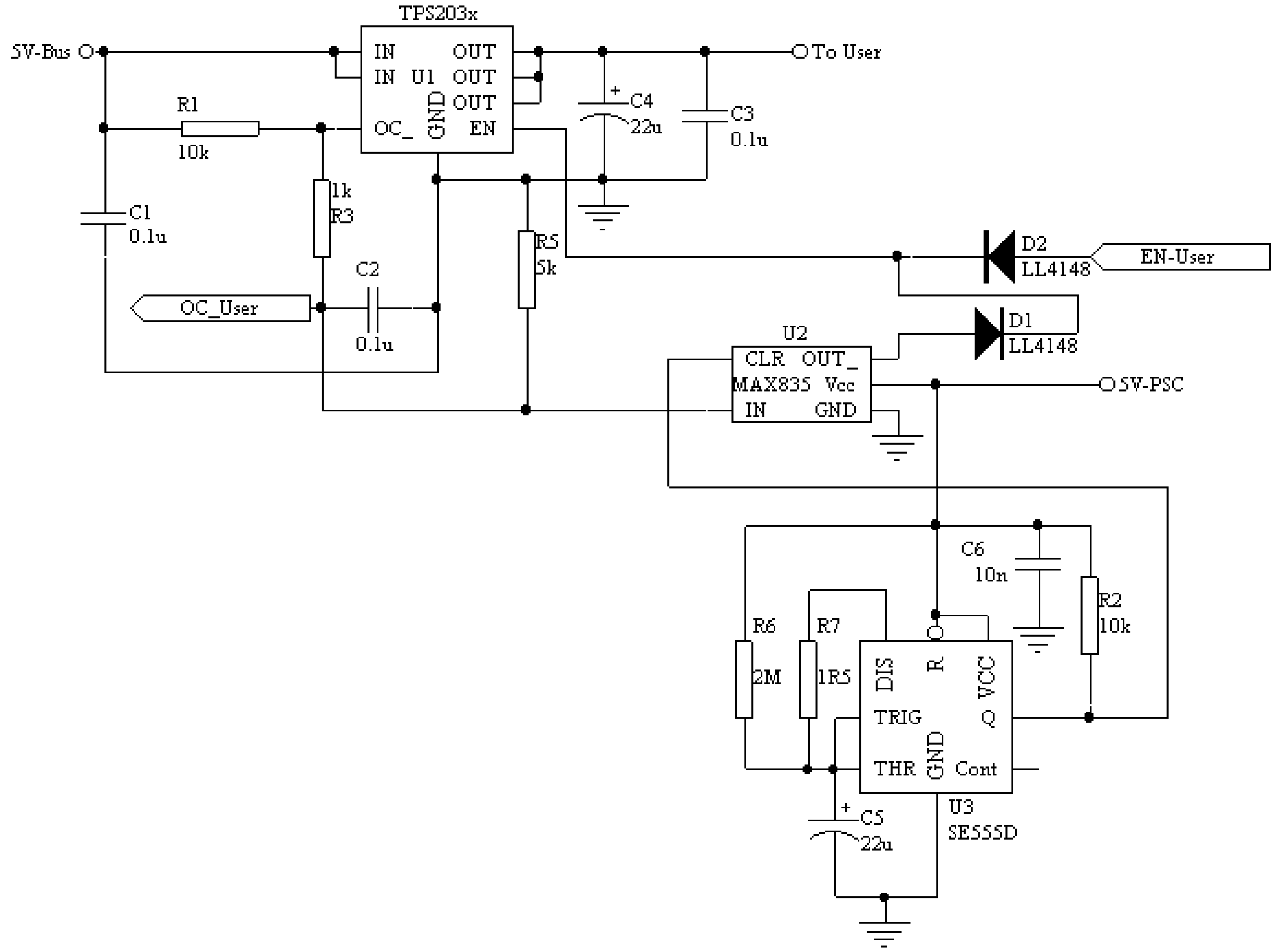

Figure 4.12 Protection circuits for each user

When the overcurent threshold is exceeded the power distribution switch TPS203x is limiting the output current and furnishing an overcurrent flag at $\overline{OC}$ output. This signal is filtered for avoiding false overcurrent signals which can occur because of the transients. The micropower voltage monitor MAX835 is comparing the filtered $\overline{OC}$ signal with its internal reference. If the signal is smaller than the reference the internal latch will put the output of the MAX835 low. The output is connected through a diode to EN pin of the TPS203x inhibiting in this way the output of the device. EN pin can be also inhibited by the MCU.

The latches are periodically cleared using an astabil. The circuit used is the precision timer SE555D configured in astable operation mode and the timing period is below one minute.

4.5.1. Power distribution switches TPS203x

The TPS203x family of power distribution switches is intended for applications where heavy capacitive loads and short circuits are likely to be encountered. These devices are 50mΩ N-channel MOSFET high-side power switches. The main characteristics of this family are:

- 33mΩ (5V Input) High-Side MOSFET Switch
- Short-Circuit and Thermal Protection
- Overcurrent Logic Output
- Operating Range . . . 2.7 V to 5.5 V
- Logic-Level Enable Input
- Typical Rise Time . . . 6.1 ms
- Undervoltage Lockout
- Maximum Standby Supply Current ...10 mA
- No Drain-Source Back-Gate Diode
- Available in 8-pin SOIC and PDIP Packages
- Ambient Temperature Range, –40°C to 85°C
- 2-kV Human-Body-Model, 200-V Machine-Model ESD Protection

The switch is controlled by a logic enable compatible with 5-V logic and 3-V logic. Gate drive is provided by an internal charge pump designed to control the power-switch rise times and fall times to minimize current surges during switching. The charge pump requires no external components and allows operation from supplies as low as 2.7 V.

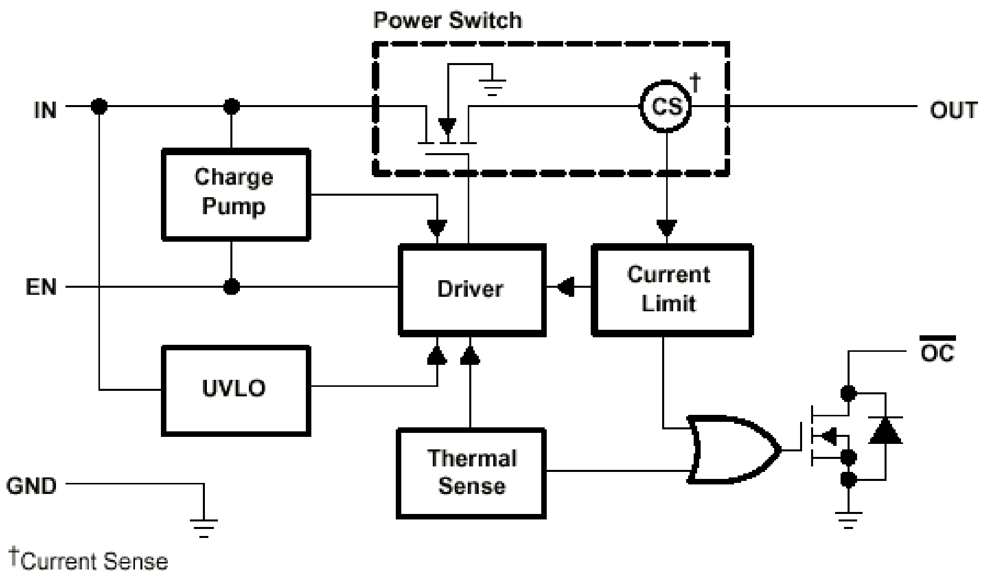

Figure 4.13 Functional diagram for power distribution switch TPS203x

Pin Description

TERMINAL		I/O	DESCRIPTION
NO.	NAME		
4	EN	I	Enable input. Logic high turns on power switch.
1	GND	I	Ground
2, 3	IN	I	Input voltage
5	$\overline{OC}$	O	Overcurrent. Logic output active low
6, 7, 8	OUT	O	Power-switch output

Detailed description

- **power switch**

The power switch is an N-channel MOSFET with a maximum on-state resistance of 50mΩ ($V_{I(IN)}$ = 5V). Configured as a high-side switch, the power switch prevents current flow from OUT to IN and IN to OUT when disabled.

- **charge pump**

An internal charge pump supplies power to the driver circuit and provides the necessary voltage to pull the gate of the MOSFET above the source. The charge pump operates from input voltages as low as 2.7 V and requires very little supply current.

- **driver**

The driver controls the gate voltage of the power switch. To limit large current surges and reduce the associated electromagnetic interference (EMI) produced, the driver incorporates circuitry that controls the rise times and fall times of the output voltage. The rise and fall times are typically in the 2-ms to 9-ms range.

- **enable (EN)**

The logic enable disables the power switch, the bias for the charge pump, driver, and other circuitry to reduce the supply current to less than 10mA when a logic low is present on EN . A logic high input on EN restores bias to the drive and control circuits and turns the power on. The enable input is compatible with both TTL and CMOS logic levels.

- **overcurrent ($\overline{OC}$)**

The $\overline{OC}$ open drain output is asserted (active low) when an overcurrent or overtemperature condition is encountered. The output will remain asserted until the overcurrent or overtemperature condition is removed.

- **current sense**

A sense FET monitors the current supplied to the load. The sense FET measures current more efficiently than conventional resistance methods. When an overload or short circuit is encountered, the current-sense circuitry sends a control signal to the driver. The driver, in turn, reduces the gate voltage and drives the power FET into its saturation region, which switches the output into a constant current mode and holds the current constant while varying the voltage on the load.

- **thermal sense**

An internal thermal-sense circuit shuts off the power switch when the junction temperature rises to approximately 140°C. Hysteresis is built into the thermal sense circuit. After the device has cooled approximately 20°C, the switch turns back on. The switch continues to cycle off and on until the fault is removed.

- **undervoltage lockout**

A voltage sense circuit monitors the input voltage. When the input voltage is below approximately 2V, a control signal turns off the power switch.

AVAILABLE OPTIONS

DEVICES	RECOMMENDED MAXIMUM CONTINUOUS LOAD CURRENT [A]	TYPICAL SHORT-CIRCUIT CURRENT LIMIT AT 25°C [A]
TPS2030D	0.2	0.3
TPS2031D	0.6	0.9
TPS2032D	1	1.5
TPS2033D	1.5	2.2
TPS2034D	2	3

Table 4.3 Available options for TPS203x ICs

Considering the table 4.3 and the consumption for each user, the following devices have been chosen, stated in table 4.4:

No.	Consumer	Power [W]	Current[A]	Device
1	OBC	0.46	0.092	TPS2030D
2	Transmitter	9	1.8	TPS2034D
3	Camera	0.3	0.06	TPS2030D
4	Attitude Control	0.25	0.05	TPS2030D

Table 4.4 Choose of the protections circuits for loads

Figure 4.14 shows the TPS203x typical application circuit.

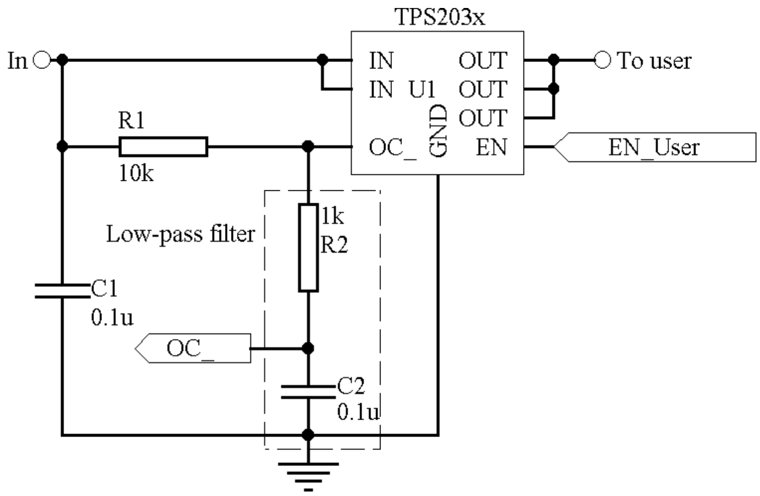

Figure 4.14 Application scheme for power distribution switch TPS203x

The filter at the $\overline{\text{OC}}$ output (R_2-C_2) is an low-pass filter and is reducing the false overcurrent reports. This can occur when heavy capacitive loads are connected and the inrush current is flowing through the device. The filter has a time constant of:

$$\tau = R_2 \cdot C_2 = 10^3 \cdot 10^{-7} = 100[\mu s] \tag{4.26}$$

and the turn-over frequency of

$$f_0 = \frac{1}{2 \cdot \pi \cdot \tau} = \frac{1}{2 \cdot 3.14 \cdot 10^{-4}} \approx 1591[\text{Hz}] \tag{4.27}$$

4.5.2. Micropower voltage monitor MAX835

The MAX835 micropower voltage monitor contains a 1.204V precision bandgap reference, comparator, and latched output in a 5-pin SOT23 package. The MAX835 has a push/pull output driver. Two external resistors set the trip-threshold voltage.

Applications

- Precision Battery Monitor
- Load Switching
- Battery-Powered Systems
- Threshold Detectors

Features

- Prevents Deep Discharge of Batteries
- Precision ±1.25% Voltage Threshold

- Latched Output (once low, stays low until cleared)
- SOT23-5 Package
- Low Cost
- Wide Operating Voltage Range, +2.5V to +11V
- <2µA Typical Supply Current
- Push/Pull Output

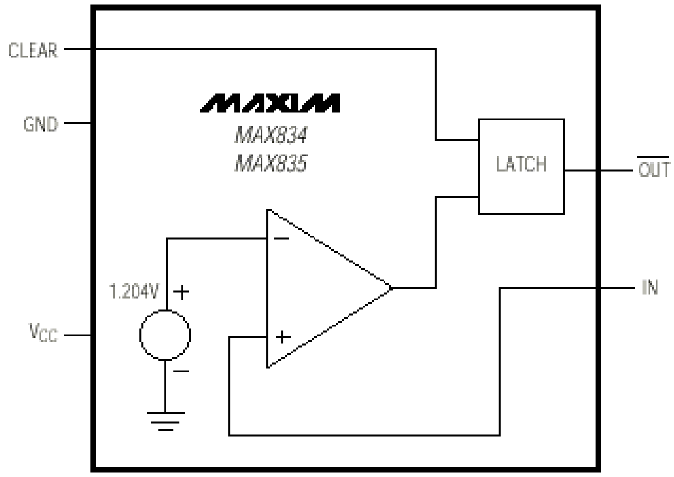

Figure 4.15 Functional diagram for MAX835 micropower voltage monitor

Programming the Trip Voltage (V_{TRIP})

Two external resistors set the trip voltage, V_{TRIP} (figure 4.16). V_{TRIP} is the point at which the falling monitored voltage causes OUT to go low. IN’s high input impedance allows the use of large-value resistors without compromising trip voltage accuracy.

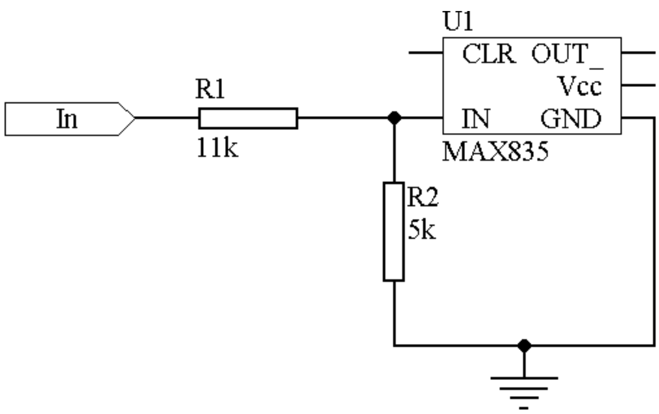

Figure 4.16 Setting the V_{TRIP} voltage

Knowing that the R_1 is form from two resistors in series (see in figure 4.12 the resistors R_1 and R_3) the resultant value for R_1 is 11kΩ. The value for R_2 is computed as it follows:

$$R_2 = \frac{R_1}{\left(\frac{V_{TRIP}}{V_{TH}} - 1\right)} \tag{4.28}$$

where V_{TRIP} is the desired trip voltage and V_{TH} is the threshold voltage and equals with 1.204V. This yields to:

$$R_2 = \frac{11 \cdot 10^3}{\left(\frac{4}{1.204} - 1\right)} = 4736.7\Omega \tag{4.29}$$

and the final value for the resistor of 5kΩ. The trip voltage was establish knowing that the input voltage should be smaller that the supplying voltage with 0.25V. Is not needed a too precise programming for the trip voltage. The most important thing is to make the difference between a high or low logical state input

Latched-Output Operation

When V_{MON} falls below V_{TRIP}, OUT goes low and remains low (even if V_{MON} rises above V_{TRIP}), until CLEAR is pulsed high again with V_{MON}>V_{TRIP}. Figure 4.17 shows the timing relationship between V_{MON}, OUT, and CLEAR.

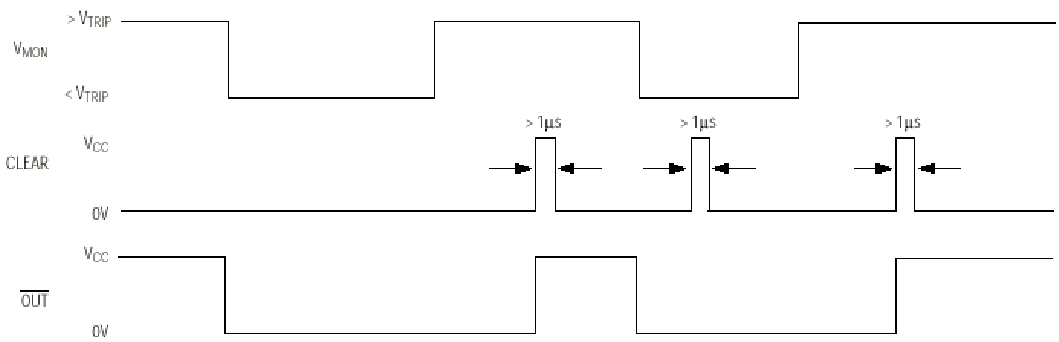

Figure 4.17 Relationship between V_{MON}, OUT, and CLEAR

4.5.3. Precision timer SE555D

Description

This device is precision monolithic timing circuit capable of producing accurate time delays or oscillations. In the time-delay or monostable mode of operation, the timed interval is controlled by a single external resistor and capacitor network. In the astable mode of operation, the frequency and duty cycle can be controlled independently with two external resistors and a single external capacitor.

The threshold and trigger levels normally are two-thirds and one-third, respectively, of VCC. These levels can be altered by use of the control-voltage terminal. When the trigger input falls below the trigger level, the flip-flop is set and the output goes high. If the trigger input is above the trigger level and the threshold input is above the threshold level, the flip-flop is reset and the output is low. RESET can override all other inputs and can be used to initiate a new timing cycle. When RESET goes low, the flip-flop is reset and the output goes low. When the output is low, a low-impedance path is provided between DISCH and ground.

The output circuit is capable of sinking or sourcing current up to 200mA. Operation is specified for supplies of 5V to 15V. With a 5V supply, output levels are compatible with TTL inputs. The SE555 and SE555C are characterized for operation over the full military range of –55°C to 125°C.

Features

- Timing From Microseconds to Hours
- Astable or Monostable Operation
- Adjustable Duty Cycle
- TTL-Compatible Output Can Sink or Source up to 200 mA

Functional diagram

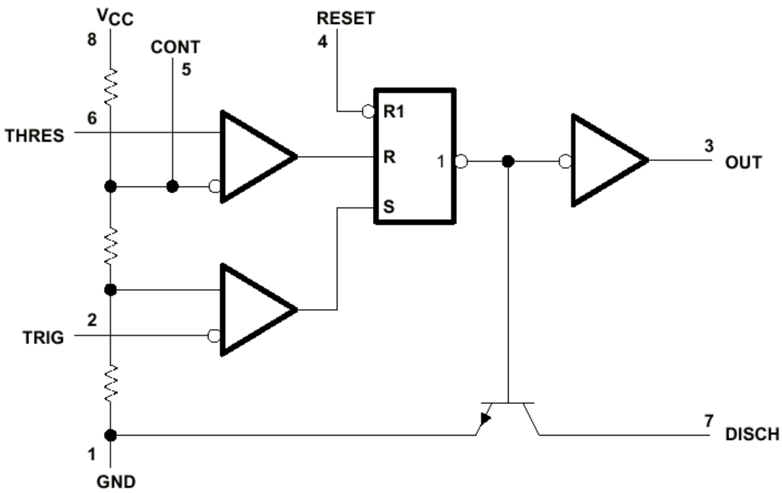

Figure 4.18 Functional diagram for SE555 IC

Application circuit

The application circuit diagram is shown in figure 4.19.

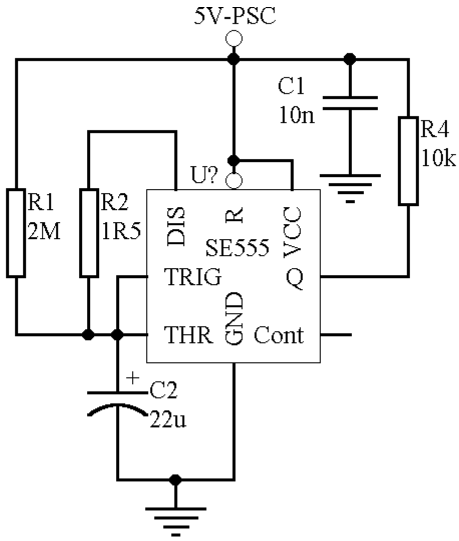

Figure 4.19 Application circuit for astable operation

Astable operation

As shown in figure 4.19, connecting the trigger input to the threshold input causes the timer to self-trigger and run as a multivibrator. The capacitor C charges through R_1 and then discharges through R_2 only. Therefore, the duty cycle is controlled by the values of R_1 and R_2.

This astable connection results in capacitor C charging and discharging between the threshold-voltage level ($0.67 \cdot V_{CC}$) and the trigger-voltage level ($0.33 \cdot V_{CC}$). The charge and discharge times (and, therefore, the frequency and duty cycle) are independent of the supply voltage.

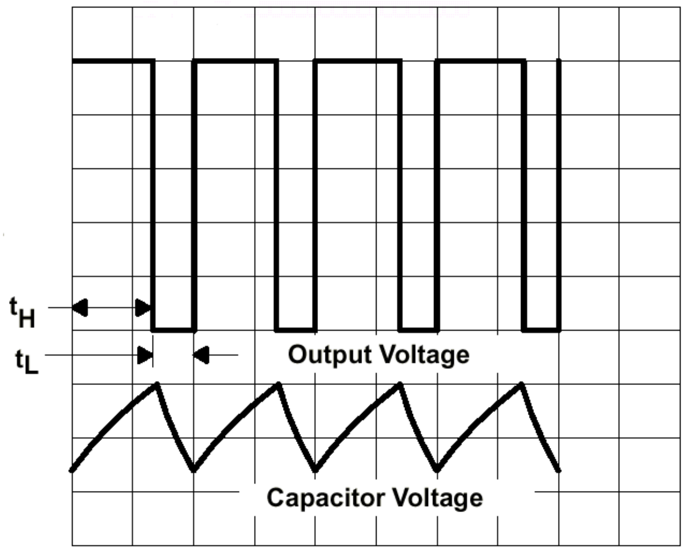

Figure 4.20 Typical astable waveforms

Figure 4.20 shows typical waveforms generated during astable operation. The output high-level duration t_H and low-level duration t_L can be calculated as follows:

$$t_H = 0.693 \cdot R_1 \cdot C_2 \tag{4.30}$$

$$t_L = 0.693 \cdot R_2 \cdot C_2 \tag{4.31}$$

For clearing the MAX835 latch it is specified in the datasheet a minimum pulse width of 1μs. For ensuring the clear, it was selected the pulse width generated by SE555 (t_H) of 20μs. The time between the pulses (t_L) it was selected a value of 30s. It yields to:

$$t_H = 0.693 \cdot R_1 \cdot C_2 = 20[\mu s] \Rightarrow R_1 \cdot C_2 = 28.86 \cdot 10^{-6}[s] \tag{4.32}$$

$$t_L = 0.693 \cdot R_2 \cdot C_2 = 45[s] \quad \Rightarrow R_2 \cdot C_2 = 43.29[s] \tag{4.33}$$

and considering the standardized values for components it was chosen: $R_1 = 1.5\Omega$, $R_2 = 2M\Omega$ and $C_2 = 22\mu F$. For these values of the components the new times are:

$$t_H = 0.693 \cdot 1.5 \cdot 22 \cdot 10^{-6} = 22.87[\mu s] \tag{4.34}$$

$$t_L = 0.693 \cdot 2 \cdot 10^6 \cdot 22 \cdot 10^{-6} = 30.49[s] \tag{4.35}$$

4.6. Load filters

For a precise computing of the output filters for each load is necessary to know the value of the filtering capacitors placed on each board of the loads. Without this information is difficult to estimate the value of the filtering capacitors on the power supply board. A too high value for the capacities can generate huge inrush currents. A small one it cannot minimize enough the voltage ripple.

4.7. Housekeeping data acquisition

Housekeeping data are data collected in the satellite and delivered to the OBC to be sent down to the ground station. Values processed are currents, voltages and temperatures.

4.7.1. Measurement of currents and voltages

As described in section 3.4.3, the measured currents in the satellite are:

- currents on each solar panel

- current flowing from step-up converter
- currents flowing to each user

Similarly, the voltages collected are:

- voltage on the solar panels, at the input of the step-up converter
- voltage of the batteries
- voltage on the regulated bus

Measurement of the currents

The current is measured using shunt resistors. The voltage drop on the shunt resistors is proportional with the current flowing through the resistor. From the specifications is known that the voltage for each user should be within 2% accuracy. This means a voltage of 100mV. For this reason the voltage drop on the shunt resistors should smaller than this value. Because the A/D converter has a 12bit resolution (approx. 1.22mV voltage step), for a voltage range lower than 100mV the error will be quite big when small currents are measured.

Taking in consideration this it seems that the small voltage drop on the shunt must be amplified to 5V, the maximum input voltage for A/D converter of the microcontroller. For this reason is used the high-side current-sense amplifier MAX4372. Because the input voltage is very low, it can be easily affected by parasites, a low-pass filter is needed at the input. The measuring scheme can be seen in the figure 4.?.

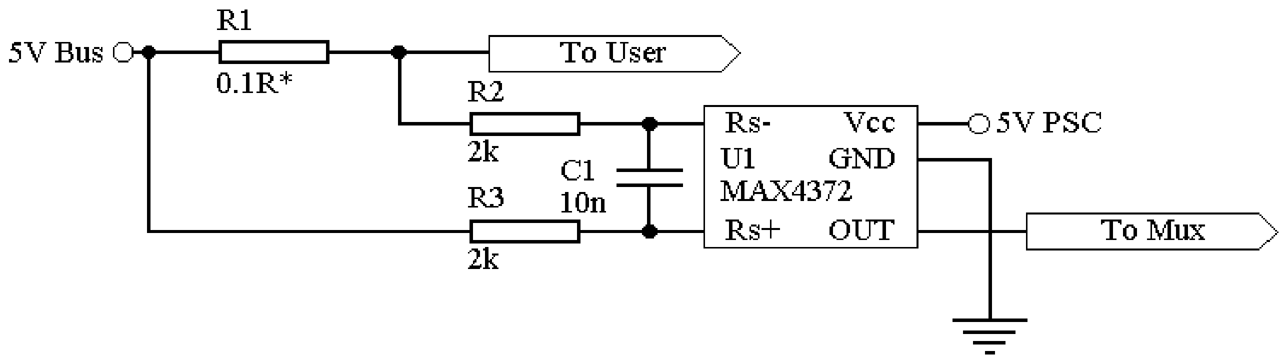

Figure 4.21 Current measuring circuitry

The differences between the measuring circuits for the current is the value for the resistor R_1 and the terminations of the MAX4372 IC's, which is indicating the voltage gain.

High-side current-sense amplifier MAX4372

The MAX4372 low-cost, precision, high-side current-sense amplifier is available in a tiny, space-saving SOT23-5 package. Offered in three gain versions (T = +20V/V, F = +50V/V, and H = +100V/V), this device operates from a single +2.7V to +28V supply and consumes only 30µA. It features a voltage output that eliminates the need for gain-setting resistors and is ideal for today's notebook computers, cell phones, and other systems where battery/DC current monitoring is critical. High-side current monitoring is especially useful in battery-powered systems since it does not interfere with the ground path of the battery charger. The full-scale current reading can be set by choosing the device (T, F, or H) with the desired voltage gain and selecting the appropriate external sense resistor. This capability offers a high level of integration and flexibility, resulting in a simple and compact current-sense solution.

Functional diagram

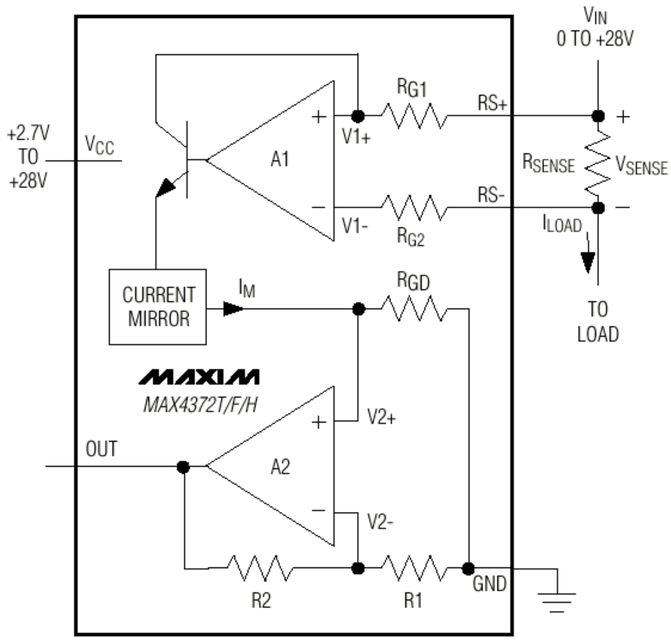

Figure4.22 Functional diagram for MAX4372

Features

- Low-cost, compact current-sense solution
- 30μA supply current
- +2.7V to +28V operating supply
- 0.18% full-scale accuracy
- Low 1.5Ω output impedance
- Three gain versions available:
  - +20V/V (MAX4372T)
  - +50V/V (MAX4372F)
  - +100V/V (MAX4372H)
- Wide 0 to +28V common-mode range, independent of supply voltage
- Available in space-saving SOT23-5 package

Pin description

Pin	Name	Function
1	GND	Ground
2	OUT	Output Voltage. V_{OUT} is proportional to the magnitude of V_{SENSE} (V_{RS+}-V_{RS-}).
3	V_{CC}	Supply Voltage
4	RS+	Power Connection to the External Sense Resistor
5	RS-	Load-Side Connection to the External Sense Resistor

Choosing R_{SENSE} (R_1)

Given the gain and maximum load current, R_{SENSE} will be selected such that V_{CC}-V_{OUT} does not exceed +0.25V. To measure lower currents more accurately, a high value for should be used for R_{SENSE}. A higher value develops a higher sense voltage, which overcomes offset voltage errors of the internal current amplifier. For monitoring high current, R_{SENSE} must be able to dissipate its own I^2R losses. If the resistor's rated power dissipation is exceeded, its value may drift or it may fail altogether, causing a differential voltage across the terminals in excess of the absolute maximum ratings.

Following the considerations above, the fact that the voltage drop on the shunt should be lower than 100mV and the voltage scale limit of 4.5V the recommended component values from datasheet and the available values for the shunt resistors it yields:

No.	Consumer	Current [A]	Maximum current [A]	Shunt resistor [Ω]	Gain [V/V]	Device	Full-scale output voltage [V]
1	Solar arrays	0.462	0.5	0.1	50	MAX4372F	2.5
2	Battery	0.5A	0.5	0.25	20	MAX4372T	2.5
3	OBC	0.092	0.3	0.1	100	MAX4372H	3
4	Transmitter	1.8	3	0.01	100	MAX4372H	3
5	Camera	0.06	0.3	0.1	100	MAX4372H	3
6	Attitude Control	0.05	0.3	0.1	100	MAX4372H	3

Table 4.5 Choose of components for currents measurements

Measurement of the voltages

The voltages measured are above the maximum input voltage for the multiplexer so, voltage dividers will be used at the input of the multiplexer. All the voltages will be processed by MCU after the conversion in digital.

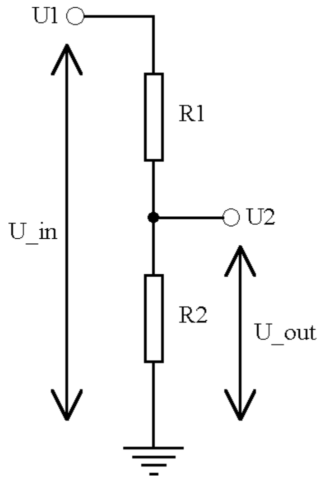

No.	Signal	Input voltage [V]	Output voltage [V]	R_1 [kΩ]	R_2 [kΩ]
1	Voltage on the solar panels	4.932	2.466	100	100
2	Voltage of the batteries	6-8.4	4.2	100	100
3	Voltage on the regulated bus	5	2.5	100	100

Figure 4.23 Values for resistors used in voltage measurement

For reducing power consumption have been selected big values for the resistances.

4.7.1. Measurement of temperatures

For housekeeping data and also for avoiding the critical state are useful values of temperatures inside the satellite. A system of 7 sensors will be distributed all over the satellite to measure temperatures on the most sensitive parts. This measure points will be selected in a virtue of thermal analysis. Results from these sensors can be used in thermal control.

The devices selected for temperature measurement must be as small as possible and must be able to operate in range of industrial standard (-55 to 85˚C). Communication with PIC controller must be also very simple, regarding to the number of wires used for communication with microcontroller. According to the specifications analog sensors are preferred, they need less wires for communication with multiplexer. Only voltage level will be sent to the multiplexer and then analog to digital converter, which is implemented in PIC controller will convert the value. For sticking device, epoxide or some special glue can be used. This system will be easy to implement and will be also very robust. The LM19 from National Semiconductors have been chosen to fulfill these specifications. The LM19 is a precision analog output CMOS integrated-circuit temperature sensor that operates over a -55°C to +130°C temperature range. Here are a few features and specifications. The attached CD contains datasheet for this sensor, also.

- rated for full -55°C to +130°C range
- available in a TO-92 package
- accuracy at +30°C ±2.5 °C (max)
- accuracy at +130°C & -55°C ±3.5 to ±3.8 °C (max)

- power supply voltage range +2.4V to +5.5V
- current drain 10 µA (max)
- nonlinearity ±0.4 % (typ)
- predictable curvature error

The accuracy of the LM19 when specified to a parabolic transfer function is ±2.5°C at an ambient temperature of +30°C. The temperature error increases linearly and reaches a maximum of ±3.8°C at the temperature range extremes. The temperature range is affected by the power supply voltage. At a power supply voltage of 2.7 V to 5.5 V the temperature range extremes are +130°C and -55°C. Decreasing the power supply voltage to 2.4 V changes the negative extreme to -30°C, while the positive remains at +130°C.

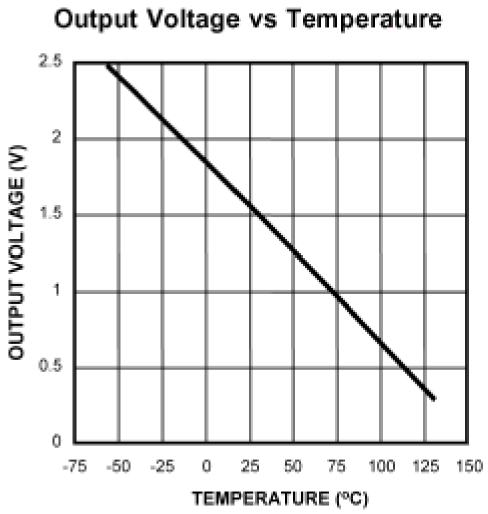

Temperature (°C)	Typical V_O (mV)
+130	+303
+100	+675
+80	+919
+30	+1515
+25	+1574
0	+1863.9
-30	+2205
-40°	+2318
-55	+2485

Figure 4.24 Output voltage vs. temperature and typical values for LM19

Shutdown capability for the LM19 is intrinsic because its inherent low power consumption allows it to be powered directly from the output of many logic gates or does not necessitate shutdown at all.

In figure 4.25 is depicted the implementation of temperature measurement. Power bus gives required voltage and the V_o is analog voltage output. For details see datasheet for LM19, on the attached CD of the report.

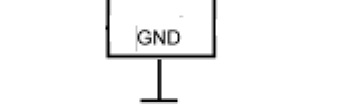

Figure 4.25 Temperature measurement circuitry

4.8. MCU – hardware and software

4.8.1. Selection of hardware

In the interface specification made by Cubesat steering committee [*interfaceV14.pdf*] are defined main parameters for hardware parts of MCU circuit and they must be fulfill. However, these parameters are only general and there is still lot of considerations to be done.

Microcontroller (MCU) must redeem these properties: it must have at least 12-bits analog-digital converter, supports I^2C bus in slave mode with 100kHz speed and it must acquire housekeeping data from the satellite. There are 14 electrical signals plus 7 temperatures to be measured.

From the demands can be evaluated minimum number of pins on the MCU. List of needed pins is on table 4.6. Number of pins for housekeeping data is calculated as a sum of needed analog input pins and digital control signals for multiplexers.

Name of the pin	Number of pins
Housekeeping data acqusition	7 pins
Boot pin	1 pin
Oscillator	2 pins
Power source	1 pin
Ground	1 pin
Fault signal from users	4 pins
Enable/Disable signal for users	4 pins
I^2C bus	2 pins
TOTAL	**21 pins**

Table 4.6 Description of needed pins

Another problem is program memory in the processor. Today's hi-tech FLASH technology could be used for space applications, but the probability that some high-energy particle from space will change memory is rising, to prevent this risk was decided to use OTP memories. For development is not good to have processor with no way how to erase it and reprogram again, so the chip that has been looking for was one with packages with erasable window (for debugging) and with OTP memory (for final product).

1. MCU

At the beginning was figured that 8-bit microcontroller is powerful enough for this task and there is no need to use processors that are more advanced. There is wide variety of types and families of 8-bit processors like AVR from Atmel, PIC from Microchip, Motorola 6800 family or

Intel 8051 family. Consumption of most of them is very high (for example 8051's consumption with 5V and 1MHz inner frequency is app. 100mW [*ADuC812_b.pdf*]), and low consumption is a priority number one for systems with limited electrical energy like Cubesat satellite. Also processors with reduced instruction set (RISC) have, because of their simplified inner structure very low consumption compare to the ones with wide instruction set. After these considerations was decided to search closely RISC microcontrollers.

After brief search of possible companies and also after consultations with other Cubesat's groups was decided to select one processor from Microchip, because ACS and COM modules will use this family so it is good idea to select same one for better compatibility and sharing development resources.

Last step was to decide which variant select. Removing chips without I^2C or without appropriate A/D converter or without enough pins only few possible solutions stayed. From them was selected PIC16C774, because it has parameters very corresponding with requested characteristics.

PIC16c774 is 8bit processor with reduced instruction set (RISC) manufactured in 40 and 44 pin packages. It has 10 possible inputs to the analog to digital converter with maximum speed of conversion 2µs.

It has two types of memory, for program it has 4kB OTP memory or 4kB EPROM memory (depending on package) and for data there is 256 bytes of RAM.

Processor has five input/output ports, where ports B, C and D are 8-bit ports, port A is 6-bit and port E is 3-bit. Not all ports can be used as a digital pins, because lot of functions are multiplexed with them (for example port A and E are multiplexed with A/D converter).

Among other features belongs PWM output, internal watchdog or low voltage detector. For more detail description, see datasheet [*30275a datasheet.pdf*].

2. Multiplexers

Multiplexer is simply described, digitally controlled switch among some inputs to the one output and the main purpose in the PSU is to collect more signals than there are free pins on the MCU. There are more possibilities which multiplexers use in PSU, as was written in specifications and analysis PSU will send 21 signals to OBC. In that case, two 16 to 1 channels multiplexers can be used or three 8 to 1 channels multiplexers are also possible. 8-1 muxes have less control wires, they need only three compare to four for 16-1 muxes, but they need one more analog input and more space on PCB, actually they are smaller but with all power supply wires and control signals result will be the same as with 16-1muxes. Finally two 16-1 multiplexers were chosen. Another advantage of them is that at this moment, only 21 signals are measured, but if in the future anyone will want to add signal, there will be no problem with it at all. As a conclusion were selected multiplexers from Analog Devices ADG706, which have very small R_{on} resistance 2.5Ω [*ADG706_7_0.pdf*], and they have acceptable size (10mmx6.5mm).

3. Switching between MPPT signals

Because there will be three types of driving signals for MPPT converter, there must be switch among them. From this is clear that some sort of arbitrate system is needed. Digital controlled switch consists only from one 4 to 1 channel multiplexer, 3 to 1 multiplexer should be sufficient for it, but they are not common on the market. Deeper look inside the problematic is done in another chapter. Final decision was made to use another multiplexer from Analog Devices (ADG704), because of their low R_{on} resistance [*ADG704_a.pdf*].

4. Oscillator

The oscillator is one of the most important parts in MCU circuits and there are more ways how to guarantee frequency for MCU: Resonant crystal, resonant oscillator or resonant *RC* circuit. First two variants are very precious, but they are sensitive to mechanical ripples and their maximum mechanical stress is 10G [*7702.pdf*] what is starting to be close to the launching start stress (7G) [*Hansen, 2001*]. After comparing these facts was decided to use resonant *RC* circuit, which is not too precise and is vulnerable to temperature, but for tasks, which MCU is going to be used, precise timing is not needed. Does not matter if frequency is 3MHz or 5MHz. This oscillator consists only of two components and these components are simple resistor and capacitor, reliability of this circuit is much higher compare to resonant crystal. On figure 4.1 is shown connection of RC circuit to MCU.

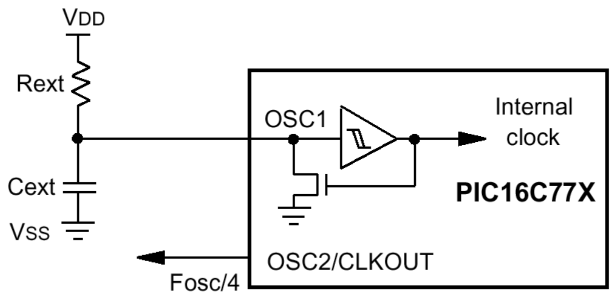

Figure 4.26 Scheme of RC oscillator

Following the recommendations from manufacturer [*Mid-Range MCU Family Reference Manual, p. 2-12*], where they recommended resistance between 3k and 100kΩ and capacitance above 20pF. Values for R_{EXT} and C_{EXT} have been selected R_{EXT} = 4.7kΩ and C_{EXT} = 22pF (experimental approach to obtain 4MHz frequency).

4.8.2. Hardware design

1. Connection of protection circuits

Protection circuits need eight digital signals for their right function. Four of them are inputs and the rest are outputs, each user has it's own pair of these signals. Input signals are called NOT_FAULT signals, because when this signal is in high state, the user works fine. When the low state is set means that protection circuit detected overcurrent. Second signal is ENABLE and provide turn on/off signal for protections. When ENABLE is in the high state user is turn on.

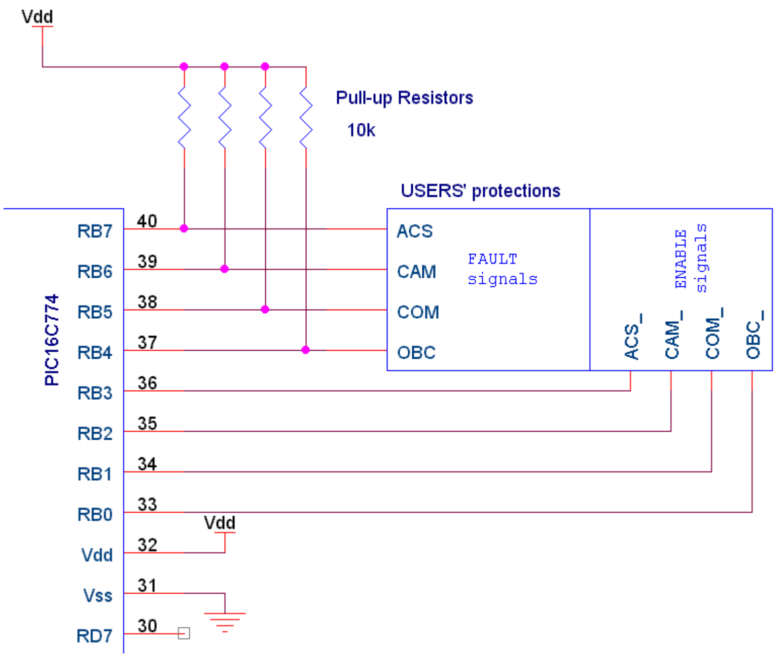

Figure 4.27 Connection of protections

Because protection circuits work as a current limiter, MCU do not need to provide turn-off of the users too quickly, but still it is better to turn off user at least in few ms. PIC16C774 has good technical solution for this problem; it is called "interrupt on change on port B". Simply explained: MCU run interrupt routine when change from low to high state (or high to low state) on port B (bits 4,5,6 and 7) occurs. When using interrupts, user could be turn off in few moments. Usually for input pins are needed pull-up resistors, otherwise signal should not has perfect high state (low level is done by connecting to the ground and high level is done by not connecting anywhere and wire is "in the air"). Solution for this these pull-up resistors, there is already weak pull-up resistors inside the MCU, but they can be used only when they are set by software. To be sure that signal will correct value was decided to use external ones too, these external pull-up resistors are already part of protection design so no more component will be added (see section 4.5).

Enable signals may be connected to any output pin on MCU, but to have all things around protections on one place, it is good to use rest of pins from port B for ENABLE.

2. Signals connection

All signals collected from PSU are connected to the MCU through the multiplexers, but because not all signals have same priority or voltage levels, some design changes must be implemented.

There are two main groups of signals: electrical and thermal. Because temperature cannot change too fast, it is not needed to read thermal sensors so often as electrical signals. All electrical signals should be put together to one multiplexer and thermal sensors to another one. The second multiplexer will be read only every few seconds. More details about this can be found in section 4.8.3.

Because analog/digital converter can convert voltages in resolution V_{ref-} to V_{ref+} (in this case from 0 to 5V), signal connected to the ADC cannot be higher or lower than these values. To decrease the voltage level a voltage divider is used, rate ½ is used for better digital processing (multiplication by two is done just by adding same value). It means all three measured voltages (solar panels, batteries and 5V bus) will be twice smaller. Rest of the signals (currents) can be measured directly.

For thermal sensors used in the satellite (LM19), which have maximum voltage around 3V, no voltage divider is needed and mux2 can be directly connected to the ADC. The scheme of implementation for the MCU is shown in Appendix C.

Each multiplexer must be driven by four control signals. Because there is no need to read both multiplexers at the same time, these four signals from each multiplexer can be connected together and only four wires connected to any four output pins on the MCU.

3. Power source connection

Separate analog and digital power supply pins (V_{dd} and AV_{dd}, respectively) allow AV_{dd} to be kept relatively free of noisy digital signals often present on the system V_{dd} line. Connection scheme is presented in figure 4.28. Smaller capacitors (0.1μF) must be connected as close to the power pins as possible to keep trace lengths short.

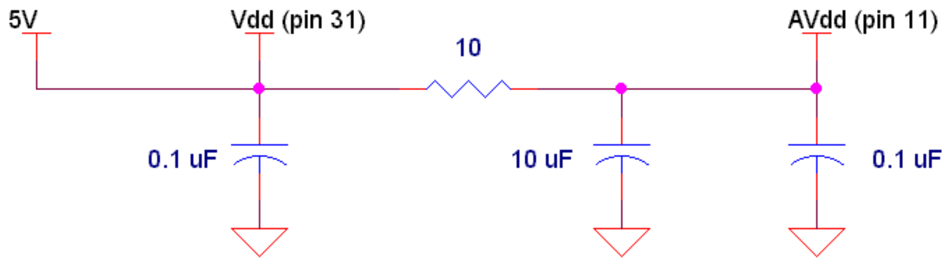

Figure 4.28 Power source connection

4. Digital MPPT circuits

For digital version of MPPT controller is needed an analog output in range from 0 to 1.5V. Unfortunately, the PIC16C774 does not have any D/A converter included. This problem can be override with MCU's PWM output and all what is needed is a low-pass filter to create an analog signal. Because MCU will run on low frequency to lower power consumption, PWM cannot run too fast without loss of resolution. Resolution was selected 9 bits when voltage step should be:

$$MaxStep = \frac{V_{REF}}{2^{rezolution}} = \frac{5(V)}{2^9} = 10(mV) \tag{4.36}$$

and the frequency can be up to 7.4kHz.

The output signal of the filter will be MPPT control signal and this signal is changing only in dependence on rotating of the satellite or when temperature change. These changes are relatively slow and bandwidth of this signal should be very low, only few hertz (it was established 100 Hz). That is the reason why 7.4KHz will be enough for PWM frequency. Values for the filter were counted from the following relation:

$$R \cdot C = \frac{1}{2 \cdot \pi \cdot f} \tag{4.37}$$

and if C is chosen as 330nF , a resistance $R = 4.8\text{k}\Omega$ is the result.

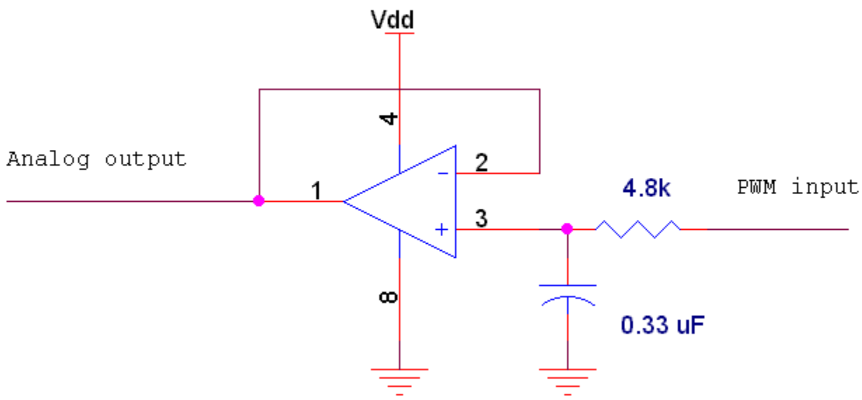

Figure 4.29 Low pass filter for PWM signal

5. System for arbitrating MPPT signals

As a system for selecting which system will drive MPPT converter was selected 4->1 multiplexer, controlled by MCU. This MCU will watch the analog signal and after it will stop work, MCU switch to another source (digital or default), when MCU hang or crash and will be unable to control multiplexer, watchdog will reset MCU and default values will be set on the pins (logic 0) and this default values on the multiplexer will select default MPPT signal (see the truth table on table 4.7).

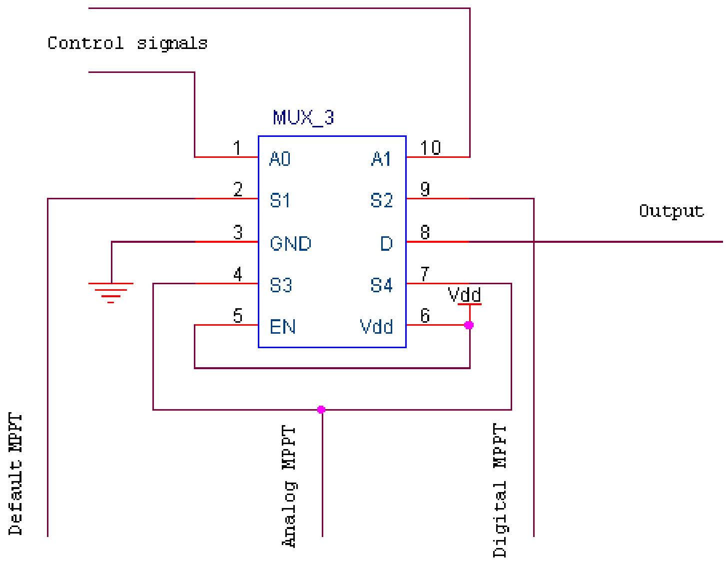

Figure 4.30 Arbitrating system

Output	A0	A1	EN	MPPT
S1	0	0	1	Default
S2	1	0	1	Digital
S3	0	1	1	Analog
S4	1	1	1	Analog
N/A	X	X	0	N/A

Table 4.7 Truth table for MUX3

4.8.3. Software for MCU

1. Basic structure

There are two main parts of the software. The first one, which is time crucial, was created as interrupt service routines. Time is important for serial communication and for protections. For the rest is not needed that fast response and they could be done as a normal code in main loop.

On figure 4.31 is displayed the structure of both parts.

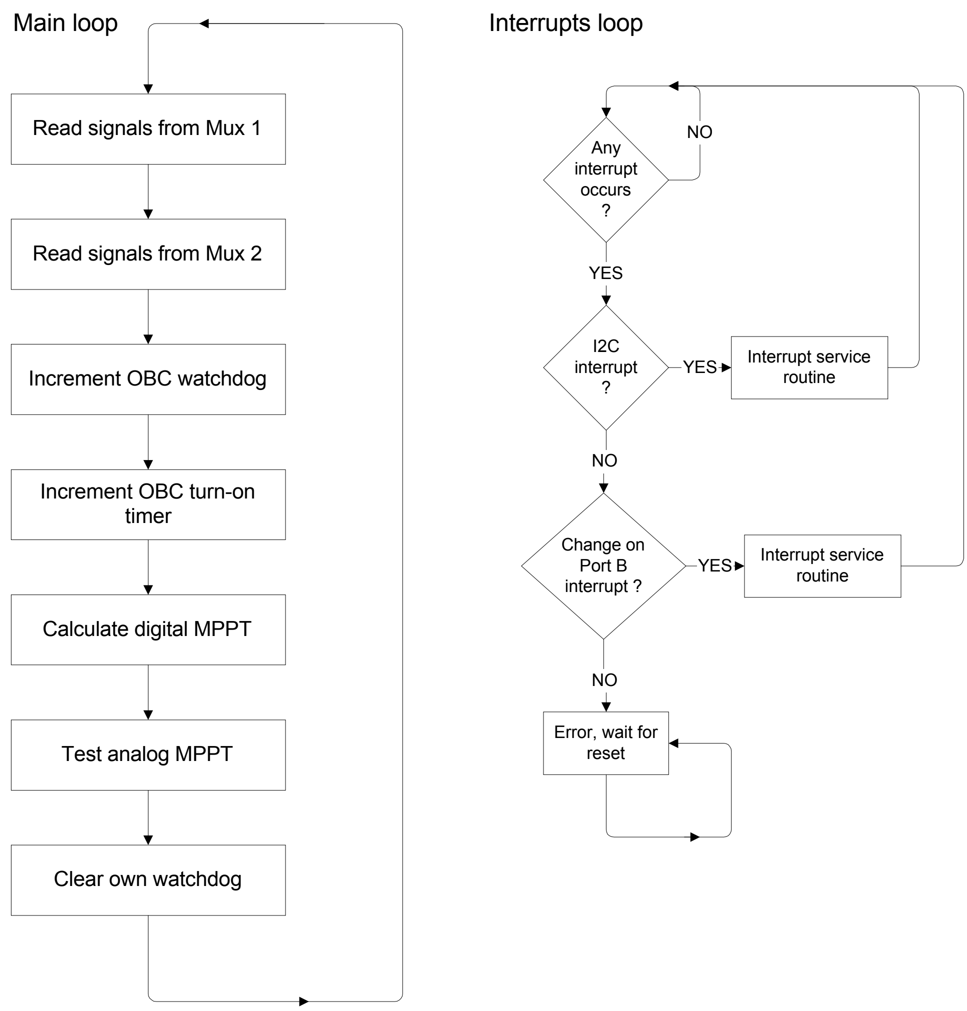

Figure 4.31 Program structure

2. Protections

Protections are systems, which need relatively fast response. It was decided to use interrupt routines to service them. After any change occurs on the pins configured as the inputs for NOT_FAULT signals, software will detect which users has overcurrent and turn off that user. The flowchart, describing algorithm, is depicted in figure 4.32a.

3. Data acquisition

Converting signal from analog voltage to digital number is very important task for MCU, because most of the functions of the MCU depending on these signals. An error in data acquisition will cause another errors in other parts of software. PIC16C774 has implemented 12bit A/D converter, which implies that for each sensor is needed two bytes of memory (not all bits will be used in these two bytes). These two bytes will be overwritten every time ADC converts updated value. No past values are stored, for calculating average, maximum or minimum values special software should be in the OBC. The algorithm of reading signals is explained on figure 4.32b.

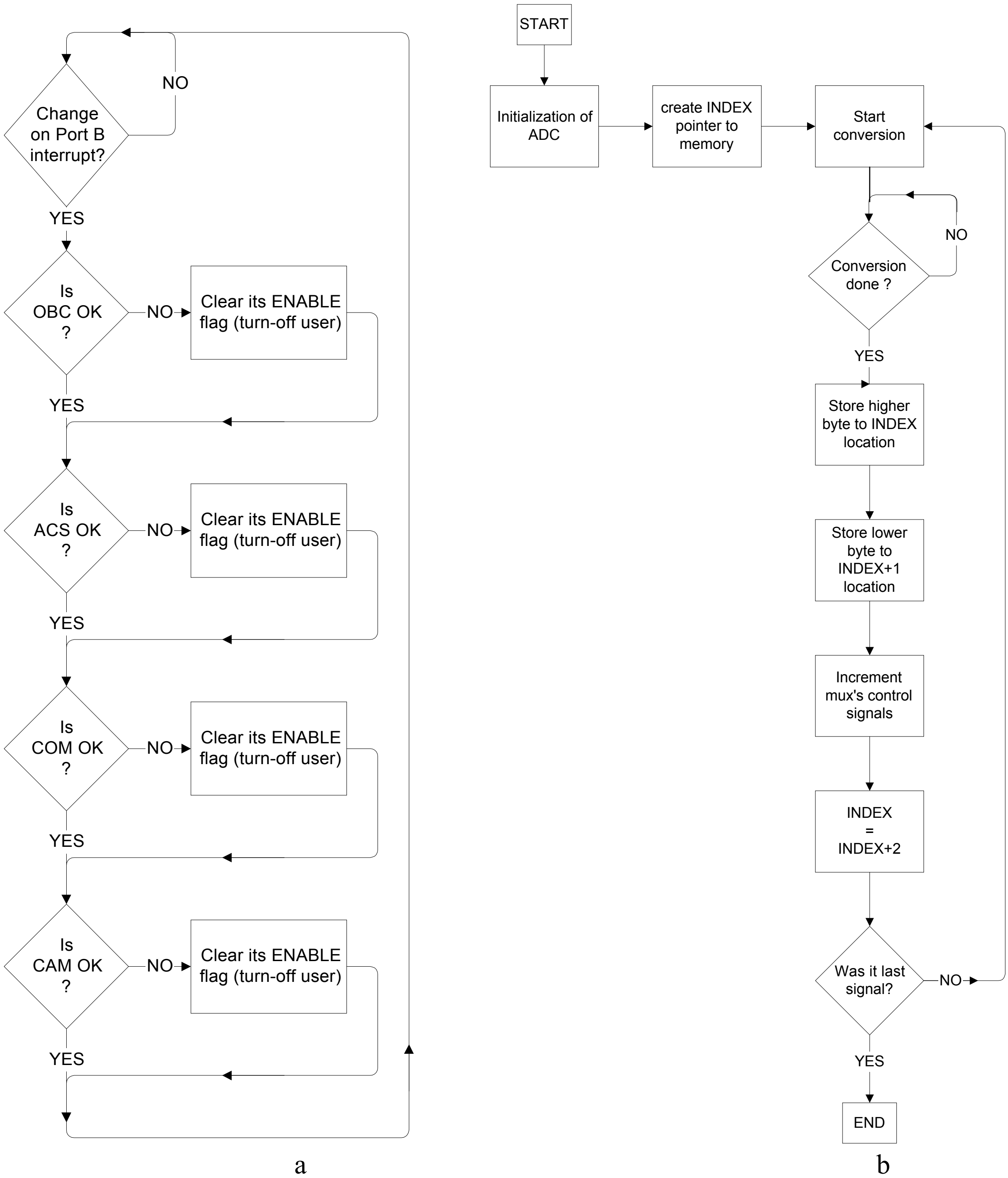

Figure 4.32 Protections' interrupt service routine (a) and algorithm for reading signals from mux1(b)

Figure 4.32b is only for one multiplexer, but both multiplexers have same function, only memory places and input pins are changing. Another difference is that values from mux2 are voltages from temperature sensors and these voltages will be converted to the degrees of Celsius. Because accuracy of the sensor is app. ± 3°C there is no need for 12-bit number and was decided to use 8-bit for better manipulation. Further was decided to use binary complement format for numbers (-1 is FFh, 0 is 0h and 1 is 1h and so on, numbers can be from –127 to 128). The fastest way how to convert numbers is to use look-up table with pre-calculated values from approximation equation for sensor [*LM19.pdf*].

$$T = \frac{1.8528 - V}{0.01179} \tag{4.38}$$

where T is the temperature [°C] and V is measured voltage [V].

4. I^{2}C bus communication

I^{2}C is two wires bi-directional bus; PSU will work as a slave on this bus. [*I2C-busv1_7.pdf*]. Each byte, which should be sent to PSU from OBC, is stored in SSPBUF and then interrupt is created. After MCU read that byte, OBC can continue with sending another byte. Similar is it with writing to bus; only interrupt is created each time when OBC read successfully byte, which MCU send through SSPBUF to the bus.

Data buffer

Because housekeeping data should be collected also during sending them to OBC, I^{2}C cannot send data directly from places in the memory where ADC saved them, because they can be changed there during transmition. It was decided to use another place in the memory to store whole module in some sort of buffer, its structure is on figure 4.33. When OBC request first byte from new module, MCU first fill this buffer with values from ADC and compute CRC and header. After OBC request another bytes, only index pointer will be incremented and prepared byte will be sent.

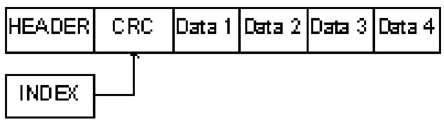

Figure 4.33 Structure of the buffer

States of the I^{2}C bus

There are five possible states on I^{2}C bus:

- State 1, Master will send data to slave and byte, which is in the SSPBUF is the address of the PSU and nothing will be done with this byte
- State 2, Master sends data to slave and byte, which is in the SSPBUF, is data package and must be read and processed.
- State 3, Slave will send data to the OBC and in SSPBUF is PSU address. Buffer must be filled and CRC calculated. Then HEADER will be written to the SSPBUF as a first byte of the module.

- <u>State 4,</u> Slave sends data to the OBC and module sending is in progress, byte where INDEX pointing will be written to the SSPBUF and after INDEX will be incremented.
- <u>State 5</u>, Master resets I2C logic, all buffer and INDEX pointer will be cleared.

Description of modules

For communication with OBC were created two types of modules, one for each direction of communication. Each module includes header and CRC and could include four bytes of data. Inner structure of the header is on figure 4.34. CRC is calculated as a sum of all bytes in module (header + data). For more detailed information about header and CRC see [*I2C-busv1_7.pdf*].

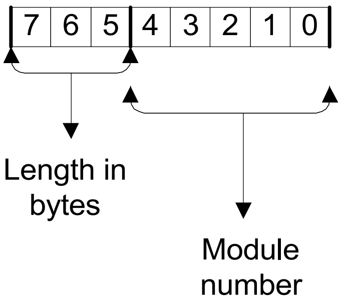

Figure 4.34 Structure of the header byte

Module nr.	1st byte	2nd byte	3rd byte	4th byte
1	Battery voltage (Higher byte)	Battery voltage (Lower byte)	Current from MPPT (Higher byte)	Current from MPPT (Lower byte)
2	SC 1 current (Higher byte)	SC 1 current (Lower byte)	SC 2 current (Higher byte)	SC 2 current (Lower byte)
3	SC 3 current (Higher byte)	SC 3 current (Lower byte)	SC 4 current (Higher byte)	SC 4 current (Lower byte)
4	SC 5 current (Higher byte)	SC 5 current (Lower byte)	SC voltage (Higher byte)	SC voltage (Lower byte)
5	5Volts bus voltage (Higher byte)	5Volts bus voltage (Lower byte)	PSU current (Higher byte)	PSU current (Lower byte)
6	Temperature 1	Temperature 2	Temperature 3	Temperature 4
7	Temperature 5	Temperature 6	Temperature 7	Protection status flag
8	OBC current (Higher byte)	OBC current (Lower byte)	CAM current (Higher byte)	CAM current (Lower byte)
9	COM current (Higher byte)	COM current (Lower byte)	ACS current (Higher byte)	ACS current (Lower byte)
19	This module has no data inside, this module will be send as a error message after wrong recalculation of CRC of message from OBC.			
20	This module has no data inside this module will be send as a OK message after successful recalculation of CRC from OBC			

Table 4.8 Modules from PSU, for OBC

Modules for communication from PSU to OBC are described in table 4.8. Modules for the other direction do not have any data inside; they consist only from header and CRC, which must be same as header. Modules from OBC are described in table 4.9.

Module nr.	Description	Module nr.	Description
1	Request for module nr.1, PSU will send module nr.1 next time.	22	Turn off ACS command
2	Request for module nr.2	23	Turn off CAM command
3	Request for module nr.3	24	Turn off COM command
4	Request for module nr.4	25	Turn on OBC command
5	Request for module nr.5	26	Turn on ACS command
6	Request for module nr.6	27	Turn on CAM command
7	Request for module nr.7	28	Turn on COM command
8	Request for module nr.8	29	Reset watchdog
9	Request for module nr.9	30	Clear bootpin (OTP PROM)
21	Turn off OBC command	31	Set bootpin (EEPROM/FLASH)

Tab 4.9 Modules from OBC, for PSU

I^{2}C data flow algorithms

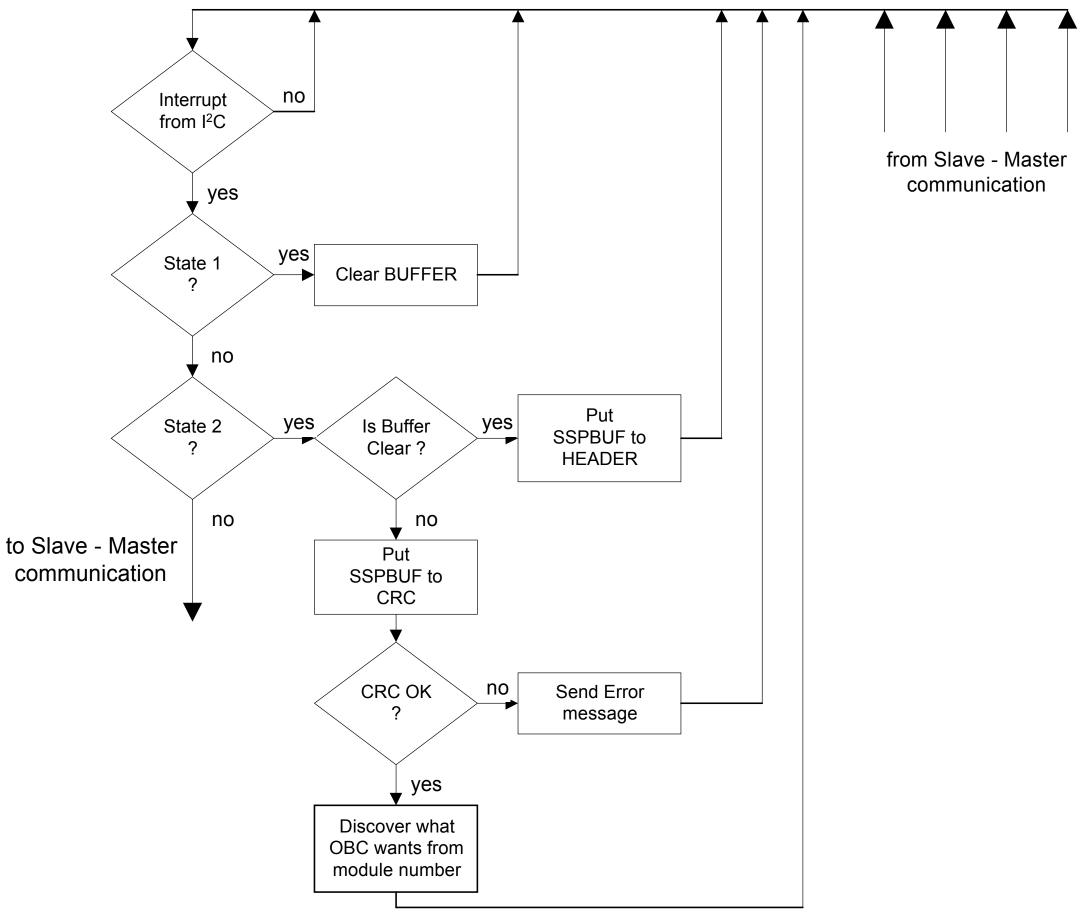

Figure 4.35 Communication from master to slave

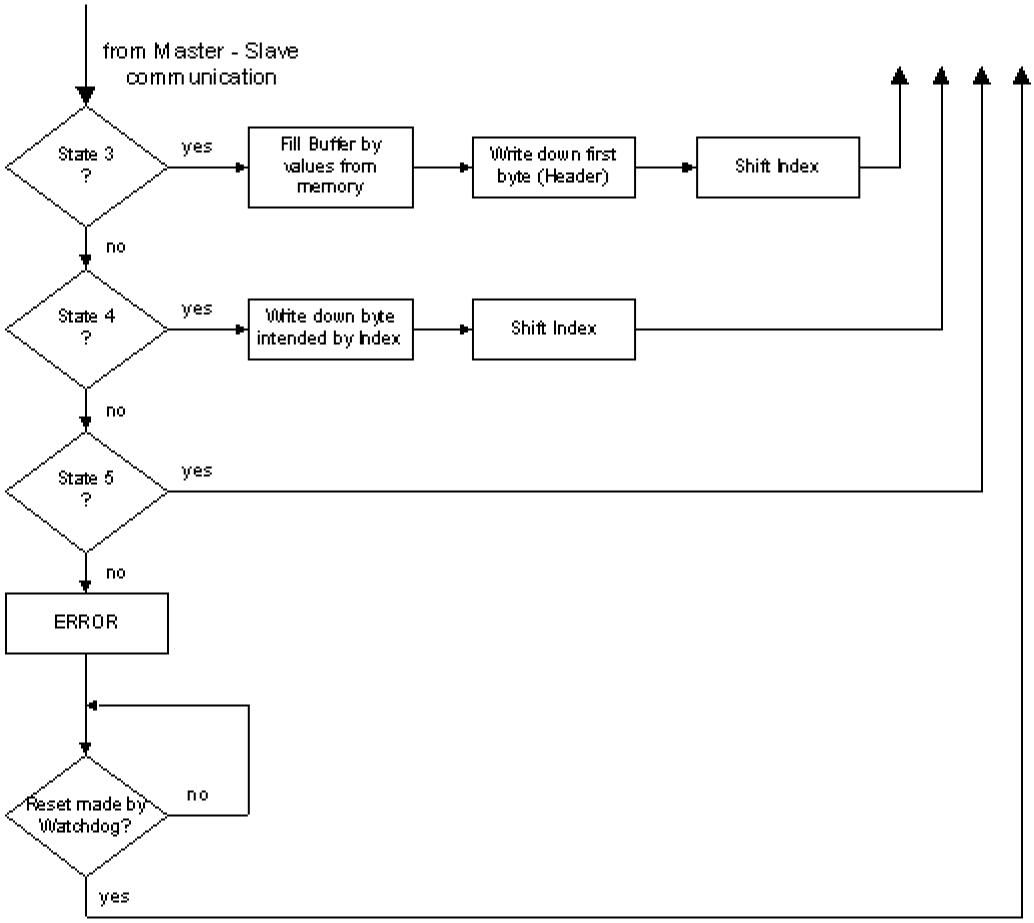

Fig 4.36 Communication from slave to master

5. Special software for OBC

External watchdog and software timer

This program will provide watchdog for the OBC. As a reset of this watchdog serves any module received from the OBC. If the PSU will not receive anything from the OBC in 10 seconds, the program will turn-off OBC (put enable signal for OBC low state).

The OBC watchdog algorithm is depicted in figure 4.37a.

When OBC is turned off, the PSU itself must provide repeated turn-on signal after some time, which was decided to be 5 minutes. That is enough time to get out the OBC processor from dangerous states. The timer algorithm is described in figure 4.37b.

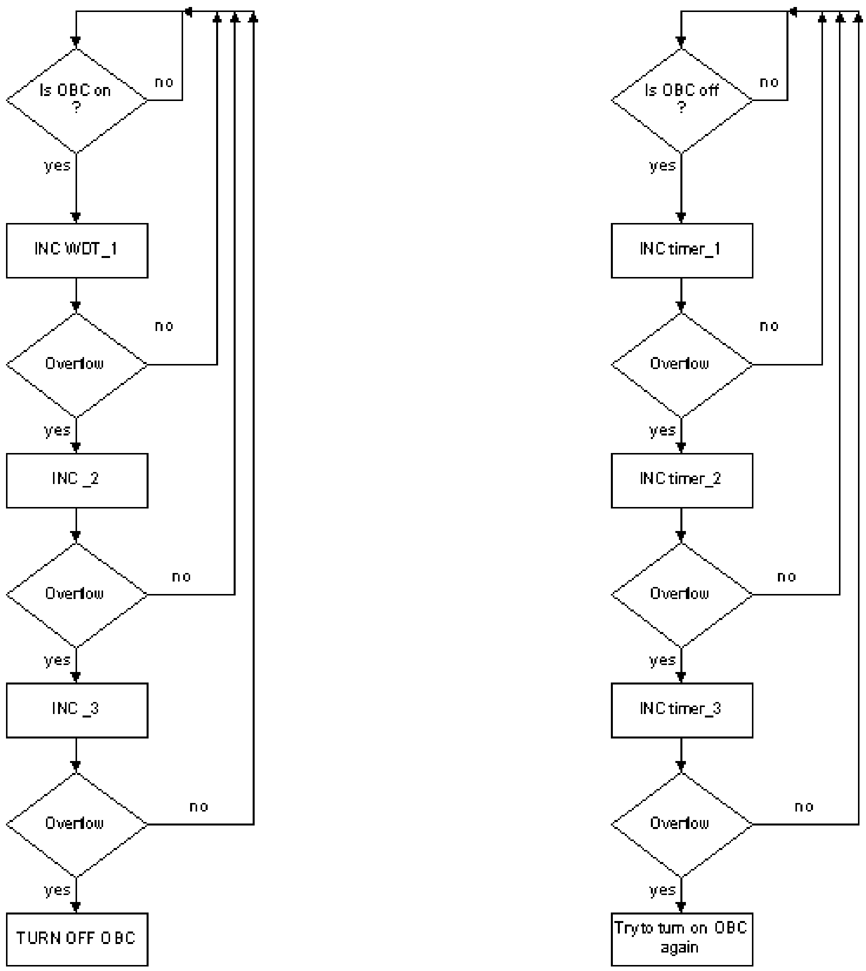

a b

Figure 4.37 OBC watchdog algorithm (a) OBC timer algorithm (b)

6. Arbitrage for MPPT signals

This part of software will guard signal from analog MPPT controller. If this signal is smaller than 30mV, program will turn-on software timer and after two minutes, if any signal is still not on analog MPPT, it will switch to another MPPT control source. If anytime in the future, an analog signal will be received from the MPPT, the program will switch back to it immediately.

7. Bootpin control

After the PSU receives module no. 30 from OBC (see table 4.9), the bootpin will be set to low level. When receiving module no. 31, the bootpin will be set to high level. The PSU will just follow the commands from OBC. After the reset of PSU's microcontroller, the bootpin will be set to low level.

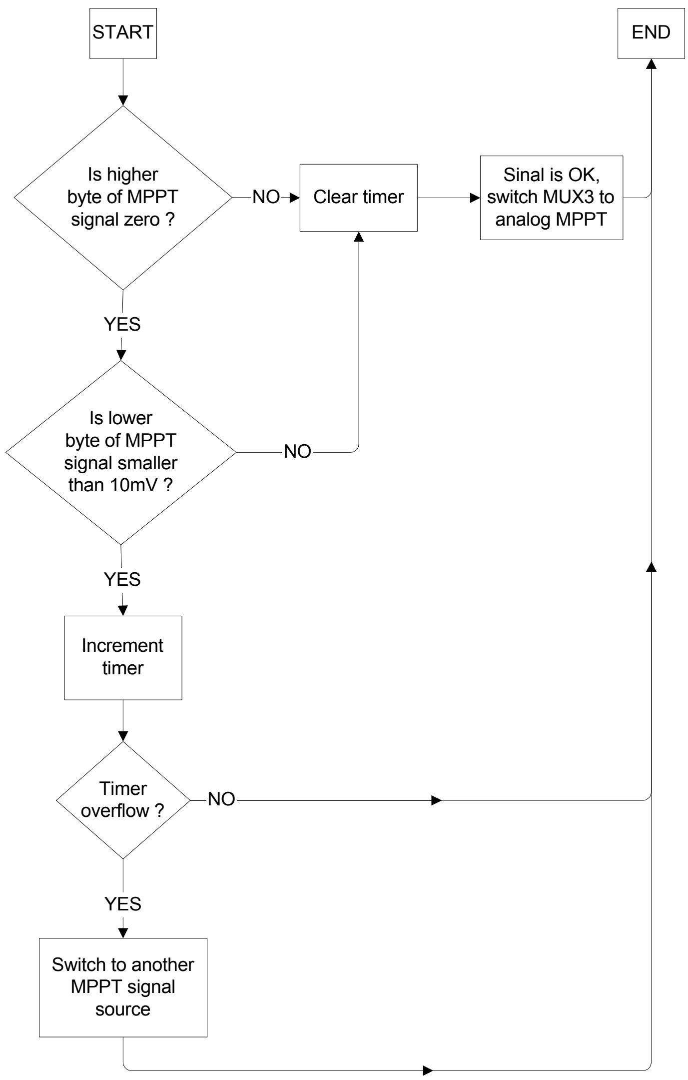

Figure 4.38 Testing algorithm for analog MPPT

8. Digital MPPT algorithm

The use of the microcontroller offers the possibility to implement a digital MPPT algorithm. Comparing to the analog one it has some significant advantages:

- Higher flexibility: it is very easy to add modifications and improvements for the algorithm.
- Lower size and mass: it is needed only the microcontroller and a operational amplifier with an input filter.

Everything is based on a fact that the used algorithm can be much more sophisticated than analog one. Of course, analog MPPT can be also very complex, but the weight and the size of system is increasing with complexity. In case of software it means few new rows in a program.

An *Incremental Conductance MPT Algorithm* (ICA) was chosen to implement. The biggest advantage of this new algorithm is, that when the proper value of maximum power point is found, than there are no other losses. This algorithm consist in comparison new measured values with previous values.

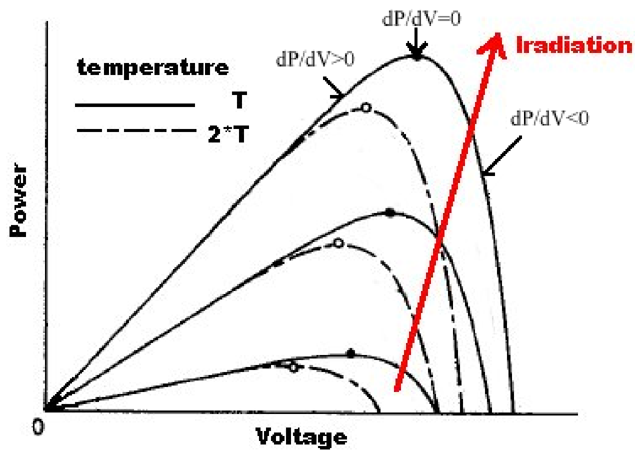

Figure 4.39 P-V curves for solar panels

As it can be seen on figure 4.39 *Maximum power operation point* (MPOP) is when $dP/dV = 0$. If the operation point is to the left of the MPOP then with increasing voltage the power is also increasing. If the operation point is to the right of the MPOP than the power is decreasing with increasing voltage. It can be written in this three formulas:

$dP/dV = 0$ at the MPOP,

$dP/dV > 0$ to the left of the MPOP,

$dP/dV < 0$ to the right of the MPOP.

If it is taken into account that $dP/dV = d(I \cdot V)/dV = I + V \cdot dI/dV$, than it is possible to rewrite previous equations as follow:

$dI/dV = -I/V$ at the MPOP,

$dI/dV > -I/V$ to the left of the MPOP,

$dI/dV < -I/V$ to the right of the MPOP.

In case of constant voltage, $dV = 0$, may change current its values. Than can be written relation for three possible conditions like this:

$dI = 0$ at the MPOP,

$dI > 0$ to the left of the MPOP,

$dI < 0$ to the right of the MPOP.

From all equations above can be easily drawn flowchart for ICA.

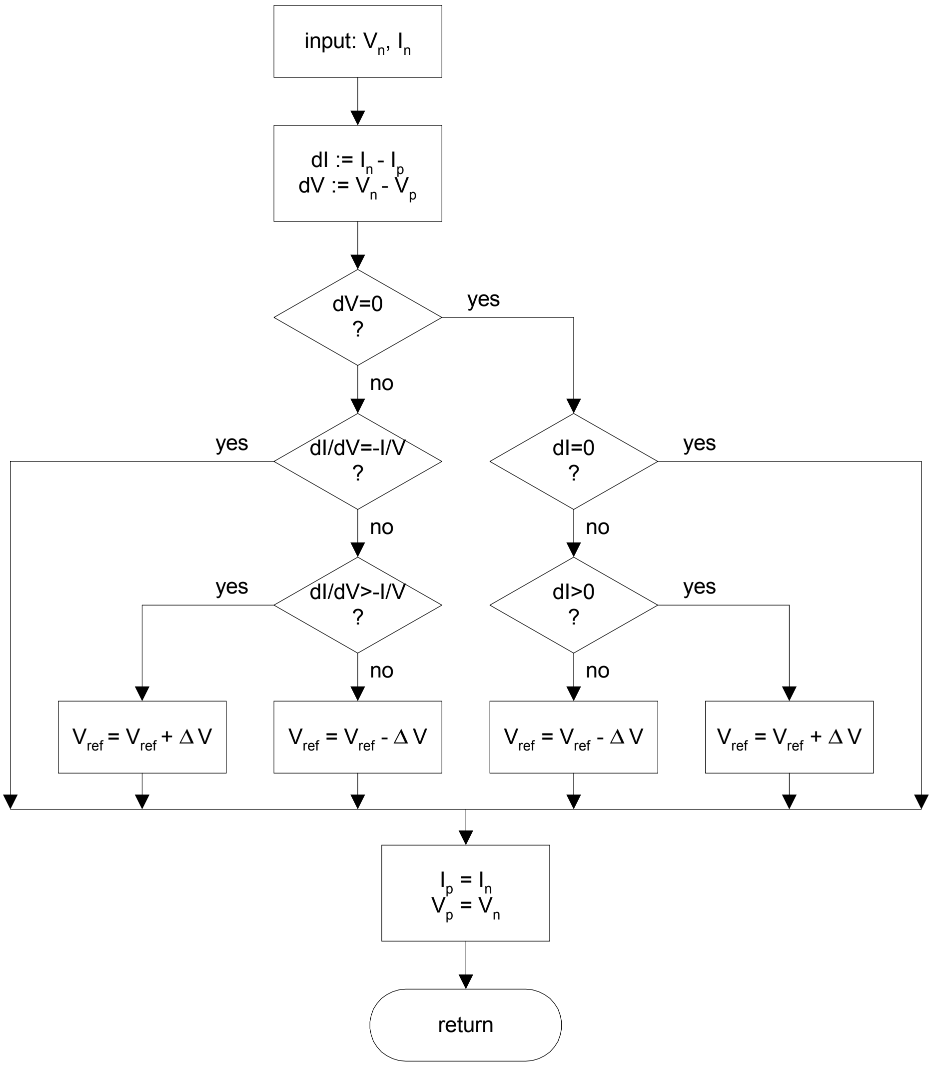

Figure 4.40 Flowchart for ICA

At the beginning of the algorithm is read the new values of *I* and *V*. Then is making differential of voltage and current by subtraction of new (*n*) and previous (*p*) values. Previous values are stored at the end of each preceding cycle. According to results from decision functions is set up a new value of reference voltage (V_{ref}) by either addition or deduction of nominal step **ΔV**.

4.9. Power supply for Power Supply Circuits

For supplying the circuits of the power supply it was chosen the linear regulator LM78L05 fed directly from the unregulated bus. Two main considerations were used for choosing this device. The first one was the small consumption of the circuits used in the interior of the power supply, so the power loses due to the linear regulation are neglectable. The second one was the fact that this IC is self-protected in case of a shortcircuit at the output and overtemperature.

Linear regulator LM78L05

General Description

The LM78L05 is three terminal positive regulator. When used as a zener diode/resistor combination replacement, the LM78L05 usually results in an effective output impedance improvement of two orders of magnitude, and lower quiescent current. The regulator can provide local on card regulation, eliminating the distribution problems associated with single point regulation.

The LM78L05 is available in the plastic TO-92 (Z) package, the plastic SO-8 (M) package and a chip sized package (8-Bump micro SMD) using National's micro SMD package technology. With adequate heat sinking the regulator can deliver 100mA output current. Current limiting is included to limit the peak output current to a safe value. Safe area protection for the output transistors is provided to limit internal power dissipation. If internal power dissipation becomes too high for the heat sinking provided, the thermal shutdown circuit takes over preventing the IC from overheating.

Features

- LM78L05 in micro SMD package
- Output voltage tolerances of ±5% over the temperature range
- Output current of 100mA
- Internal thermal overload protection
- Output transistor safe area protection
- Internal short circuit current limit
- Available in plastic TO-92 and plastic SO-8 low profile packages
- No external components

Typical Application

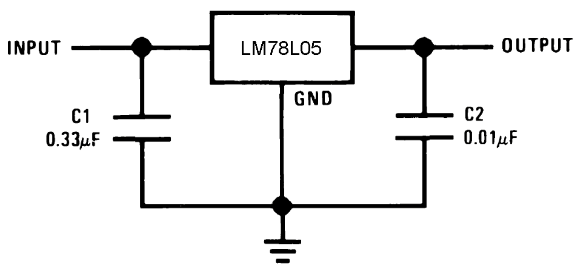

Figure 4.41 Typical application circuit for LM78L05

4.10. Summary

This chapter presents the implementation of the practical circuits that can be found in the power supply subsystem. All the most important modules have been detailed and computations performed. An important space is reserved for description of the devices used. It has been tried to use small outline components, due to the constrains about mass and geometrical dimensions for the power supply board, detailed previously in Chapter 2.

The functioning of the MCU used for the power supply board is described in section 4.9. Various flowcharts for specific parts of software are presented. Also, there is included an algorithm for the digital MPPT, as an alternative to the analog one, already implemented and described in section 4.1. For supplying the components on the board, it has been chosen a self-protected 5V integrated power supply, described briefly in section 4.9.

Chapter 5
EMC and thermal analysis

Abstract

This chapter deals mainly with problems related with the thermal analysis for the power supply subsystem and for the whole satellite. A section about electromagnetic compatibility is also included.

5.1. Introduction

An important space in the present chapter is reserved for the thermal analysis. The mechanisms of the heat transfer are presented, as well as some methods of thermal modeling and control. It is important to have a control of the temperature inside the satellite, due to the hostile environment in which the electronic components and other parts have to function. The analysis is performed in several sections, starting with section 5.2.

Some basic knowledge about electromagnetic compatibility (EMC) is presented in section 5.5. This part contains also some recommendations to follow in order to avoid electromagnetic interferences and to minimize the parasitic emissions, due to digital circuits or power electronic circuits.

5.2. Thermal analysis

One of the necessary parts of Cubesat's design is the thermal analysis. It will provide us operating temperatures an their distribution for all device inside satellite. For decision, which temperature standard can be used for components it is necessary to know the maximum and the minimum value of temperature. In virtue of this results the position of the all device must be also optimized. Some methods for thermal control are also proposed. There are two main source of heat in Cubesat, the Sun from outside and the electrical power from inside generated by all working components

5.2.1. Conditions for Low Earth Orbit

In Chapter 2, section 2.4, the specifications for the Low Earth Orbit are described. As it has been shown in section 2.3.1 (Table 2.1), the heat in space comes from three main sources:

- The Sun – energy 1358±5 [W/m^2]
- Albedo – energy 406 [W/m^2]
- Infrared – energy 237 [W/m^2]

The temperature surrounding the satellite in space is 2.7K and the pressure surrounding is very close to vacuum. In figure 5.1, are illustrated the sources of heat in space [*Sellers, p.67, 1994*].

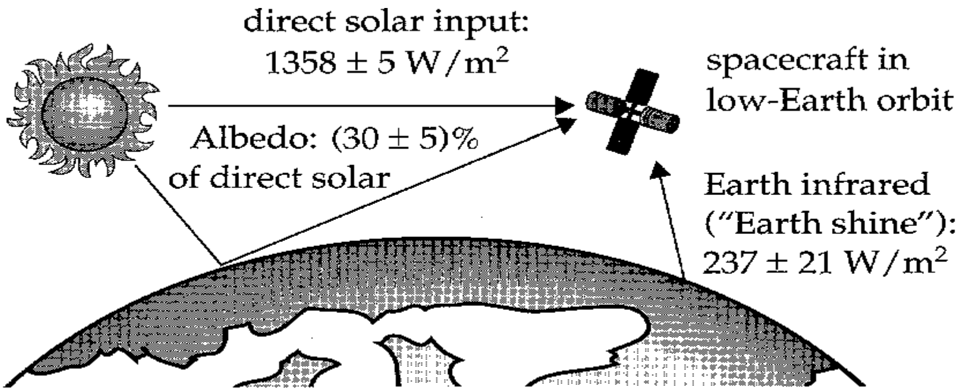

Figure 5. 1 Sources of radiation in space

5.2.2. Heat transfer

There are three mechanisms by which thermal energy is transported:

1. Convection
2. Conduction
3. Radiation

In space convection can be neglected. As said before, the surrounding temperature in space is 2.7°K, very close to absolute zero. Then there is no transfer between hot and cold air as on the Earth. The vacuum is also cause for this problem, because there is no difference in density of gasses.

Conduction

In definition of heat transferred through conduction, the following formula is used:

$$P_{cond} = \frac{\lambda \cdot A \cdot \Delta T}{L} \tag{5.1}$$

where λ is thermal conductivity [J/s·m·K]

A is a cross section area [m^2]

L represents the length of the conduction path [m]

ΔT is difference temperatures between the two bodies, T_1 and T_2

In figure 5.2 is shown an illustration of the heat conduction mechanism.

Thermal resistance is defined by formula:

$$R_{th\_cond} = \frac{\Delta T}{P_{cond}} [\text{K/W}] \tag{5.2}$$

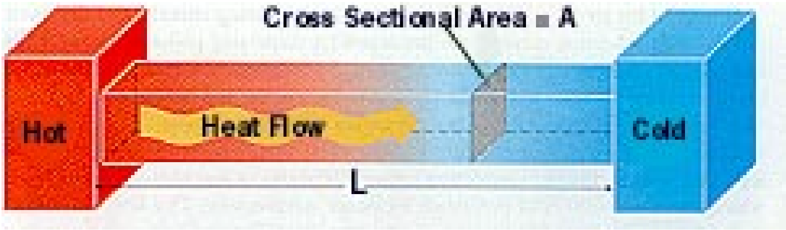

Figure 5.2 Illustration of heat conduction mechanism
[http://sol.sci.uop.edu/~jfalward/heattransfer/heattransfer.html]

Replacing the expression of P_{cond} from equation (5.1), it yields:

$$R_{th\_cond} = \frac{L}{\lambda \cdot A} [\mathrm{K/W}] \tag{5.3}$$

Conduction will apply only for components on the same board and R_{jc} (thermal resistance junction case) can be assumed as a thermal resistance for this transfer.

Radiation

All matter and space contains electromagnetic radiation. A particle of electromagnetic energy is a photon, and heat transfer by radiation can be viewed either in terms of electromagnetic waves or in terms of photons.

For calculation of the amount of heat transferred through radiation is valid Stefan-Boltzmann law:

$$P_{rad} = \varepsilon \cdot \sigma \cdot A \cdot T^4 \tag{5.4}$$

where, ε = emissivity (value between 0÷1)

σ = Stefan-Boltzmann constant equal with $5.67 \cdot 10^{-8}$ [W/m^{2}K^4]

A = surface area of object [m^2]

T = temperature [K]

From this equation may be observed that for modifying the radiated power for an object, the only parameter which can be changed is the emissivity of radiating object, supposing that the object maintains its physical dimensions. This can be realized by modifying the color and surface of component. Figure 5.3 shows the difference between the absorbtion and emission of radiation. [http://sol.sci.uop.edu/~jfalward/heattransfer/heattransfer.html]

For a dark-color material, the absorbtion of a radiated amount of heat is higher than for a light-color material, supposing the same geometric dimensions for the two bodies.

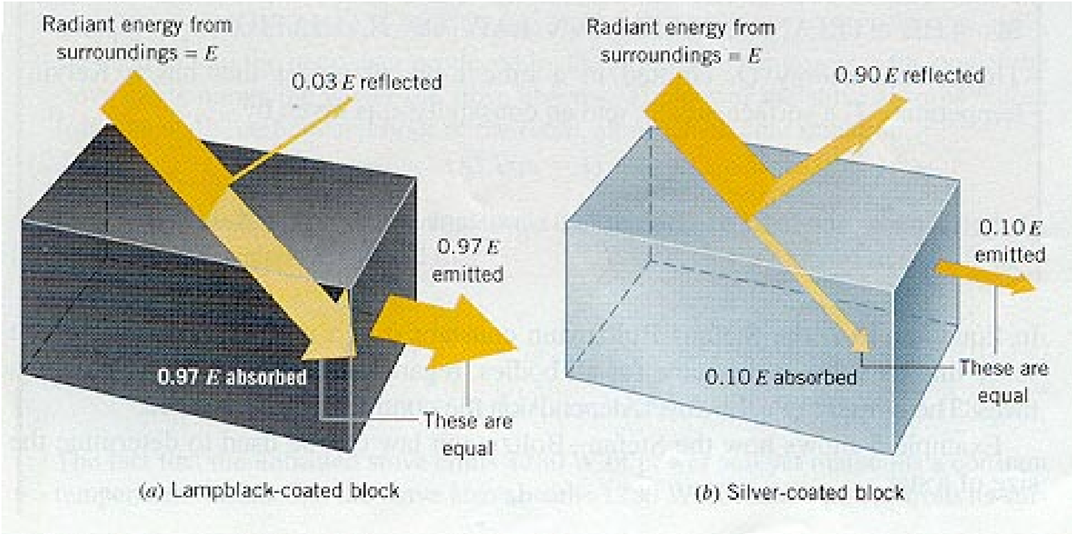

Figure 5.3 Absorption and emission of radiation

The thermal resistance for radiation can be defined as:

$$R_{th\_rad} = \frac{\Delta T}{P_{rad}} [\text{K/W}] \tag{5.5}$$

Combining equations (5.4) and (5.5), the thermal resistance may be written in the following form:

$$R_{th\_rad} = \frac{1}{h_r \cdot A} [\text{K/W}] \tag{5.6}$$

where, $h_r = 4 \cdot \varepsilon \cdot \sigma \cdot T_m^3$ is called the *radiation heat transfer coefficient* [W/m^{2}K].

For normal room temperature, 25°C (= 298K), h_r is about six times the surface emmitance. This can be easily proved, replacing in the definition relation the corresponding numbers [*Mills, p.16, 1995*]:

$$h_r = 4 \cdot \varepsilon \cdot 5.67 \cdot 10^{-8} [\text{W/m}^2\text{K}^4] \cdot (298)^3 [\text{K}] \cong 6 \cdot \varepsilon [\text{W/m}^2\text{K}] \tag{5.7}$$

5.2.3. Temperature equilibrium

A temperature equilibrium will be always reached after the solar irradiation has begun. It is helpful to know this temperature for the first idea about thermal conditions in the Cubesat. There is presented only instance without internal heat sources. The temperature equilibrium is obtained when the absorbed power Q_A is equal to emitted power by radiation Q_E. These values are given by the following equations:

$$Q_A = S_0 \cdot \alpha \cdot A_{in} \tag{5.8a}$$

$$Q_E = \varepsilon \cdot \sigma \cdot A_{out} \cdot T_e^{\ 4} \qquad (5.8b)$$

where the symbols in the equations have the following significances:

S_0 is solar irradiation (1353 [W/m^2], in case of sunlight, 237 [W/m^2], in case of eclipse),

α represents the absorbitivity of the material,

A_{in} is area illuminated by solar irradiation [m^2],

ε is the emissivity of the material,

σ is Stephan-Boltzmann constant, equal with 5.67 x 10^{-8} [W/m^{2}K^4],

A_{out} is the radiating area [m^2], and

T_e represents the equilibrium temperature [K].

The equilibrium temperature is obtained from condition $Q_A = Q_E$. Replacing the expressions for the two amounts of heat, from equations (5.8a, b), it yields:

$$T_e = \sqrt[4]{\frac{A_{in}}{A_{out}} \cdot \frac{\alpha}{\varepsilon} \cdot \frac{S_0}{\sigma}} \qquad (5.9)$$

In the satellite are used these materials with their constants as is shown in table follows.

	Solar cells (InGaP,GaAs,Ge)	Material of sides (Carbon)	Material on side with camera (Aluminum)
α	0.75	0.96	0.55
ε	0.83	0.9	0.3
Coverage of one side (%)	57	43	100

Table 5.1 Absorbitivity and emissivity for materials used in the satellite

Case of sunlight

Solar irradiation is taken into account without respect of Albedo and infrared heat from the Earth. The illuminated sides are only the sides with solar cells (side with camera is still pointed to the Earth). For material constants can be put only values with respect of coverage of sides. It can be calculated as below:

$$\overline{\alpha} = \alpha_{cell} \cdot 0.57 + \alpha_{mat} \cdot 0.43 = 0.75 \cdot 0.57 + 0.96 \cdot 0.43 = 0.8403 \qquad (5.10a)$$

$$\overline{\varepsilon} = \varepsilon_{cell} \cdot 0.57 + \varepsilon_{mat} \cdot 0.43 = 0.83 \cdot 0.57 + 0.9 \cdot 0.43 = 0.8601 \qquad (5.10b)$$

Due to assumption, that the satellite will stay in position with camera side pointed to the Earth, there are these boundary conditions:

- One side illuminated
- Three sides illuminated

From equations (5.10a, b) the equilibrium temperature can be calculated as follows:

$$T_e = \sqrt[4]{\frac{\sqrt{N}\cdot A_1}{A_1}\cdot\frac{\overline{\alpha}}{5\cdot\overline{\varepsilon}+1\cdot\varepsilon_{cam}}\cdot\frac{S_0}{\sigma}} = \sqrt[4]{\frac{\sqrt{N}\cdot\overline{\alpha}\cdot S_0}{\left(5\cdot\overline{\varepsilon}+1\cdot\varepsilon_{cam}\right)\cdot\sigma}} \tag{5.11}$$

where A_1 is the area of one side [m^2],

N is number of illuminated sides, and

ε_{cam} represents the emissivity of material on side with camera.

The illuminated area is dependent on the angle of sunlight and its maximum is respected by $\sqrt{N}$ (section 3.3.1). That is why this value is placed in numerator.

In radiation must be taken in account that all of sides are radiating. But not all of them are the same. One side (with camera) has different conditions. This is a reason for writing such a shape of denominator as in equation (5.11).

Then by inserting these values into the equation (5.11) is obtained:

- One side illuminated:

$$T_e = \sqrt[4]{\frac{0.8403\cdot 1353\,[\mathrm{W/m^2}]}{\left(5\cdot 0.8601+1\cdot 0.3\right)\cdot 5.67\cdot 10^{-8}\,[\mathrm{W/m^2K^4}]}} = 256.94\,[\mathrm{K}] = -18.19\,[^{\circ}\mathrm{C}] \tag{5.12}$$

- Three sides illuminated:

$$T_e = \sqrt[4]{\frac{\sqrt{3}\cdot 0.8403\cdot 1353\,[\mathrm{W/m^2}]}{\left(5\cdot 0.8601+1\cdot 0.3\right)\cdot 5.67\cdot 10^{-8}\,[\mathrm{W/m^2K^4}]}} = 294.77\,[\mathrm{K}] = 21.62\,[^{\circ}\mathrm{C}] \tag{5.13}$$

- Three sides illuminated simultaneously by direct solar irradiation, Albedo, infrared heat of the Earth:

$$T_e = \sqrt[4]{\frac{\sqrt{3}\cdot 0.8403\cdot\left(1353+406+237\right)[\mathrm{W/m^2}]}{\left(5\cdot 0.8601+1\cdot 0.3\right)\cdot 5.67\cdot 10^{-8}\,[\mathrm{W/m^2K^4}]}} = 327.99\,[\mathrm{K}] = 54.84\,[^{\circ}\mathrm{C}] \tag{5.14}$$

Case of eclipse

The source of power for this case is only infrared heat produced by the Earth by itself. In this case are counted all possible boundary conditions that can appear:

- One side pointed to the Earth
  - Side with camera (case 1)
  - Side without camera (case 2)
- Three sides pointed to the Earth
  - Including side with camera (case 3)

- Without side with camera (case 4)

In all of these cases is the denominator still the same due to radiation of all sides. Then the general equation can be written as follows:

$$T_e = \sqrt[4]{\frac{\frac{\sqrt{N_{cam} + N_{cells}}}{N_{cam} + N_{cells}} \cdot \left(N_{cells} \cdot \overline{\alpha} + N_{cam} \cdot \alpha_{cam}\right) \cdot S_0}{\left(5 \cdot \overline{\varepsilon} + 1 \cdot \varepsilon_{cam}\right) \cdot \sigma}} \tag{5.15}$$

where N_{cam} = 1 if the side with camera is illuminated,

0 if the side with camera is not illuminated,

N_{cells} is the number of sides with cells illuminated,

$\overline{\alpha}$ is the absorbtivity with respect of coverage,

$\overline{\varepsilon}$ represents the emissivity with respect of coverage,

α_{cam} is the absorbtivity of side with camera,

ε_{cam} is the emissivity of side with camera,

S_0 = 237 [W/m^2] represents the irradiation due to infrared heat from the Earth, and

σ is Stephan-Boltzmann constant (5.67 x 10^{-8} [W/m^{2}K^4]).

Then by inserting these values into the equation (5.15) the following results are obtained:

case 1: $$T_e = \sqrt[4]{\frac{\frac{\sqrt{1+0}}{1+0} \cdot \left(0 \cdot 0.8403 + 1 \cdot 0.55\right) \cdot 237\,[\mathrm{W/m^2}]}{\left(5 \cdot 0.8601 + 1 \cdot 0.3\right) \cdot 5.67 \cdot 10^{-8}\,[\mathrm{W/m^2K^4}]}} = 149.51\,[\mathrm{K}] = -123.64\,[^\circ\mathrm{C}] \tag{5.16}$$

case 2: $$T_e = \sqrt[4]{\frac{\frac{\sqrt{0+1}}{0+1} \cdot \left(1 \cdot 0.8403 + 0 \cdot 0.55\right) \cdot 237\,[\mathrm{W/m^2}]}{\left(5 \cdot 0.8601 + 1 \cdot 0.3\right) \cdot 5.67 \cdot 10^{-8}\,[\mathrm{W/m^2K^4}]}} = 166.23\,[\mathrm{K}] = -106.92\,[^\circ\mathrm{C}] \tag{5.17}$$

Case 3: $$T_e = \sqrt[4]{\frac{\frac{\sqrt{1+2}}{1+2} \cdot \left(2 \cdot 0.8403 + 1 \cdot 0.55\right) \cdot 237\,[\mathrm{W/m^2}]}{\left(5 \cdot 0.8601 + 1 \cdot 0.3\right) \cdot 5.67 \cdot 10^{-8}\,[\mathrm{W/m^2K^4}]}} = 184.95\,[\mathrm{K}] = -88.2\,[^\circ\mathrm{C}] \tag{5.18}$$

Case 4: $$T_e = \sqrt[4]{\frac{\frac{\sqrt{0+3}}{0+3} \cdot \left(3 \cdot 0.8403 + 0 \cdot 0.55\right) \cdot 237\,[\mathrm{W/m^2}]}{\left(5 \cdot 0.8601 + 1 \cdot 0.3\right) \cdot 5.67 \cdot 10^{-8}\,[\mathrm{W/m^2K^4}]}} = 190.69\,[\mathrm{K}] = -82.46\,[^\circ\mathrm{C}] \tag{5.19}$$

Conclusion

The goal was to compute the equilibrium temperature for the satellite, considering no internal heat sources. If all equilibrium temperatures are compared than can be seen that the worst case for the satellite is in eclipse when only side with camera is pointed to the Earth.

Then, it is accepted the smallest amount of energy in comparison with other cases. In addition, in all cases are radiating all sides. But must be mentioned, that no internal heat made by equipments is taken into account. So temperature range according to the temperature equilibrium is:

$T_{max} = 55$ [˚C]

$T_{min} = -124$ [˚C]

From this numbers can be derived that satellite has a trend to keep lower temperature than higher one. This is advantage for us, because no internal sources of heat are included. Internal heat sources will raise temperature inside.

5.3. Methods of modeling

5.3.1. Two-dimensional model of board

In this part of analysis the method of modeling for the electrical board is suggested. Whole Cubesat will be divided into separate layers, corresponding to the number of boards and each layer will be meshed, as shown in figure 5.4.

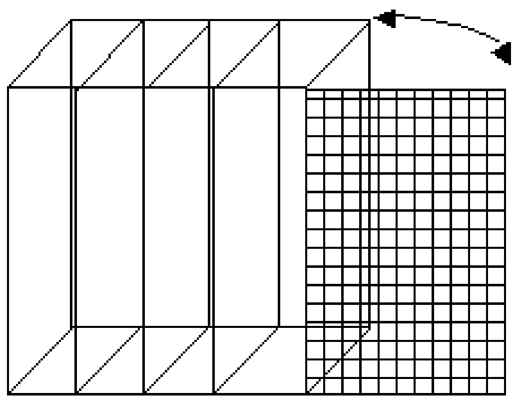

Figure 5.4 Meshed layer of the satellite

Then the components from the board will be projected into the mesh such a way, that thermal source and thermal resistances will represent each component. An example is depicted in figure 5.5. The thermal models for the components are implemented by use of Saber software. On the attached CD-ROM can be found all files concerning this simulation.

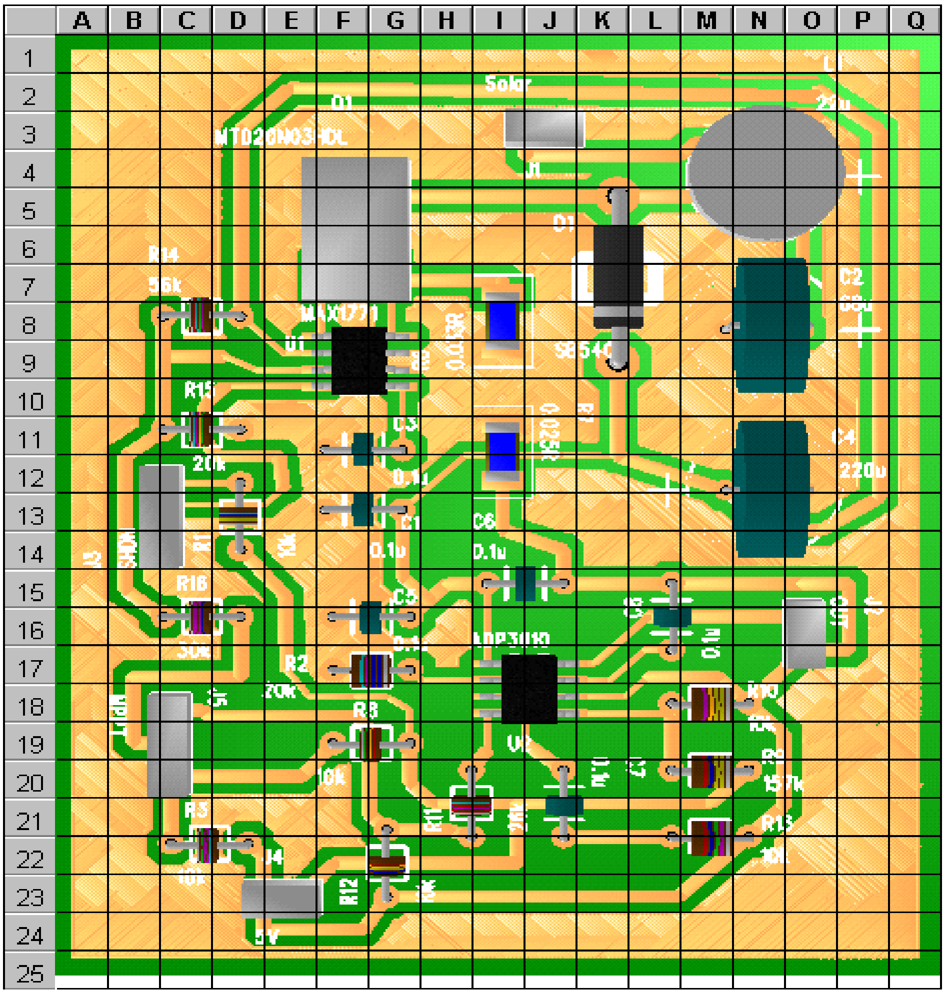

Figure 5.5 Meshed surfaces for the board

From figure 5.6 can be seen the thermal model for a power MOSFET (MTD20N03HDL), which includes the heat source corresponding to operating values and 3 thermal resistances, which represent thermal resistance of each PIN. The library of all components was created the same way. Thermal resistances include only the junction-case resistance and radiation is neglected. The thermal resistance of PCB is not considered.

Table 5.2, which includes operating values of power and thermal resistance is shown further, Thermal resistances R_{thjc} are not known for some components (in tab they are written in italic) so some of them were estimated. The estimation is based on type of package, it is assumed that if the same technology is used, then the thermal resistances will be the same.

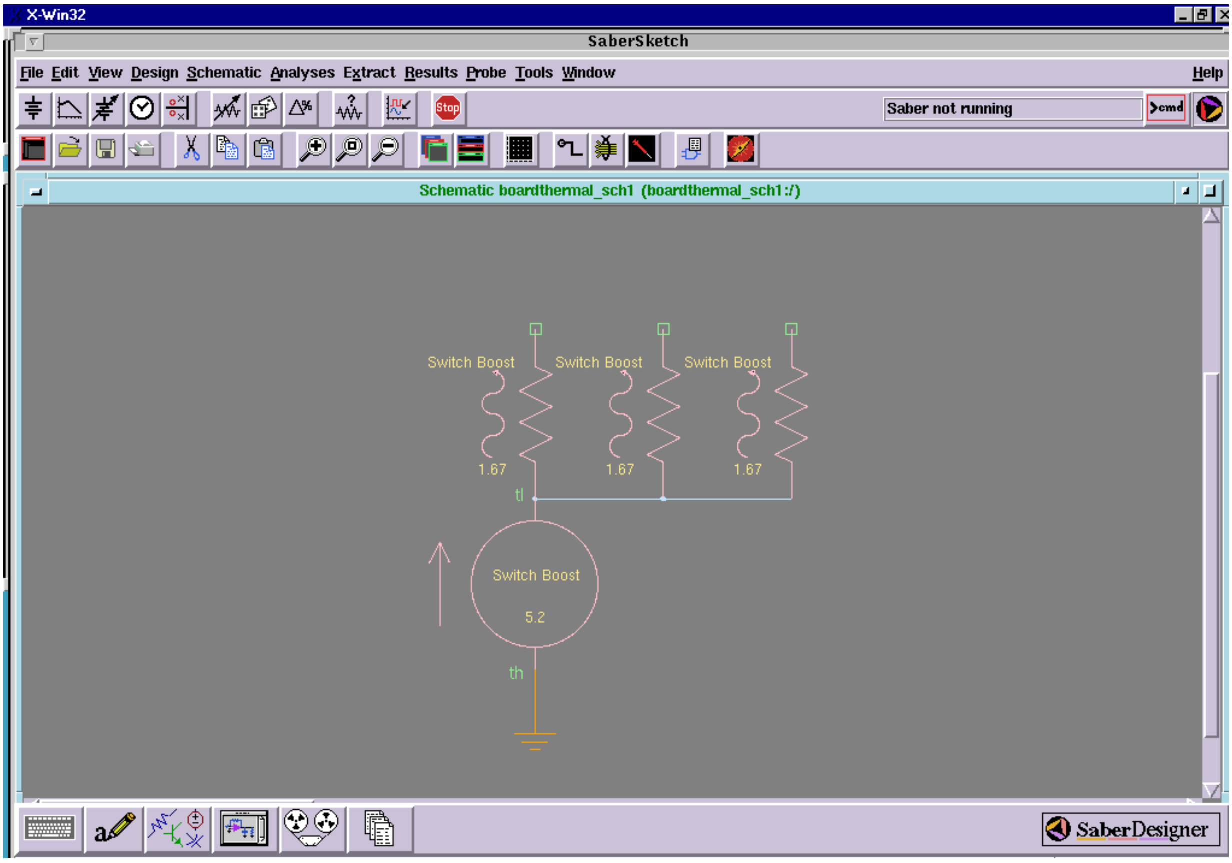

Figure 5.6 Thermal model for a power transistor

Component name	Function	Number of pieces	Number of legs	$R_{th\ j\text{-}c}$ (K/W)	Working conditions			Included in model?
					Current (A)	Voltage (V)	Power (W)	
MTD20N03HDL	switch for step-up convertor	1	3	1.67	0.58	5.23	3	yes
NDT 456P	switch for step-down convertor	1	3	12	2	3.4	6.8	yes
TPS2034	protection for transmitter	1	8	*10*	1.8	5	9	yes
TPS2030	protection for ACS,CAM, MCU, OBC	4	8	*10*	0.05; 0.06; 0.003; 0.092	5	0.25; 0.3; 0.015; 0.46	yes
MAX1771	step-up convertor	1	8	*10*	110µ	5	0.55m	yes
MAX1744	step-down convertor	1	8	*10*	221µ	8.4	1.86m	yes

UCC3911	protection for 2 batteries in series	2	16	*12*	0.92	8.4	7.728	yes
SB540	diodes for convertors	2	2	*2*	0.5	0.43	0.215	yes
PRLL5817	string diodes for solarcells	5	2	*5*	0.5	0.35	0.175	yes
MAX4372	current-sence amplifier	10	5	*7*	30μ	5	0.15m	no
LM78L05	terminal positive regulator	1	8	*7*	0.1	5	0.5	yes
MAX835	latching voltage monitor	4	5	*7*	15μ	5	0.075m	no

Table 5.2 Operating values of components

From these components MAX4372 and MAX835 were neglected.

The restrictions of 2D model are stated as follows:

- The thermal resistance of PCB is not considered.
- Number of nodes is directly connected to the accuracy of the model. The more nodes we have the higher accurate model we obtain.
- In our case only main sources of heat will be taken in account.
- Radiation is not included in this model; it is supposed that the conduction through the copper is main way for heat transfer.
- Distances between components are not included.
- The model is only two-dimensional and it is a problem to transfer into 3D.
- The thermal resistances for radiation (R_{thca} case-ambient) are not included in datasheets and must be computed for each component.
- Saber software is not optimal for this type of analysis.
- Creating of the model is elaborate and requires a large amount of work.
- Thermal resistances R_{thjc} are not known for all device.

5.3.2 Implementation of the model and results

The whole thermal model of the PSU board is depicted in figure 5.7. In model there are included only main sources of heat. Position of components is respecting the electrical layout, because final board wasn't at disposal. It is assumed that the copper on a board is conducting the most of the heat, because its thermal conductivity is thousand times higher then for the board. Pins, which are not connected to other components and have no function have zero value. If it is not like this, the Saber software will assume them as a nonfinite value and it will alter the results.

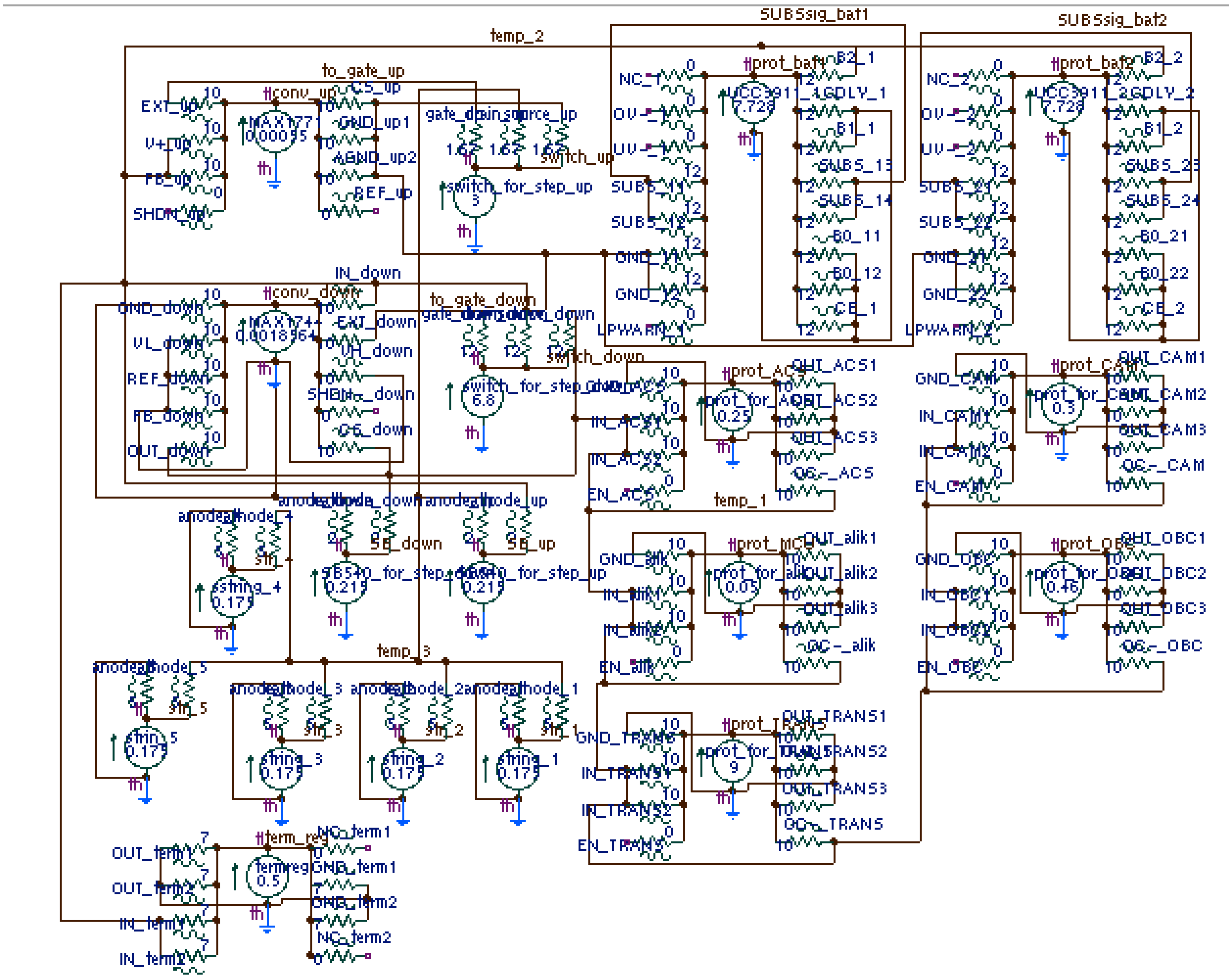

Figure 5.7 Final layout for thermal model

The results are presented in table 5.3 and in figure 5.8.

All temperatures are acceptable and are following the industrial standard. The highest temperature is on the switch of step-down converter (40.9°C). It is exactly according to the expectances, because of the highest power. Also protections for batteries and for communication module will have temperatures near to 20°C.

	Device	Temperature (^oC)
Convertors	Step-up	13.3
	Step-down	5.3
Protections	ACS	3.1
	Batteries	16.6
	CAM	3.2
	MCU	2.8
	OBC	3.4
	Transmitter	15.6
Diodes	String	4.9
	SB540 for step-up	11.3
	SB540 for step-down	3.4
Switches	For step-up	13.6
	For step-down	**40.9**
	Terminal positive regulator	5.0

Table 5.3 temperatures of main components

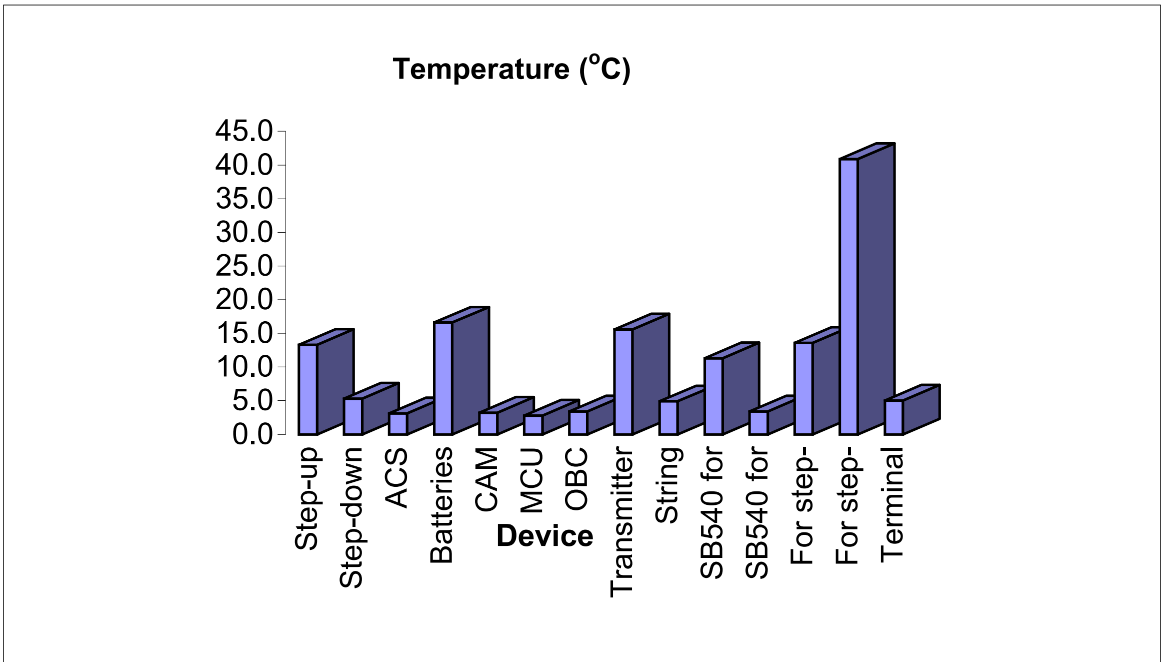

Figure 5.8 Temperatures of main components

Conclusion

Sequent model is not the final one, because it does not consider the geometrical distribution of components. For successful completion of it, the final board is necessary. The method for it, is shown in figure 5.5. The model has many restrictions and imperfections. The main problem is that the material properties of the board are not included and if two components are very close and their electrical connection is far distant then the conduction by board can apply more than by copper.

Anyway, this model gives the basic idea about thermal conditions on a PSU board. The main sources of heat and the temperature amount are known. The problem is with verifying values of resulting temperatures in our laboratory. For this it is necessary to eliminate convection so vacuum chamber is needed. It is also clear that the temperatures are strongly dependent on thermal resistances, which were just estimated.

5.3.4. Three-dimensional model of satellite

In reference to mentioned restrictions of previous model, another solution for 3D model needed to be found. In this case, a software using method of finite elements have to be used. ANSYS software has been chosen as a most suitable for our application. Its biggest advantage is that it consider the material properties and it works in three dimensions. On the other hand it is very sophisticated tool and it requires a lot of time to learn it.

To simplify the realization of model it will include only main parts of the satellite:

- Side walls
- Solar cells
- It is assumed steady state for all the computations

For proper function of this software, it is necessary to choose a proper element. As was mentioned before, between heat conduction mechanisms, only radiation and conduction are applicable in a space application. For a 3D analysis only LINK31, SHELL57 and SURF152 elements can work in ANSYS software with respect to radiation.

LINK31 element can be used only for calculating the heat flow between two nodes. It only has these two nodes and cannot be meshed. SHELL57 has four nodes and capability to define in each node different thickness. There is not problem with meshing of this element.

SURF152 (also called superelement) may be used for various load and surface effect applications.

If a radiation simulation between some surfaces and surroundings has to be performed, then the SHELL57 element must be chosen. After setting the thickness, the geometry of the satellite can be done by creating key points, from them lines and finally from lines can be constructed areas of each hand side. Figure 5.9 shows an example of a meshed surfaces for the satellite.

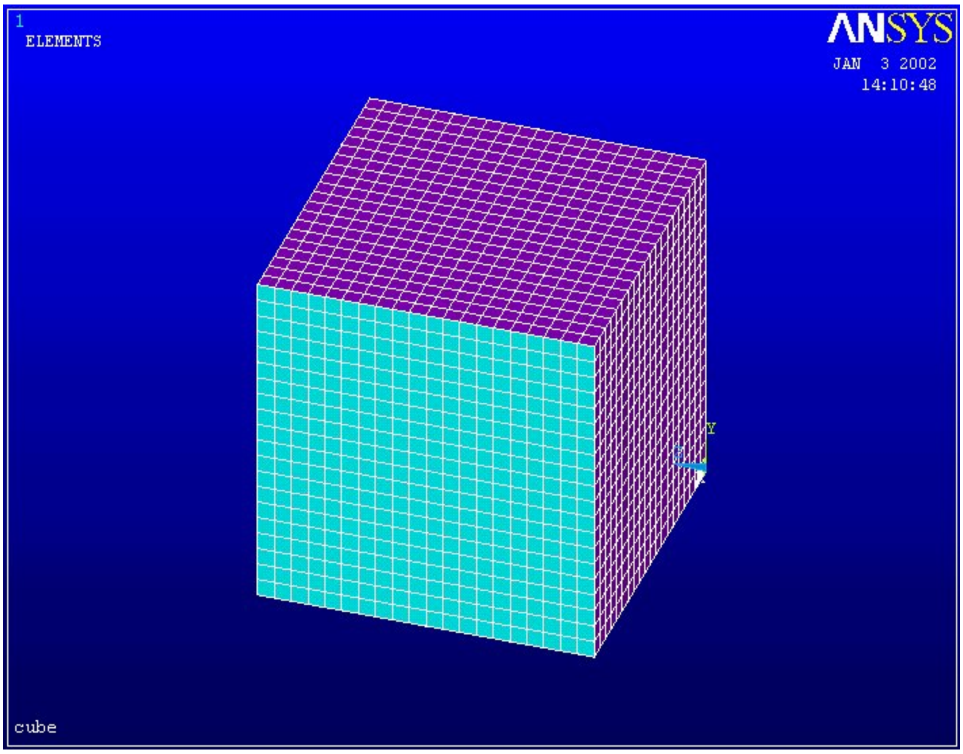

Figure 5.9 Example of meshed structure for the satellite

Following, there are two methods of doing simulation with reference to radiation problem:

- AUX12 Radiation Matrix Method
- Radiosity Solver Method.

For the AUX12 method must be SHELL57 superimposed by superelement on which must be defined conditions for radiation.

Assigning edge conditions for the model

Because there was not possible to establish temperature distribution only from heat flux and material properties, boundary conditions had to be calculated.

For calculation the edge temperature on the sun side (T_1), can be used Stefan-Boltzmann law:

$$S_{rad} = \sigma \cdot T^4 \cdot \varepsilon \tag{5.20}$$

From this, the expression of temperature resides:

$$T = \sqrt[4]{\frac{S_{rad}}{\sigma \cdot \varepsilon}} \tag{5.21}$$

where the symbols in the equations have the following significances:

S_{rad} is the solar heat flux, equal with 1353 [W/m^2]

ε is the emissivity of the material, and

σ is Stephan-Boltzmann constant, equal with 5.67 x 10^{-8} [W/m^{2}K^4].

Assuming the emissivity ε equal with 1, and replacing the numbers in equation (5.21), it yields:

$$T_1 = \sqrt[4]{\frac{1353[\mathrm{W/m^2}]}{1\cdot 5.67\cdot 10^{-8}[\mathrm{W/m^2K^4}]}} = 393[\mathrm{K}] = 120[^\circ\mathrm{C}] \tag{5.22}$$

A similar value can be obtained also by computing thermal equilibrium for solar cells. The same equation can be used for infra radiation from the side of the Earth, only now the heat flux for infrared is 237 [W/m^2].

$$T_2 = \sqrt[4]{\frac{237[\mathrm{W/m^2}]}{1\cdot 5.67\cdot 10^{-8}[\mathrm{W/m^2K^4}]}} = 254[\mathrm{K}] = -19[^\circ\mathrm{C}] \tag{5.23}$$

By using these edge conditions it has been obtained the picture shown in figure 5.10 (using SHELL57 element), which shows temperature distribution in Cubesat, but this model is including only conduction. It is necessary to build similar model for radiation, but this was not possible at the time of doing the analysis.

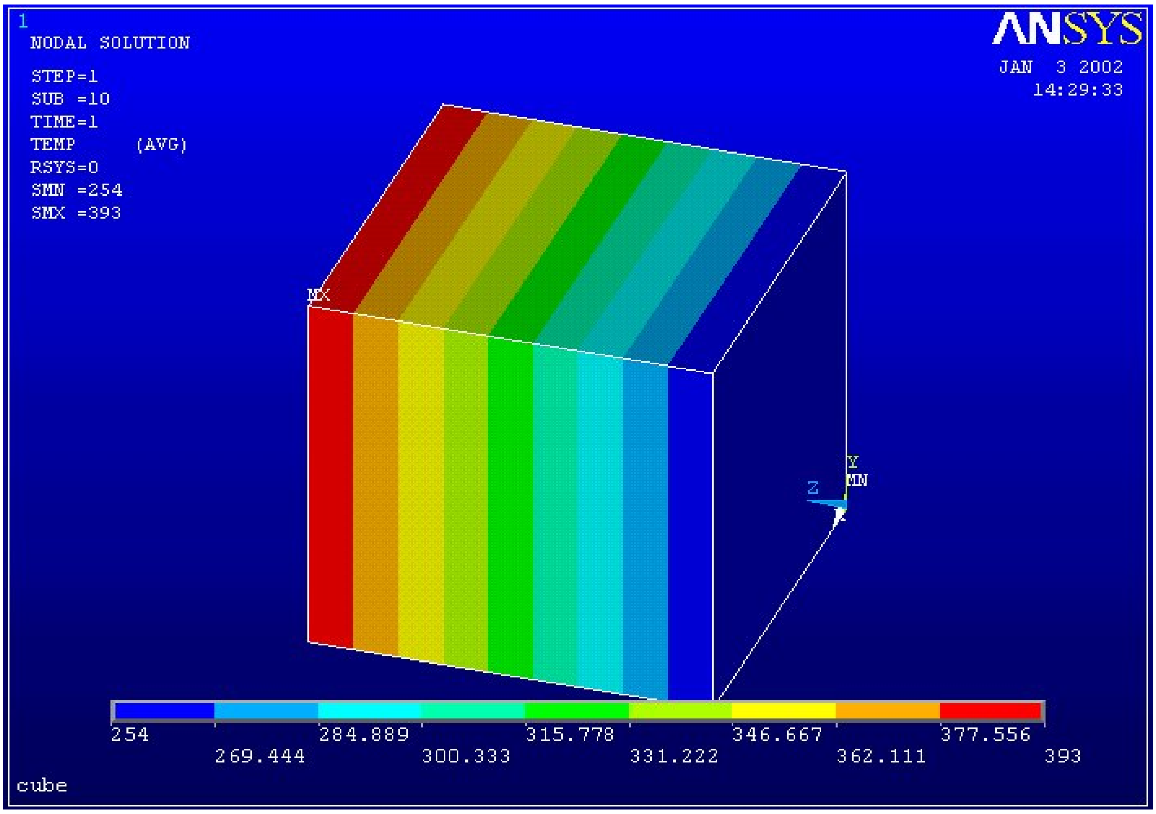

Figure 5.10 Distribution of temperature on the satellite surface

Conclusion

The built model is very simple and couldn't satisfy our recommendations. It is necessary to find a solution for radiation element. And connect both models together.

5.4. Thermal control

It is necessary to keep the temperature in Cubesat during the mission in the industrial standard, because all electronic devices are designed to operate in this temperature range. The methods of realizing this goal are described in the following.

The methods of thermal control can be split into two categories, passive methods and active methods. In respect to the size of the satellite, passive methods will be preferred.

Heat insulation is needed to keep an instrument sufficiently warm or to prevent heat from body-mounted solar panels from propagating into the spacecraft or for separation the heat-sensitive parts. Used material is MLI (multilayer insulation), with a structure like the one depicted in figure 5.11 [*Hansen, 2001*].

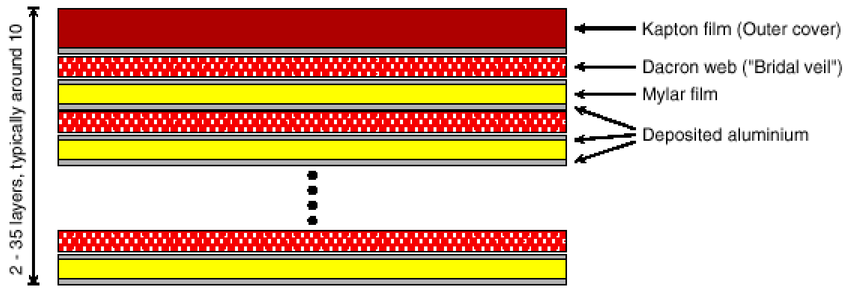

Figure 5.11 Thermal insulating material

This material is very light and thin and can be simple used for a small satellite. This material will be probably used as a thermal shielding for our batteries. This can help us to avoid fast temperature changes.

Another passive form is *changing value of* α/ε *factor***.** This can be realized by changing the color or surface materials. This method is very easy to implement and is also reliable. Temperature equilibriums for different values of α/ε factor can be seen in a table 5.4 [*Hansen, 2001*].

No.	Material	Measure-ment temp.(K)	Surface condition	Solar absorbitivity α	Infrared emissivity ε	α/ε ratio	Equili-brium temp.(^{o}C)
1	Aluminum (6061-T6)	294	As received	0.379	0.0346	10.95	450
2	Aluminum (6061-T6)	422	As received	0.379	0.0393	9.64	428
3	Aluminum (6061-T6)	294	Polished	0.2	0.031	6.45	361
4	Aluminum (6061-T6)	422	Polished	0.2	0.034	5.88	346
5	Gold	294	As rolled	0.299	0.023	13.00	482

6	Titanium (6AL-4V)	294	As received	0.766	0.472	1.62	176
7	Titanium (6AL-4V)	422	As received	0.766	0.513	1.49	166
8	Titanium (6AL-4V)	294	Polished	0.448	0.129	3.47	270
9	Titanium (6AL-4V)	422	Polished	0.488	0.148	3.30	251
10	White enamel	294	Al. substrate	0.252	0.853	0.30	20
11	White epoxy	294	Al. substrate	0.248	0.924	0.27	13
12	White epoxy	422	Al. substrate	0.248	0.888	0.28	16
13	Black paint	294	Al. substrate	0.975	0.874	1.12	136
14	Silvered Teflon	295		0.08	0.66	0.12	-39
15	Aluminized Teflon	295		0.163	0.8	0.20	-6
16	Quartz Over Silver	295		0.077	0.79	0.10	-51
17	Sol.Cell-Fused Silica Cover			0.805	0.825	0.98	122
18	Crushed Carbon Graphit			0.88	0.96	0.92	

Table 5.4 Temperature equilibrium for different materials

From the active methods of thermal control, the *rotating method* can be mentioned. If large amounts of heat are located on a board the satellite, this can start slowly to rotate. There exists a critical value of temperature, which can be measured by temperature sensors and this signal can be used as a control signal for the attitude control system to rotate the satellite. This method is dependent on speed of rotation, which is connected to the induced current into the magnetotorquers. We cannot rotate very fast or very slow, the speed of rotation must be optimized in transient thermal analysis. And it is a task for thermal stabilization.

Also h*eaters* are used to avoid low temperatures. They can be realized as electrical blankets or as small resistances. For our application they seem to be so inefficient, because of power problems. Only one possible application can be realized for heating batteries. The necessary amount of the heat has to be computed.

Heat pipes are the last active method. Heat pipes can transfer much higher powers for a given temperature gradient than even the best metallic conductors. They are hollow tubes closed on both ends filled with some fluid like ammonia, as shown in figure 5.12. As one end of the pipe is exposed to a heat source, the ammonia absorbs this heat and vaporizes. The ammonia vapor then flows through the pipe and carries the heat away to the cold end. There the ammonia losses its heat and recondenses as a liquid. It then flows back to the other end. This is a form of convection in which the work is being done not by gravity but by the wicking effect. This system can be effective for higher temperatures, depends on boiling point of inner fluid. (But in case of our system the problem is to avoid low temperatures during the eclipse). Its light weight (generally less than 40 grams), small, compact profile, and its passive operation, allow it to meet the demanding requirements of mini satellites. Their application needs deeper analysis. They can be used for transporting heat from hot (illuminated) sides to cold one.

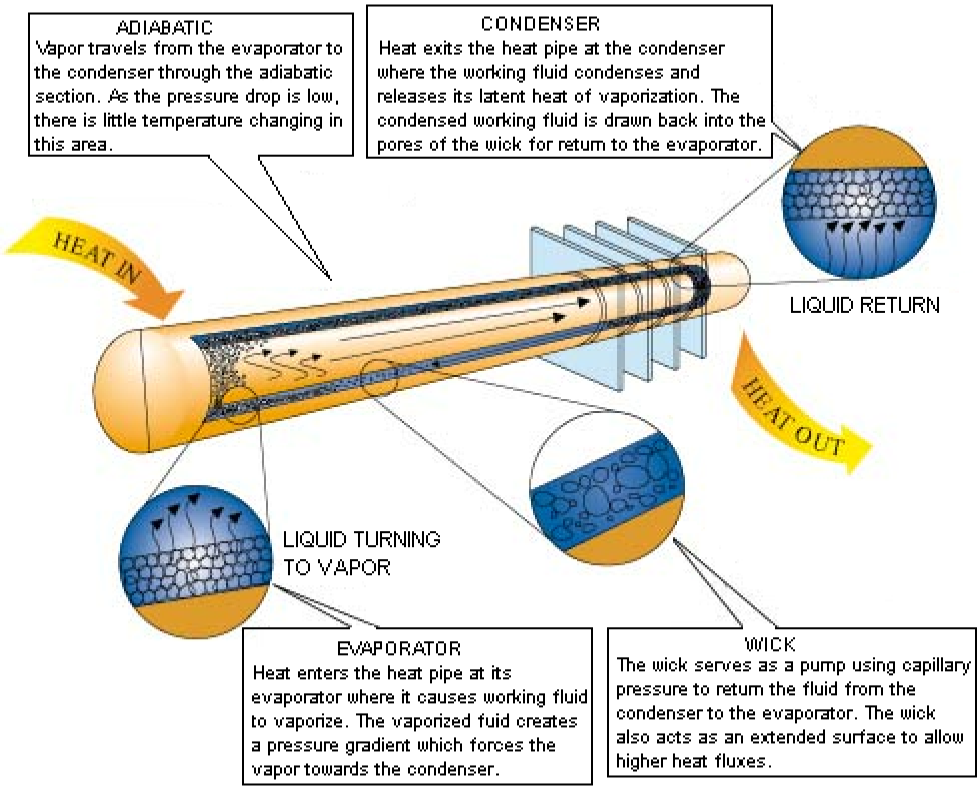

Figure 5.12 Heat pipes – principle of operation
[http://www.electronics-cooling.com/Resources/EC_Articles/SEP96/sep96_02.htm]

5.5. EMC considerations

Power supply must also fulfill requirements for EMC. It means that the level of the electromagnetic noise of our device should be below admissible value for other parts of Cubesat. And on the other hand our device must be resistant enough against foreign sources of noise [http://www.its.bldrdoc.gov/fs-1037/dir-013/_1932.htm].

Definitions

Electromagnetic compatibility (EMC):

1. Electromagnetic compatibility is the condition, which prevails when equipment is performing its individually designed function in a common electromagnetic environment without causing or suffering unacceptable degradation due to unintentional electromagnetic interference to or from other equipment in the same environment.

2. The ability of systems, equipment, and devices that utilize the electromagnetic spectrum to operate in their intended operational environments without suffering unacceptable degradation or causing unintentional degradation because of electromagnetic radiation or response. It involves the application of sound electromagnetic spectrum management; system, equipment, and device design configuration that ensures interference-free operation; and clear concepts and doctrines that maximize operational effectiveness.

Electromagnetic environment (EME):

1. For a telecommunications system, the spatial distribution of electromagnetic fields surrounding a given site. The electromagnetic environment may be expressed in terms of the spatial and temporal distribution of electric field strength [V/m], irradiance [W/m^2], or energy density [J/m^3].

2. The resulting product of the power and time distribution, in various frequency ranges, of the radiated or conducted electromagnetic emission levels that may be encountered by a military force, system, or platform when performing its assigned mission in its intended operational environment. It is the sum of electromagnetic interference; electromagnetic pulse; hazards of electromagnetic radiation to personnel, ordnance, and volatile materials; and natural phenomena effects of lightning.

Electromagnetic interference (EMI):

1. Any electromagnetic disturbance that interrupts, obstructs, or otherwise degrades or limits the effective performance of electronics/electrical equipment. It can be induced intentionally, as in some forms of electronic warfare, or unintentionally, as a result of spurious emissions and responses, intermodulation products

2. An engineering term used to designate interference in a piece of electronic equipment caused by another piece of electronic or other equipment. EMI sometimes refers to interference caused by nuclear explosion [JP 1-02].

Level of noise

- High frequencies >1MHz
- Low frequencies our case <1MHz

Digital circuits as a noise sources

Digital circuits generate mainly narrow-band noise, that means energy is concentrated on single frequency. The biggest emission is normally between 50 and 500 MHz depends on clock frequency. The highest energy appears normally as a harmonic of clock frequency. Our microcontroller works on 1MHz. There is also direct emission from the PCB, which works as a magnetic loop antenna. The emission level depends on the current in the loop. From this is obvious that the board must be as small as possible. It is also important to use a PCB with ground plan (gridded ground system).

The emission from PCB loop (figure 5.13), which has diameter much smaller than a wavelength (λ), can be described as:

$$H_{\max} = \frac{A}{2\pi \cdot r^3} \cdot i \ , \ \left(r < \frac{\lambda}{6} \right) \tag{5.24}$$

where, H is magnetic field strength [A/m]

E represents the electric field strength [V/m]

A is area of the loop [m^2], and

r is the distance from the current loop to measure point [m]

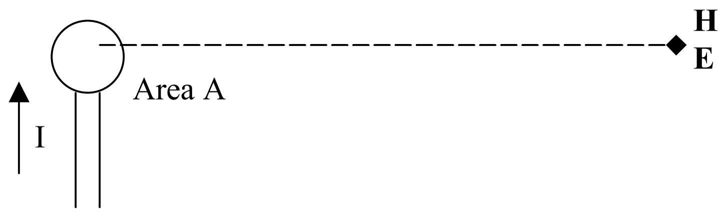

Figure 5.13 Emission from a PCB loop

Recommendations for minimizing emission of digital circuits:

- Use the lowest possible clock frequency.
- Do not use digital circuit with faster rise time than it is necessary.
- Use parallel power supply for 0 V and for V_{cc}.
- Minimize the area of all printed circuit loops. Especially for clock and bus circuit. The best place is in the middle of the board.
- Make the connection to PCB on the same side, the smaller impedance will be obtained.
- Make HF filters on all connection to the PCB. All filter capacitors should have reference to one ground plane.

Noise from power electronics

If it is made a comparison between the power electronic circuits and digital circuits, it might be observed that the rise times are higher in digital circuits, but the current is higher in power electronics. This can lead to emission of high levels of noise and electromagnetic interferences, if proper methods to avoid this are not considered.

Recommendations to prevent noise:

- Loops in circuit as short as possible: long loops works by certain frequencies as magnetic loop antenna.
- Shielding: It reduces or absorbs the coupling between noise source and the victim. The cause of this effect is, that the conductive shield hit by electromagnetic field will induce current in the plate, which transform the field energy into the heat.

The damping ability of a shield depends on:

- The frequency of the field
- The field impedance
- The shield material
- The dimensions and the placing of the shield

Absorption loss in shield are given by the following formula:

$$A = 131\sqrt{f \cdot \mu_r \cdot \sigma_r} \cdot t \tag{5.25}$$

where, f represents the frequency of electromagnetic signal [Hz]

μ_r is the relative permeability of shield material

σ_r is the material relative conductivity in relation to copper, and

t represents the shield thickness.

Reflection loss are given as:

$$R = 168 + 10\log\left(\frac{\sigma_r}{\mu_r} \cdot \frac{1}{f}\right)[\mathrm{dB}] \tag{5.26}$$

where, f is the frequency of the perturbing signal [Hz],

σ_r is the material relative conductivity in relation to copper, and

μ_r represents the relative permeability of shield material

5.6. Summary

The goal of thermal analysis developed in this chapter, is to have basic idea about temperature distribution in Cubesat and suggest some methods for thermal control. For this different approaches were used. First of all was computed the temperature equilibrium for the satellite, considering no internal heat sources. If all equilibrium temperatures are compared than can be seen that the worst case for Cubesat is in eclipse when only side with camera is pointed to the Earth. So temperature range according to the temperature equilibrium is:

$T_{\max} = 55$ [˚C]

$T_{\min} = -124$ [˚C]

From this numbers can be derived that satellite has a trend to keep lower temperature than higher one. This is advantage for us, because no internal sources of heat are included and they will raise temperature inside.

Second part was model of the board in Saber , which gives us basic idea about temperatures on a board. Highest obtained temperature for switch of step-down converter is 40.9˚C, which is far away from maximum for industrial standard. Of course, this temperatures will add up with the temperatures of surroundings and they are not final.

Next most problematic part was model of whole Cubesat in ANSYS: The built model is very simple and couldn't satisfy our recommendations. It is necessary to find a solution for radiation element. And connect both models together.

From thermal control shielding for batteries is suggested (as the most temperature sensitive part of power subsystem). MLI can be easily used for this. Also heat pipes seem to be relevant for the current application.

Some basic considerations about electromagnetic compatibility problems are presented in section 5.5. Potential sources of noise are analyzed and a comparison between them is made. Measurement of noise for final board on spectrum analyzer will be done.

Chapter 6
Evaluation of the power supply design

Abstract

In this chapter, the design work developed previously in Chapter 4 is being verified through an experimental setup. Tests over the available setups are performed, and results are presented.

6.1. Introduction

The goal of this chapter is to verify the design of the power supply, previously described in Chapter 4. It has been decided to realize separate PCB boards for each module of the entire power supply, and to evaluate each separately. The experimental setups are described, and the results available at the moment are shown.

Note that, for practical reasons, detailed in the summary, not all the proposed measurements could be performed.

6.2. MCU measurements

In this section, the methods and results of measurement and testing of the MCU module are described.

The first test consists only of testing of MCU's clock. The result was achieved at pin OSC2 (pin 14) and the waveform acquired from the oscilloscope can be seen in figure 6.1.

The output frequency on this pin is four times lower than inner clock frequency. From figure may be observed that time period is approximately 1µs, what means a frequency of 1MHz respectively oscillator frequency is 4Mz.

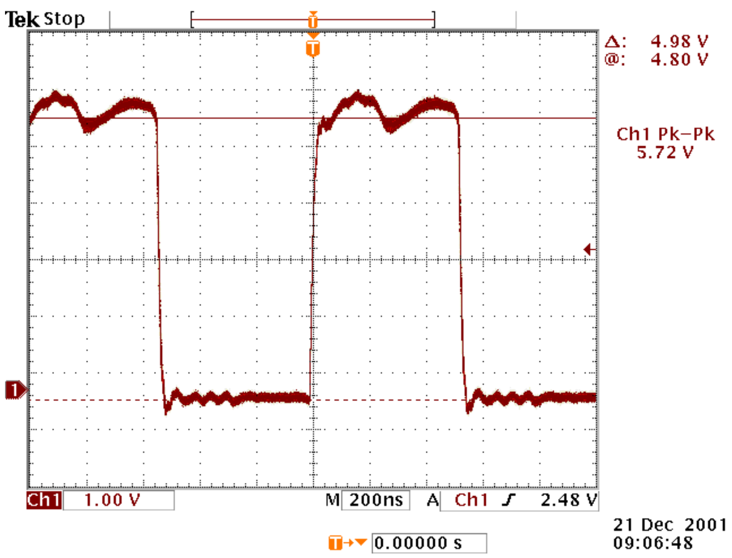

Figure 6.1 Oscillator waveform

Evaluation of protections

The scheme of the test circuit is depicted in figure 6.2. For the real measurement setup it was used a logical analyzer instead of light-emitting diodes, but diodes are in the figure for better understandability, because only two states were measured: high state (diode glows) and low state (diode not glows).

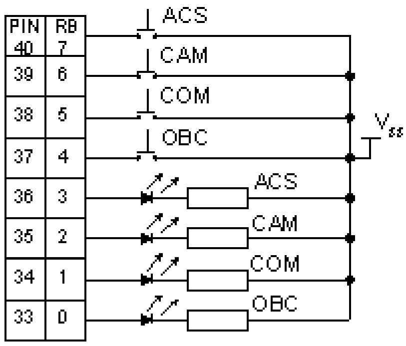

Figure 6.2 Simplified scheme of connection for testing protections

Protections for ACS, COM and CAM

These protection should work only as a turn-off: after NOT_FAULT signal switch to low level (logic 0) appropriate ENABLE signal must switch to low level too, but if the NOT_FAULT signal will switch to high level afterwards, ENABLE signal must stay on low level, because user can be turn-on only after command from OBC via I^2C bus. These functions were tested for all protections with positive function.

Protection for OBC

Protection for OBC works same way as the rest of the protections, the only difference is that the OBC cannot be turned on by itself and PSU must provide the turn-on signal.

This protection was tested in the same way as the other protections; only the time between turn off/on signals was measured. Because OBC can be turn-off also when watchdog overflow, time for this overflow was measured too. Result was that OBC was turned off after app. 12 seconds and turned on again after app. 5.5 minutes, these times are sufficient for it’s purpose, because there is no request for precise times. Assignment was to have times around 10 seconds and 5 minutes and these times were achieved.

Testing of AD converter

For testing if A/D converter works well had been written special software, which write bytes from memory to output pins, for easier code was used port C for this output (see figure 6.3a). Because some pins from this port is used for another function (I^2C, bootpin etc.) rest of program had to be changed too. To select which byte from memory will be on output was decided to use four input pins on port D (figure 6.3b).

As a result 16 different bytes from memory could be read. AD converter was connected to the variable voltage source and from port C was read value of higher and lower byte. From them were extracted 12bit final value and this value was recalculated from equation:

$$V = \frac{V_{ref}}{2^{res}} \cdot N$$

where V_{ref} is the reference voltage for AD converter (5V),

res is resolution of the ADC (12bit) and

N is the value from memory converted from binary to decimal format; result is in volts.

In Table 6.1 are shown some tested values. All results remain under 1% error and it is concluded that this error is acceptable.

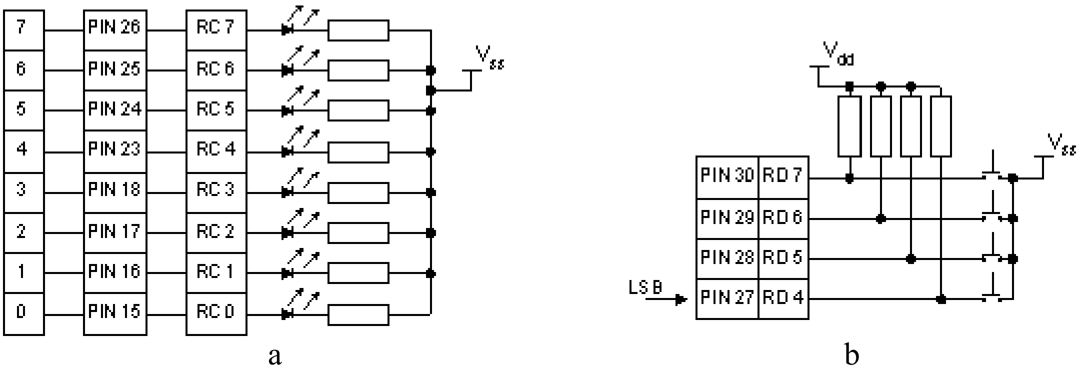

Figure 6.3 Simplified scheme of connection for reading memory (a) and scheme of byte selector (b)

Voltage on source (Multimeter)	Higher byte bit format	Lower byte bit format	Final number from ADC	Recalculated voltage	Difference
1.4720V	100	10110111	1207	1.47339V	1.4mV
2.990V	1001	10010100	2452	2.99316V	3.2mV
0.521V	1	10101001	425	0.5187V	2.2mV

Table 6.1 Measured values

Next test is about control signals for multiplexers, these signals are on port D, pins 19-22. During one reading period, these control signals must produce numbers from 0 to 15. These pins were connected to the logic analyzer and result is shown in the figure 6.4, where is clear that each pin switching from 0 to 1 with half frequency then the previous one. That means that all combinations occur and multiplexer switches to each input signal.

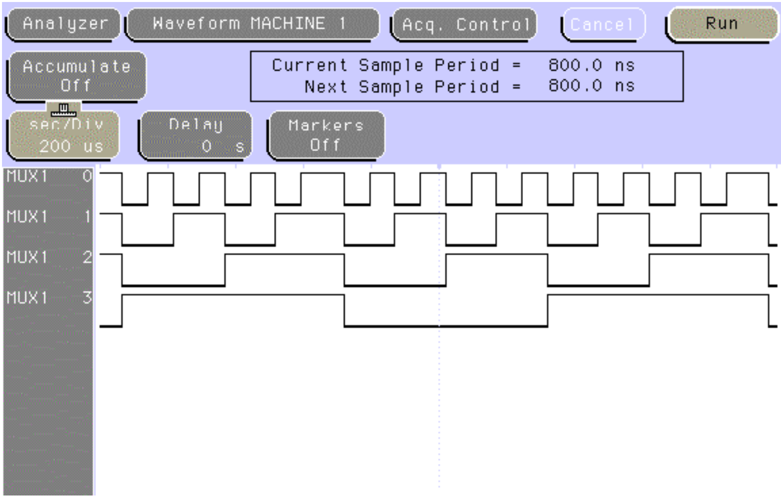

Figure 6.4 Signals for driving multiplexers

Last test is nearly the same as the tests above; only change is that on PORTC will be 8-bit value from temperature sensor in degrees of Celsius. First temperature sensors were substituted with voltage source and whole temperature resolution was tested. Second real thermal sensor LM19 was connected and it was measured that temperature in laboratory was 21°C.

4. PWM signal testing

This test was done to be sure about PWM capability of the processor and to test low-pass filter on the end of the PWM. Both signals: PWM and analog one were measured with oscilloscope and result is shown in the figure 6.5. Frequency of the PWM signal is 7174Hz, compare to expected 7.3kHz, but this error is neglectable and was caused by binary rounding of the processor. Duty cycle was set to 30% because it is theoretically 1.5 volts and it is the maximum value for the MPPT converter. Real measured signal is smaller than expected 1.5volts, because amplitude of the PWM signal is not exact 5 volts and because of the voltage drop on the resistor. Measured waveforms are on the figure 6.5

5. I^{2}C communication test

Test on the I^{2}C bus must be performed on special testing facility with simulated master processor, this facility is now developing in CDH Cubesat group, after they finish the station, tests will be perform. Only tests in simulator on PC were done, but the simulator from MPLAB software has no utility for testing serial communication and these tests are not too evidential to say that software is working right.

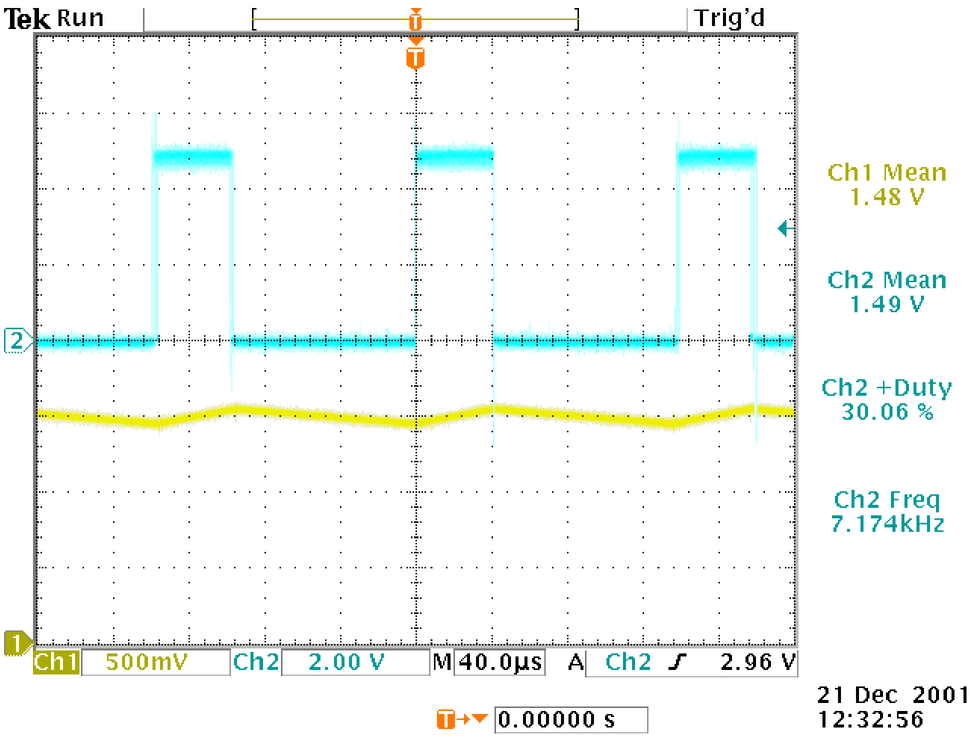

Figure 6.5 PWM signals test

6. Power consumption

During all tests current flowing to the microcontroller was measured and maximum value, when all peripherals were in use, was 3mA, what means 15mW. That is comparable to values in datasheet, where are values between 2.5mA and 5mA.

6.3. Battery protection verification

This section presents experimental results about behavior of the batteries at charging and discharging at normal room temperature.

6.3.1. Charging characteristic

In the experimental setup, a protection circuit for batteries UCC3911 has been used, and a string of two batteries have been tested.

Conditions:

- charging current: 460mA (half of capacity)

- charging voltage: constant
- charging time: approx. 100 min, until the protection circuit acts.

The protection circuit will disconnect the batteries when the voltage level will rise above the established limit: 8.45V.

In table 6.2, are presented the measured values, and the plotted charging characteristic is shown in figure 6.6.

Time [min]	0	1	2	3	4	5	6	7	8	9	10	12	15	20	25
Voltage[V]	5.83	6.97	7.1	7.35	7.42	7.42	7.5	7.55	7.59	7.62	7.64	7.67	7.69	7.74	7.79
Time [min]	30	35	40	45	50	55	60	65	70	75	80	85	90	95	100
Voltage[V]	7.82	7.83	7.85	7.87	7.89	7.91	7.94	7.97	8.02	8.05	8.1	8.15	8.2	8.27	8.35

Table 6.2 Measured voltage values for charging of batteries

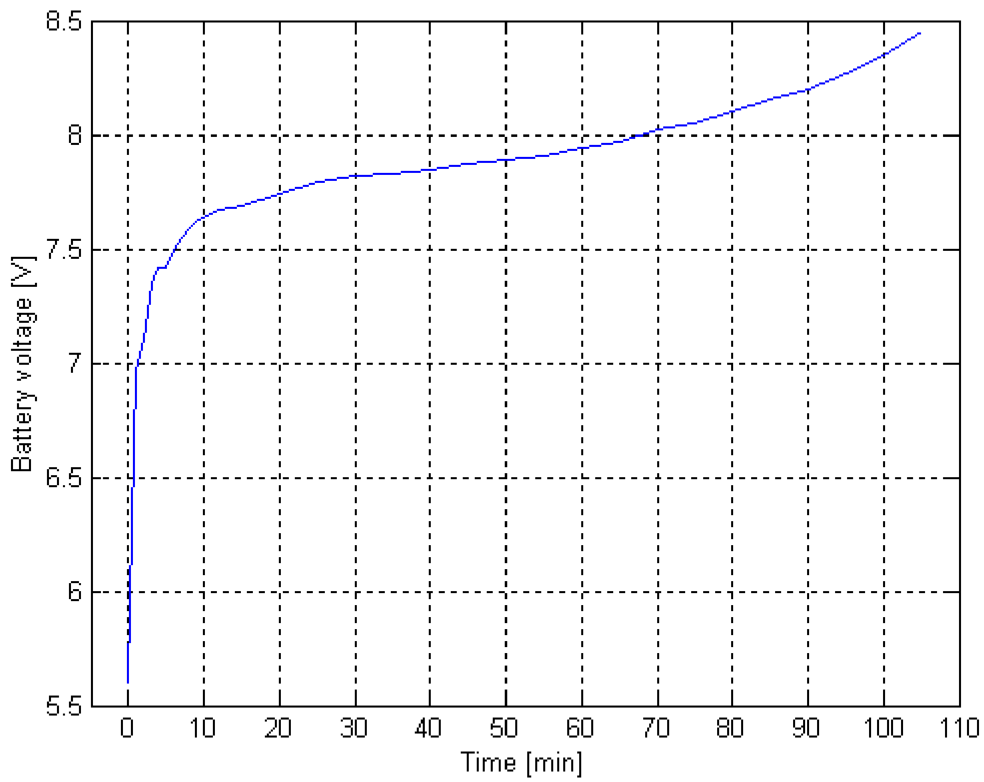

Figure 6.6 Experimental charging characteristic for the batteries

6.3.2. Discharging characteristic

The conditions for discharging batteries test are the same as for the previous performed test, for charging batteries. In table 6.3 are shown the measured values and figure 6.7 presents the discharging characteristic.

Time [min]	0	1	2	3	4	5	6	7	8	9	10	12	15	20	25
Voltage[V]	8.45	8.44	8.07	8.03	7.97	7.85	7.82	7.8	7.78	7.77	7.75	7.73	7.68	7.6	7.56
Time [min]	30	35	40	45	50	55	60	65	70	75	80	85	90	95	100
Voltage[V]	7.53	7.5	7.46	7.43	7.38	7.36	7.31	7.27	7.24	7.22	7.19	7.17	7.13	7.06	6.74

Table 6.3 Measured voltage values for discharging of batteries

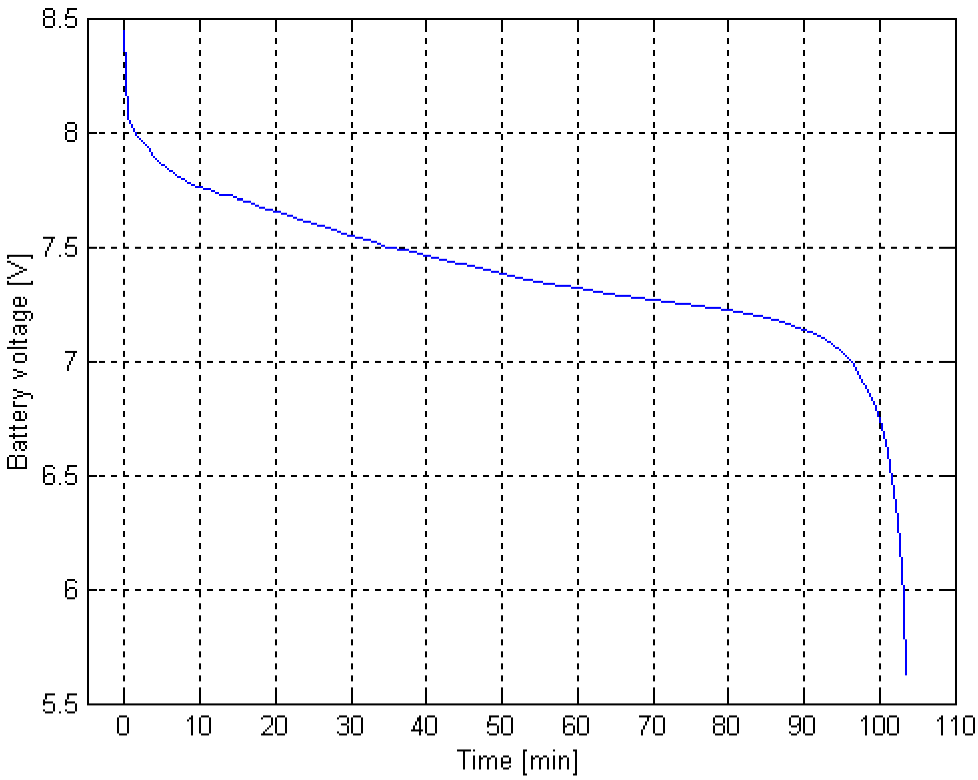

Figure 6.7 Experimental discharging characteristic for the batteries

There are a few points after t = 100 min, unregistered in the table, but visible in the figure. The protection circuit disconnects the batteries at V = 6.09V.

6.4. Summary

Experimental results are captured and shown in this chapter.

As written in the introduction, there were several reasons for not performing all the necessary tests at the time of delivering the report. One of the strongest reasons has been lack of components, due to long delivery time from the manufacturers. Due to constrains about mass and dimensions of the power supply board, all the electronic components have been chosen in respect with reliability (brand-name, well-known manufacturers), small outline packages and high-efficiency. This led to some delays in practical implementation of the designed board. One result is that it has been decided to realize separate PCBs for each module of the power supply and to test them independently, further connections between modules being easy to be done later.

All possible tests, available at this time, were performed on microcontroller and the results obtained are satisfying the demands for the software and hardware. Tests of the communication with OBC must be performed later after testing facility will be prepared. Also tests on real solar cells must be done to test the digital version of MPPT control signal.

The tests performed over the battery protection circuit shown that this device is working properly, implementing an efficient overcharging and overdischarging protection, as expected from the analysis performed in section 4.3. Charging and discharging characteristic for a string of two batteries are depicted in section 6.3.

Chapter 7
Conclusions

Abstract

This chapter concludes on the electronic scheme, which has been implemented for the power supply subsystem, in the CubeSat satellite. The scheme is evaluated, in respect with the demands of the application stated in Chapter 1 and conclusion are drawn.

7.1. Conclusion

Solar cells

It was supposed to receive triple junction solar cells fabricated by EMCORE company. But still we have not got any more accurate data about them. As can be seen from equation used in SABER simulation, the behavior of solar cell is dependent on a lot of parameters. So far as simulation has been performed, majority of parameters were guess. Due to this statement, results obtained from simulation can be taken only for general conception. There is not any problem, after receiving real data, to run simulation again and profit proper results.

The final scheme of the power supply is presented in figure 3.4 in chapter 3.

Input power

In section 3.3, the input power from the solar arrays is computed.

- Average input power, per one side: P_{av} = 2.07 [W]
- Albedo radiation power, for one side: $P^{*}_{ALB} = 0.554$ [W]
- Infrared radiation power, for one side: $P^{*}_{IR} = 0.324$ [W]

It is shown that the most favorable situation is when three sides of the satellite are illuminated by Sun. From characteristic of the solar cells, it is deducted that a certain amount of power can be delivered considering the infrared and albedo energy radiated by Earth. This quantity is calculated and it has been proposed as a mission statement to verify it through housekeeping data which will be sent back to Earth.

A theoretical background about photovoltaic and batteries is presented, as well as an overview of different possibilities of implementation, existent on the market.

Concerning the application and the specifications for the system, batteries are chosen to be four Li-Ion type.

Thermal model

First of all was computed the temperature equilibrium for the satellite, considering no internal heat sources. If all equilibrium temperatures are compared than can be seen that the worst case for Cubesat is in eclipse when only side with camera is pointed to the Earth. Temperature range according to the temperature equilibrium is:

$T_{\max}$ = 55 [˚C]

$T_{\min}$ = -124 [˚C]

Model of the board in Saber

Highest obtained temperature for switch of step-down converter is 40.9°C, which is far away from maximum for industrial standard. Of course this temperatures will add up with the temperatures of surroundings and they are not final.

From thermal control shielding for batteries is suggested (as the most temperature sensitive part of power subsystem). MLI can be easily used for this. Also heat pipes seem to be relevant for the current application.

Some basic considerations about electromagnetic compatibility problems are presented in section 5.5. Potential sources of noise are analyzed and a comparison between them is made.

There were a few reasons for not performing all the necessary tests at the time of delivering the report. One of the strongest reasons has been lack of components, due to long delivery time from the manufacturers. Due to constrains about mass and dimensions of the power supply board, all the electronic components have been chosen in respect with reliability (brand-name, well-known manufacturers), small outline packages and high-efficiency. This led to some delays in practical implementation of the designed board. One result is that it has been decided to realize separate PCBs for each module of the power supply and to test them independently, further connections between modules being easy to be done later.

Analog part of the PSU

Test boards have been made for different circuits, which are included in the analog part of the PSU. Until now have been completed tests for battery protection circuit, the step-up converter and battery charger. These circuits are working properly. It has been observed bigger voltage ripple than it was expected at the output of the step-up converter. This was due to the output filtering capacitor used, being general purpose with a large ESR.

MCU

For MCU and it's additional circuits were selected proper components and then final design scheme was created (Appendix C). Also software for supervising power supply unit were designed and written. Program guards protection circuits for each user and in case of failure turn-off user. With measured signals from whole unit MCU can provide OBC with precise information about situation in the PSU. Also from these signals digital MPPT control signal is calculated, furthermore selecting which signal should drive the MPPT converter. As a last function, MCU provide external watchdog and bootpin selector for the OBC. Source code for the software is included on the enclosed CD.

After the development all possible tests, available at the time, were performed on microcontroller and the results obtained are satisfying the demands for the software and hardware, which was described in chapter 2.

Only tests of the communication with OBC must be performed later after testing facility will be prepared. Also tests on the real solar cells must be done to test the digital version of MPPT control signal.

Batteries

The tests performed over the battery protection circuit shown that this device is working properly, implementing an efficient overcharging and overdischarging protection, as expected from the analysis performed in section 4.3. Charging and discharging characteristic for a string of two batteries are depicted in section 6.3.

7.2. Future work

System engineering

It will be necessary to cooperate with other groups next semester and keep track on interfaces. It is still a lot of work to implicate PSU subsystem to the entire design.

Thermal analysis

- Verify 2D model by measurement in vacuum chamber at low temperatures.

2D model:

- It is necessary to find exact values for R_{thjc} for specification of model.
- Make 2D model according to the final PCB, which respecting geometrical position of device.
- Models for other boards if parameters will be delivered.
- Try to include radiation.

3D model:

- Define more sophisticated geometry.
- Connect models for conduction and also for radiation in ANSYS, run them simultaneously.
- Make transient thermal analysis.

Thermal control:

- Consult with MK9 group about using of heat pipes and find hardware
- Design thermal shield for batteries in cooperation with MK9

EMC

- Measurement by using spectrum analyzer on our board must be done

MCU

- Tests of the communication with OBC must be performed later after testing facility will be prepared.
- Tests on the real solar cells must be done to test the digital version of MPPT control signal.

Analog part of the PSU

In order to verify well-functioning of all the modules and to prove the accuracy of the design, further separate experimental tests for each circuit must be performed. After that a general test must be made for proving expected behaviour. In respect with the design work done so far, it is necessary to finish the final board for the power supply. Because of the small outline components selected for the application, this will imply cooperation with some specialized companies in mounting SMD components. A prototype of the entire board is programmed to be finished in the near future.

Appendix A

Input power calculation

Abstract

This appendix presents the Matlab file used in calculation of input power. The listing of the file is attached and the results from the program are shown.

A.1. Matlab file used in computations

The listing of the Matlab file used to compute the input power is giving in the following. The results, returned by the program, may be found after the listing.

```
function InputPower
%all values here are only coefficients not power!!!
MaxSize=100;
StepSize=100;
fi=0:pi/(StepSize*2):pi/2;
theta=0:pi/(StepSize*2):pi/2;

for i=1:StepSize
    for j=1:StepSize

power(i,j)=cos(fi(i))*sin(theta(j))+sin(fi(i))*sin(theta(j))+cos(theta(j));
    end
end
%f=power;
surface(power);
set(gca,'XTickLabel',{'0°','9°','18°','27°','36°','45°','54°','63°','72°','81°',
'90°'})
set(gca,'YTickLabel',{'0°','9°','18°','27°','36°','45°','54°','63°','72°','81°',
'90°'})
xlabel('\vartheta 0-90°')
ylabel('fi 0-90°')
zlabel('Power coefficient')
grid on
%colormap(autumn);

%find maximum value
max_value=-inf;
Max_fi=0;
Max_theta=0;
for i=1:MaxSize
    for j=1:MaxSize
        if power(i,j)>max_value
            max_value=power(i,j);
            Max_fi=i;
            Max_theta=j;
        end
    end
end

%values for maximum angle in degrees
maximum_angle_fi=(Max_fi*pi/(MaxSize*2))*180/pi
maximum_angle_theta=(Max_theta*pi/(MaxSize*2))*180/pi
max_value

%find average value
average_value=0;

for i=1:MaxSize
    for j=1:MaxSize
            average_value = average_value + power(i,j);
    end
end
```

```
average_value = average_value/(MaxSize*MaxSize)
```

Results from running the program:

```
maximum_angle_fi =

   45.9000

maximum_angle_theta =

   55.8000

max_value =

    1.7320

average_value =

    1.4458
```

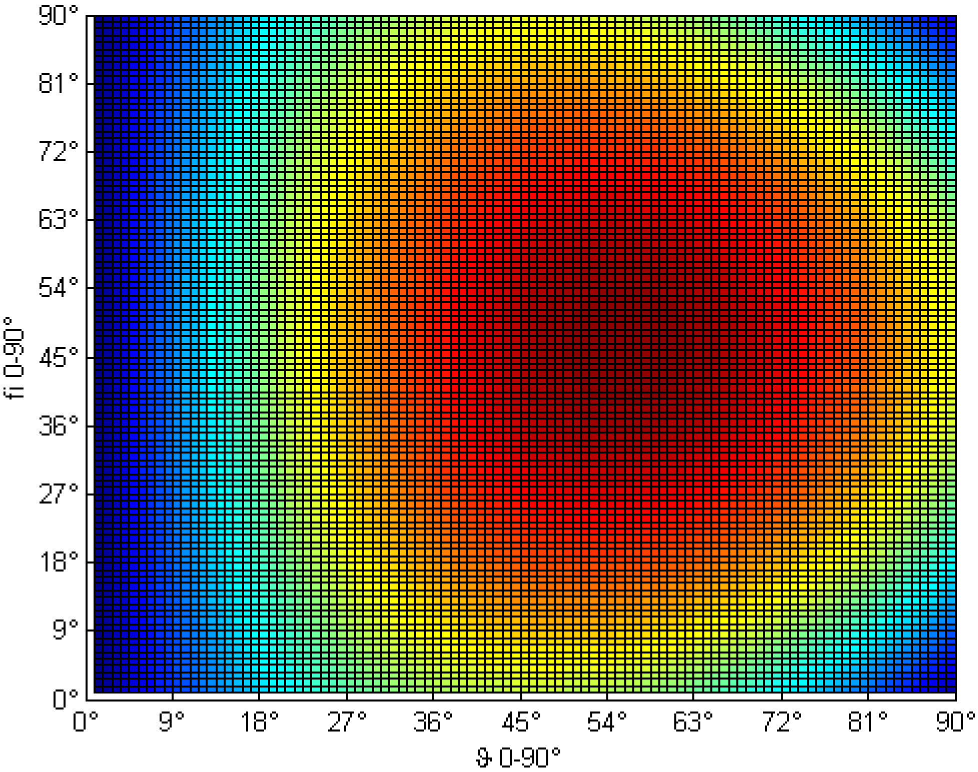

Figure A.1 Plotted result of the program

Appendix B
Spherical coordinates

Abstract

This appendix presents a mathematical abstract, about spherical coordinates. This is necessary for a better understanding of the computations performed in section 3.3.2 about the input power.

B.1. Introduction of spherical coordinates

The spherical coordinates reference system is used in situation when important things about a point are its distance from the origin and, using terms from geography, its latitude and longitude.

This reference system is designated as (rho, phi, theta) or (ρ, ϕ, θ), where each element has the following meaning:

- ρ – denotes the the point's distance from the origin.
- ϕ – is the angle of ascension, between the modulus of the point's vector distance from the origin and the *z*-axis. ϕ is positive for positive values of *z*-axis, and f ∈ [0, π].
- θ – is the angle of declination, or the angle from *xz* plane to the point.

Figure B.1 shows a graphical approach of the definition of the spherical coordinates.

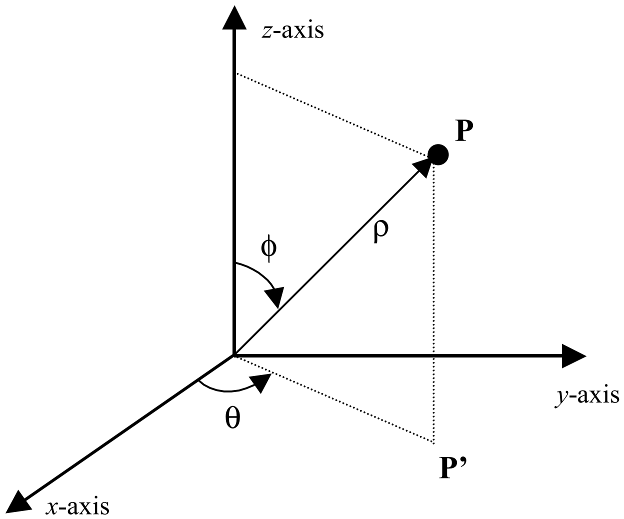

Figure B.1 Definition of spherical coordinates

B.2. Conversion of coordinate systems

Figure B.2 shows the conversion from spherical to cartesian coordinates and vice-versa. Figure B.2b, on the right shows the *xy*-plane from the figure B.2a, on the left.

Notice that, by the Pythagorean Theorem:

$$S = \sqrt{x^2 + y^2} = \rho \cdot \sin\phi \tag{B.1}$$

$$\rho = \sqrt{S^2 + z^2} = \sqrt{x^2 + y^2 + z^2} \tag{B.2}$$

$$x = S \cdot \cos\theta = \rho \cdot \sin\phi \cdot \cos\theta \tag{B.3}$$

$$y = S \cdot \sin\theta = \rho \cdot \sin\phi \cdot \sin\theta \tag{B.4}$$

$$z = \rho \cdot \cos\theta \tag{B.5}$$

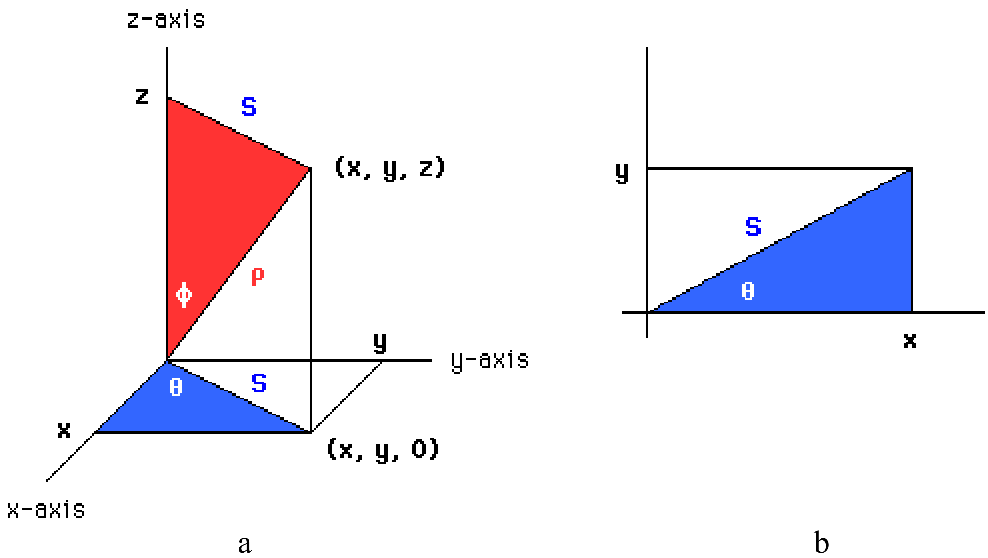

Figure B.2 Transformation of coordinate reference system
[http://www.math.montana.edu/]

The last three equations, (B.3)÷(B.5) represents the conversion from spherical to cartesian coordinates.

The conversion from cartesian to spherical coordinates is achieved through the following equations:

$$\rho = \sqrt{x^2 + y^2 + z^2} \tag{B.6}$$

$$S = \sqrt{x^2 + y^2} \tag{B.7}$$

$$\phi = \arccos\left(\frac{z}{\rho}\right) \tag{B.8}$$

$$\theta = \begin{cases} \arcsin\left(\frac{y}{S}\right), & \text{if } 0 \le x \\ \pi - \arcsin\left(\frac{y}{S}\right), & \text{if } x < 0 \end{cases} \tag{B.9}$$

Appendix C
Circuit diagrams

Abstract

In this appendix are presented the electronic schemes for analog part of the power supply subsystem and for MCU.

C.1. Implementation scheme for MCU

The scheme used to implement the digital part of the power supply subsystem, the MCU, is presented in figure C.1.

C.2. Implementation scheme for analog part

The analog part of the power supply refers to the other circuitry described in detail in Chapter 4. The scheme is presented in figure C.2.

C.3. List of components

In table C.3 is stated the bill of material, both for the MCU and for the rest of the power supply board.

Designator	PartType	Designator	PartType	Designator	PartType
Batt100	3.7V	C207	0.33u	R145	20k
Batt101	3.7V	D100	PRLL5817	R146	560R
Batt102	3.7V	D101	PRLL5817	R147	1k15
Batt103	3.7V	D102	PRLL5817	R148	250R
C100	220u	D103	PRLL5817	R149	1k
C101	220u	D104	PRLL5817	R150	1k
C102	1u	D105	SB540	R151	1k
C103	0.1u	D106	SB540	R152	1k
C104	0.1u	D107	LL4148	R153	5k
C105	0.1u	D108	LL4148	R154	5k
C106	0.1u	D109	LL4148	R155	5k
C107	0.1u	D110	LL4148	R156	5k
C108	0.1u	D111	LL4148	R157	0.01R
C109	0.1u	D112	LL4148	R158	2M
C110	0.1u	D113	LL4148	R159	1R5
C111	0.1u	D114	LL4148	R200	100k
C112	0.1u	JP100	JUMPER	R201	100k
C113	0.1u	JP101	JUMPER	R202	100k
C114	0.1u	L100	22u	R203	100k
C115	0.1u	L101	12u	R204	100k
C116	0.1u	Q100	MTD20N03HDL	R205	100k
C117	0.1u	Q101	NTD456P	R206	100k
C118	0.1u	R100	10k	R207	10R
C119	0.1u	R101	10k	R208	4k7
C120	0.1u	R102	10k	R209	240k
C121	0.1u	R103	10k	R210	4k8

C122	68u	R104	10k	S100	Kill switch
C123	68u	R105	10k	SC100	2.6V
C124	300u	R106	10k	SC101	2.6V
C125	300u	R107	0.033R	SC102	2.6V
C126	100p	R108	0.033R	SC103	2.6V
C127	100p	R109	93k3	SC104	2.6V
C128	1u	R110	0.25R	SC105	2.6V
C129	1u	R111	200R	SC106	2.6V
C130	1u	R112	200R	SC107	2.6V
C131	10u	R113	0.1R	SC108	2.6V
C132	10u	R114	0.1R	SC109	2.6V
C133	10n	R115	0.1R	U100	MAX1771
C134	10n	R116	0.1R	U101	UCC3911-DP1
C135	10n	R117	0.1R	U102	UCC3911-DP1
C136	10n	R118	0.1R	U103	MAX4372F
C137	10n	R119	0.1R	U104	MAX4372F
C138	10n	R120	0.1R	U105	MAX4372F
C139	10n	R121	2k	U106	MAX4372F
C140	10n	R122	2k	U107	MAX4372F
C141	10n	R123	2k	U108	ADP3810
C142	10n	R124	2k	U109	MAX4372T
C143	10n	R125	2k	U110	LM78L05
C144	0.22u	R126	2k	U111	TPS2034
C145	47u	R127	2k	U112	TPS2030
C146	0.33u	R128	2k	U113	TPS2030
C147	22u	R129	2k	U114	TPS2030
C148	22u	R130	2k	U115	MAX835
C149	22u	R131	2k	U116	MAX835
C150	22u	R132	2k	U117	MAX835
C151	22u	R133	2k	U118	MAX835
C152	0.47u	R134	2k	U119	MAX4372H
C153	4.7u	R135	2k	U120	MAX4372H
C154	4.7u	R136	2k	U121	MAX4372H
C155	4.7u	R137	2k	U122	MAX4372H
C200	0.1u	R138	2k	U123	MAX1744
C201	0.1u	R139	2k	U124	SE555D
C202	0.1u	R140	2k	U200	ADG706
C203	0.1u	R141	2k	U201	ADG706
C204	0.1u	R142	90k	U202	PIC16C774
C205	10u	R143	20k	U203	ADG704
C206	22p	R144	20k	U204	AD8072

Appendix D
Nomenclature

Abstract

This appendix presents all the common used abbreviations and symbols. The items are listed in groups of units, e.g. [V], [A] *and so forth. Instantaneous values are presented with lower case letters. Average and RMS values are written with uppercase letters and peak values are distinguished with a hat.*
A list of computer terminology is also included in the final part of the appendix.
Items from all the lists are arranged in alphabetical order.

Common used abbreviations

ACS – Attitude Control System

BAT – Battery Unit

COM – Communication Module

CAM – Camera Module

EMC – Electromagnetic Compatibility

EME – Electromagnetic Environment

EMI – Electromagnetic Interference

LEO – Low Earth Orbit

MCU – Microcontroller Unit

MLI – Multilayer Insulation

MPPT – Maximum Power Point Tracker

OBC – Onboard Computer

PSU – Power Supply Unit

PSC – Power Supply Source (referred to MCU)

PV – Photovoltaics

RTG – Radioisotope Thermal Generator

Symbols

Parameter/Symbol	Description	Unit
V_{OC}	Open circuit voltage	[V]
V_{mpp}	Maximum power point voltage	[V]
V_D	Voltage drop across diode	[V]
V_{serial}	Batteries voltage on serial connection	[V]
$V_{parallel}$	Batteries voltage on parallel connection	[V]
V_{batt}	Battery voltage	[V]
V_d	Input voltage for converter	[V]
V_o	Output voltage for converters	[V]
U_{min}	Minimum voltage for a Li-Ion battery	[V]
U_{max}	Maximum voltage for a Li-Ion battery	[V]
$V+$, V_{cc}	Positive supply voltage	[V]
V_{OUT}	Output voltage	[V]
V_{IN}	Input voltage	[V]

Parameter/Symbol	Description	Unit
$C_{parallel}$	Equivalent capacity for parallel connection of batteries	[Ah]
C_{series}	Equivalent capacity for serial connection of batteries	[Ah]
C_{batt}	Battery capacity	[Ah]
I_D	Current across diode	[A]
I_{rs}	Reverse saturation current	[A]
I_{ph}	Photocurrent in the solar cells	[A]
I_{sc}	Shortcircuit current	[A]
I_{RR}	Reverse saturation current at cell reference temperature	[A]
I_o	Output current for the converter	[A]
I_d	Input current for the converter	[A]
I_{GATE}	Gate current for switch	[A]
I_{LIM}	Limit current	[A]

Parameter/Symbol	Description	Unit
R_P	Series resistance of the cell	[Ω]
R_S	Parallel resistance of the cell	[Ω]
$R_{DS(\mathrm{on})}$, $r_{DS(\mathrm{on})}$	Switch on-resistance	[Ω]
R_{thjc}	Thermal resistance junction-case	[°C/W]
R_{thca}	Thermal resistance case-ambient	[°C/W]
R_{th_rad}	Thermal resistance due to radiation	[K/W]
R_{th_cond}	Thermal resistance due to conduction	[K/W]

Parameter/Symbol	Description	Unit
P^{*}_{in1}	Input power for one side of the satellite	[W]
P_{sun}	Amount of energy radiated by Sun	[W/m^2]
P_{diode}	Losses across Schottky diode	[W]
P_{in1}	One side input power, considering Schottky diode losses	[W]
P_{av}	Average input power	[W]
P_{max}	Maximum power for three sides illuminated	[W]
P_{in2}	Input power for two sides illuminated	[W]
P^{*}_{IR}	Input power from infrared radiation	[W]
P_{IR_Earth}	Amount of infrared radiation, due to Earth	[W]
P_{mIR}	Maximum of input power, due to infrared radiation	[W]
P^{*}_{ALB}	Input power from albedo radiation	[W]
P_{mALB}	Maximum of input power, due to albedo radiation	[W]
P_{ALB_Earth}	Amount of albedo radiated energy	[W]
P_{cond}	Heat transferred through conduction	[W]
P_{rad}	Heat transferred through radiation	[W]
E_{total}	Minimum available energy	[J]
E_{sun}	Energy from solar cells	[J]
E^{n}_{batt}	Energy needed from batteries	[J]
E_{OBC}	Energy required by OBC	[J]
E_{ATC}	Energy required by ACS	[J]
E_{charge}	Energy available at each orbit to charge batteries	[J]
E^{r}_{charge}	Energy required to charge the batteries from solar panels	[J]
E_G	Band-gap energy of semiconductor used in cells	[eV]
S	Solar irradiation	[mW/cm^2]

Parameter/Symbol	Description	Unit
L	Inductor	[H]

Parameter/Symbol	Description	Unit
T	Absolute temperature	[K]
ΔT	Temperature difference	[K]
T_e	Equilibrium temperature	[K]

Parameter/Symbol	Description	Value	Unit
A	Cross sectional area		[m^2]
α	Absorbitivity for a material		
D	Duty cycle ratio	[0,1]	
E	Electric field strength		[V/m]
ε	Emissivity for a material		
f	Frequency		[Hz]
H	Magnetic field strength		[A/m]
h_r	Radiation heat transfer coefficient		[W/m^{2}K]
k_i	Shortcircuit current temperature coefficient		
k	Boltzmann constant	$1.38 \cdot 10^{-23}$	[J/K]
λ	Thermal conductivity		[J/s·m·K]
n	Number of cells		
η	Efficiency		[%]
q	Charge of an electron	$1.6 \cdot 10^{-19}$	[eV]
Q_g	Charge		[C]
σ	Steffan-Boltzmann constant	$5.67 \cdot 10^{-8}$	[W/m^{2}K^4]
σ_r	Material relative conductivity in relation with copper		
μ_r	Relative permeability		
t_{on}	Switch conduction period		[s]
t_{DLY}	Delay time		[s]
T_s	Switching period		[s]

Computer terminology

EEPROM (Electrically Erasable Program Memory) – type of stable memory, which can be erased after programming by electric current.

EPROM (Erasable Program Memory) – type of stable memory, which can be deleted after programming, this deletion is done by illumination by UV light, these memories have ceramic window for the die.

FLASH – Subtype of EEPROM memory type family, usually have thousands of possible rewrites.

High level (high state) – logic status of the MCU pin, high state represents logic 1 and is implemented as a supply voltage.

Interrupt – special state of processor, when after some event normal run of code is interrupted and special part of code is started.

ISR (Interrupt Service Routine) – part of code, which will be started after an interrupt occurs.

Low level (low state) – logic status of the MCU pin, low state represents logic 0 and is implemented as a zero volts.

OTP (One Time Programmable) – type of stable memory, which can be programmed only once and after programming is not possible to change memory content. Technology is the same as EPROM only window is covered.

Port – input/output pins on microcontrollers are associated to the groups with similar properties and behaviors. These groups are called *ports.* Usually ports are 8-bit, but is not a rule.

RAM (Random Access Memory) – type of memory, which can be read and write without any limitation. Memory content is not stable, so after disconnecting power supply everything is deleted which can be read and write without any limitation.

RISC (Reduced Instruction Set Computer) – A RISC CPU contains fewer instructions than a non CISC CPU (Complete Instruction Set Computer). On first thought, one might think the RISC would be inferior to the CISC one. Actually a RISC CPU is faster because of the fewer instructions. Some of the eliminated instructions are deemed fairly obsolete anyway. A disadvantage might be that a RISC CPU may make software more complex if the program has to work around the eliminated instruction(s).

Watchdog – autonomous part of the microcontroller, which consist of independent oscillator and timer. This timer must be cleared in software or when overflows, watchdog resets microcontroller. This function is useful to prevent never-ending loops.

Appendix E
The attached CD-ROM

Abstract

This appendix is describing the content of the attached CD-ROM of the report.

The enclosed CD-ROM contains various computation script files, datasheet, articles concerning the present project work. Also, are included complete set of circuit diagrams, done by means of Protel and OrCad software.

The directory structure of the CD-ROM is depicted in figure D.1.

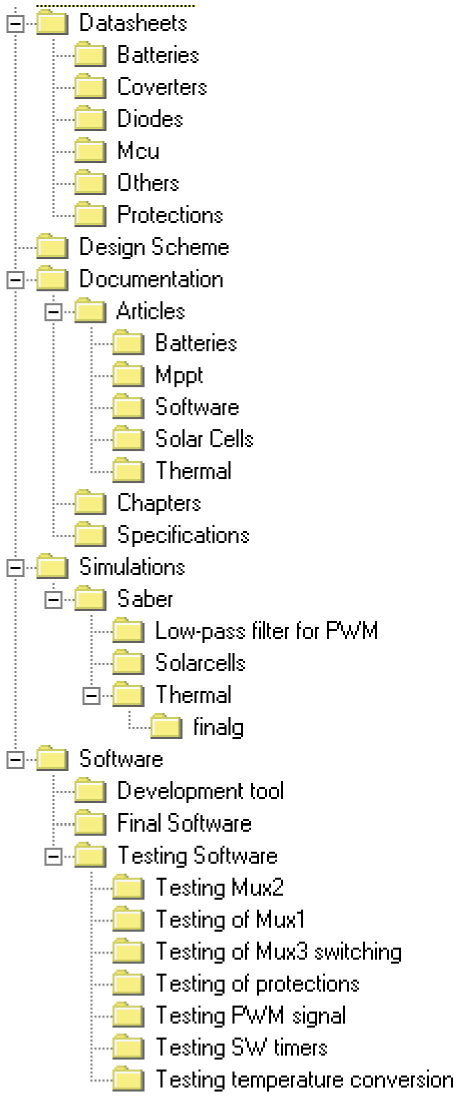

Figure D.1 Directory structure for the enclosed CD-ROM

The contents of the different folders are summarized in the following:

Datasheets – contains all the datasheet of the components used in design of the power supply, as well as complementary files.

Design scheme – this directory contains the schematic and PCB files for the entire board and for the test boards used. The file is a Protel database and it comprises the entire scheme for the power supply, schemes for test boards and test PCBs. The Protel version used is Client 99 Trial with Service Pack 4.

Documentation – besides all the articles referred to the project, this folder contains other articles and complementary data which are relevant for the project work.

Simulations – here are the files from Saber software used in thermal analysis.

Software – in this folder, various files referred to the software code used in programming the microcontroller unit are included, as well as the software code used to test parts of the board. The results are included in Chapter 6.

References

Benford, P. – *50 things to do with a PIC*, 1998, Bluebird Tech. Press Ltd., ISBN 1-901631-06-0

Hansen, A., Sørensen, P., Hansen, L., Bindner, H. – *Models for stand-alone PV system*, 2000, Risø National Laboratory, Roskilde, Denmark, ISBN 87-550-2774-1

Mills, A. F. – *Heat and mass transfer*, 1995, Irwin, ISBN 0-256-11443-9

Mohan, Undeland, Robbins – *Powers Electronics - Converters, Applications, and Design*, 1995, John Wiley & Sons Inc., ISBN 0-471-58408-8

Sellers J. – *Understanding space. An introduction to Astronautics*, 1994, McGraw-Hill Inc., ISBN 0-07-057027-2

Articles & other papers

El-Shibini, Rakha – *Maximum power point tracking technique*, Mediterranean Electrotechnical Conference, MELECON '89, "Integrating Research, Industry and Education in Energy and Communication Engineering", 1989

Enslin, Wolf, Snyman, Swiegers – *Integrated photovoltaic maximum power point tracking converter*, IEEE Transactions on Industrial Electronics, Vol. 44, Issue 6, Dec. 1997

Enslin, Snyman – *Simplified feed-forward control of the maximum power point in PV installations*, Industrial Electronics, Control, Instrumentation, and Automation, Proceedings of the 1992 International Conference on Power Electronics and Motion Control, Vol. 1, 1992

Fatemi – *Emcore presentation – solar cells. Advanced triple-junction cells*, Emcore Corp., November 1, 2001

Fitzgerald - *Advanced laboratory: Solar cell characterization,* Spring 2001

Hansen – *Notes on lectures. Design of small satellite*, Autumn 2001, Aalborg University

Hussein, Muta, Hoshino, Osakada - *Maximum photovoltaic power tracking: an algorithm for rapidly changing atmospheric conditions*, IEEE Proceedings - Gener.Transm.Distrib., Vol.142, No.1, January 1995

Irisawa, Saito, Takano, Sawada – *Maximum power point tracking control of photovoltaic generation systems under non-uniform isolation by means of monitoring cells*, IEEE Transactions on Power Electronics, 2000

Masoum, Mohammad, Dehbonei, Hooman - *Design, construction and testing of a voltage-based maximum power point tracker (VMPPT) for small satellite power supply*

Midya, Krein, Turnbull, Reppa, Kimball – *Dynamic maximum power point tracker for photovoltaic applications*, Power Electronics Specialists Conference PESC '96, 27th Annual IEEE Record, Vol. 2, 1996

Sharps, Aiken, Stan, Thang, Fatemi – *Electron and proton radiation study of $GaInP_2$/GaAs/Ge solar cells*, Emcore Photovoltaics

Shimizu, Hirakata, Kamezawa, Watanabe - *Generation control circuit for photovoltaic modules,* IEEE Transactions on Power Electronics, Vol. 16, No. 3, May 2001

Snyman, Enslin – *Simplified maximum power point controller for PV installations*, Photovoltaic Specialists Conference, 23rd IEEE Conference Record, 1993

Teulings, Marpinard, Capel, O'Sullivan – *A new maximum power point tracking system*, IEEE Transactions on Power Electronics, 1993

Yan Hong Lim, Hamill – *Simple maximum power point tracker for photovoltaic arrays*, IEEE Electronics Letters, Vol. 36, Issue 11, 25 May 2000

Standards

EN 50081-2, *Electromagnetic compatibility – Generic emission standard. Part 2: Industrial environment*, CENELEC, August 1993

IEC 61000-6-2, *Electromagnetic compatibility (EMC). Part 6.2: Generic standards – Immunity for industrial environments*, IEC, January 1999